

DISSERTATION

BIPYRIDYL COBALT COMPLEX MEDIATORS IN
DYE-SENSITIZED SOLAR CELLS

Submitted by

Michael J. Scott

Department of Chemistry

In partial fulfillment of the requirements

For the degree of Doctor of Philosophy

Colorado State University

Fort Collins, Colorado

Spring 2008

UMI Number: 3321310

INFORMATION TO USERS

The quality of this reproduction is dependent upon the quality of the copy submitted. Broken or indistinct print, colored or poor quality illustrations and photographs, print bleed-through, substandard margins, and improper alignment can adversely affect reproduction.

In the unlikely event that the author did not send a complete manuscript and there are missing pages, these will be noted. Also, if unauthorized copyright material had to be removed, a note will indicate the deletion.

UMI[®]

UMI Microform 3321310

Copyright 2008 by ProQuest LLC.

All rights reserved. This microform edition is protected against unauthorized copying under Title 17, United States Code.

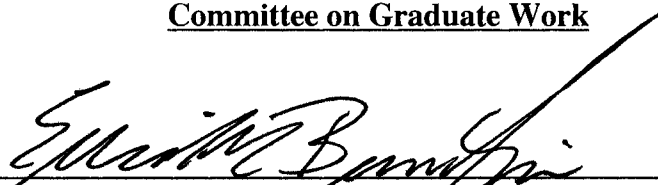
ProQuest LLC
789 E. Eisenhower Parkway
PO Box 1346
Ann Arbor, MI 48106-1346

COLORADO STATE UNIVERSITY

December 17, 2007

WE HEREBY RECOMMEND THAT THE DISSERTATION PREPARED UNDER OUR SUPERVISION BY MICHAEL J. SCOTT ENTITLED **BIPYRIDYL COBALT COMPLEX MEDIATORS IN DYE-SENSITIZED SOLAR CELLS** BE ACCEPTED AS FULFILLING IN PART THE REQUIREMENTS FOR THE DEGREE OF DOCTOR OF PHILOSOPHY.

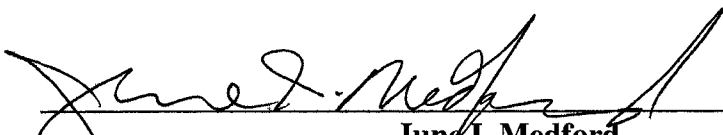
Committee on Graduate Work



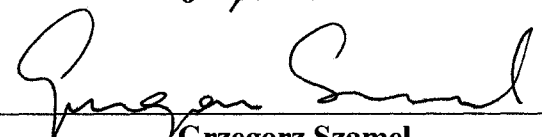
Elliot R. Bernstein



Ellen R. Fisher



June I. Medford



Grzegorz Szamel



C. Michael Elliott, Advisor



Anthony K. Rappe, Department Head

ABSTRACT OF DISSERTATION

BIPYRIDYL COBALT COMPLEX MEDIATORS IN DYE-SENSITIZED SOLAR CELLS

Dye-sensitization of semiconductor substrates allows for photo-induced charge injection of an electron from the dye's excited state into the semiconductor conduction band with near unit efficiency. Dye-sensitized solar cells (DSSCs) exploit this photo-induced charge separation for conversion of sunlight energy into electrical energy. By employing high surface area, mesoporous TiO_2 , and a darkly colored ruthenium metal complex dye for sensitization, a significant portion of the visible spectrum can be absorbed.

The mesoporous TiO_2 semiconductor, deposited on a transparent conducting oxide (TCO) medium, constitutes the photoanode of the DSSC. A wide range of materials, including gold and modified TCO, may be used as a cathode. An electrolyte solution, containing a redox couple completes the cell. Typically, the iodide/tri-iodide (I^-/I_3^-) redox couple has been employed in DSSCs, however the use of bipyridyl cobalt complexes not only avoids some of the negative aspects of I^-/I_3^- , but also allows for tuning of the cell's electrochemistry, exploration of diverse cathode materials, and investigation of mediator solution additives to enhance cell performance, among other things. Three cobalt complexes were considered throughout this body of work: one with alkyl functionalities on the bipyridyl ligands, one with ester functionalities on the bipyridyl ligands, and one with amide functionalities on the bipyridyl ligands.

The three cobalt complexes were investigated on the basis of mediator solution time dependence and electrode dependence. It was discovered that the three cobalt complexes are stable for at least a period of one week when dissolved in γ -butyrolactone.

Additionally, while gold, carbon, and modified TCO cathodes perform well in cells employing the cobalt complex with alkyl groups substituted on the bipyridyl ligands, when electron withdrawing ester and amide functionalities were substituted on the bipyridyl ligands gold cathodes provide the best performance.

An optically transparent cathode, comprising TCO glass modified with an osmium(II) complex, was developed for use in stacked DSSCs. This transparent cathode allows light that is not absorbed by the first DSSC in a stack to be absorbed by a second cell. It was also demonstrated that using a spectrally complementary dye in the second cell of the stack extends the stacked DSSCs light absorption into the longer wavelength portion of the visible spectrum.

Spatial current imaging, completed by rastering a laser over the surface of a DSSC, was described as a technique for investigating the local current behavior of cobalt mediated cells. Intentional electrode damage was visualized using the scanning technique, and the effects of increased pressure on the cell were discussed.

Finally, the use of phenothiazine (PTZ) moieties as co-mediators in cobalt mediated DSSCs was investigated. It was determined that an anionic PTZ salt was most effective at reducing the photo-oxidized sensitizing dye. Additionally, this anionic PTZ salt enhanced the performance of operational DSSCs employing the alkyl substituted cobalt complex. However, poor electronic coupling and decreased driving force prevents the anionic PTZ salt from enhancing the performance of DSSCs mediated with the cobalt complexes that contain electron withdrawing functionalities.

Michael J. Scott
Chemistry Department
Colorado State University
Fort Collins, CO 80523
Spring 2008

ACKNOWLEDGEMENTS

First and foremost I must thank Professor Mike Elliott for his research interests in dye-sensitized solar cells, his limitless knowledge of chemistry, and his ability to throw great cabin parties and ski trips. The Chemistry Department of Colorado State University for providing such excellent facilities for the pursuit of my graduate education. Most importantly I must thank my wife, Rebecca Dumeyer, for her unflagging love and relentless encouragement over the years. She has been my rock, without her I would never have come this far. Also I must thank my parents, Dr. Stuart Scott and Ruth Scott for their continuing love and support.

I must also thank the members of the Elliott group: John Weber for getting me started with the laser system when I first arrived at CSU, Shawn Sapp for starting the DSSC project, Jeremy Nelson for his assistance in the lab, for being a good sounding board for ideas, and for our daily rants against all that ails the world, Di Xue and Stefano Caramori for oxidizing $\text{Co}(\text{DTB})_3^{2+}$ with a modified TCO electrode, and everyone else for being friendly, accepting, and a great group to work with.

Professors Nancy Levinger, Elliot Bernstein, and both of their research groups for helpful advise on laser systems, and generous lending of optics. Professor Ellen Fisher for her assistance navigating graduate school, her insight on the professional world, and for her tolerance and patience with endless loud music across the hall. Bruce Parkinson and his research group for the use of the scanning electrochemistry setup and IPCE instrument. Professor Grzegorz Szamel for patiently helping me learn Physical Chemistry. Mrs. Roberta Ivy Nissen Haugh for establishing the Gary Maciel Fellowship.

The Staff of the CSU Chemistry Department are the unsung heroes of any Graduate Student. In the front office, Shelly Swanson, Tach Costello, Kathy Martinolich, and Jan Moder make the world go around. Without them the building would certainly implode. In the basement, Elden Burke, Mike Olson, Tom Frederick, and Ron Costello provide the expertise needed to design and fabricate any experimental setup and apparatus imaginable. Dr. Chris Rithner presides over an impressive instrument facility and Dr. Terry Gray keeps the computer networks running smoothly.

Finally I must thank New Belgium Brewery. They make what I believe are some of the best beers available. And they have incorporated renewable energy, sustainable practices, and positivity into their brewery, making the beer taste even better!

TABLE OF CONTENTS

ABSTRACT OF DISSERTATION		iii
ACKNOWLEDGEMENTS		iv
TABLE OF CONTENTS		vii
CHAPTER 1	Introduction	1
1.1	History of Dye-Sensitization	2
1.2	Components of Dye-Sensitized Solar Cells	3
1.3	Operational Principles of Dye-Sensitized Solar Cells	6
1.4	References	10
CHAPTER 2	Experimental Methods	13
2.1	Materials	14
2.2	Electrode Preparation	20
2.3	Experimental Techniques	25
2.4	References	32
CHAPTER 3	Stability and Electrode Dependence of Cobalt Mediator Solutions	34
3.1	Introduction	35
3.2	Results and Discussion	38
3.3	Conclusions	55
3.4	References	57
CHAPTER 4	<i>cis</i>-Dichloro-bis(2,2'-bipyridyl-4,4'-dicarboxylic acid) osmium(II)-Modified Optically Transparent Electrodes: Applications as Cathodes in Stacked Dye-Sensitized Solar Cells	58
4.1	Abstract	59
4.2	Introduction	60
4.3	Results and Discussion	64
4.4	Conclusions	76
4.5	Acknowledgements	77
4.6	Supplemental Information	78
4.7	References	81

CHAPTER 5	Spatially Resolved Current-Voltage Measurements—Evidence for Non-Uniform Photocurrents in Dye Sensitized Solar Cells	84
5.1	Abstract	85
5.2	Introduction	86
5.3	Results and Discussion	87
5.4	Conclusions	95
5.5	Acknowledgements	95
5.6	References	96
CHAPTER 6	Catalytic Phenothiazine Mediator Additives: Transient Laser Spectroscopy, Dye-Sensitized Solar Cell Performance, and Catalytic Activity	97
6.1	Introduction	98
6.2	Results and Discussion	104
6.3	Conclusions	122
6.4	References	124
APPENDIX A	Transient Absorption Spectroscopy Data	126

CHAPTER 1

INTRODUCTION

This dissertation chapter contains background information on solar conversion technology and dye-sensitized solar cells.

1.1 History of Dye-Sensitization

French scientist Edmond Becquerel first discovered the photovoltaic effect in 1839.¹ Since then humankind has been fascinated with the prospect of direct conversion of sunlight energy to electrical energy. After the fuel crisis of 1973 much attention was focused on efficient solar conversion, with a renewed interest in recent years as it has become clear that the continued use of fossil fuels is not only an environmental threat, but also a security threat. The sun supplies the earth with about 3×10^{24} joules of energy per year, or about 10^4 times more than the entire global population currently uses. This means that if 0.1 % of the earth's surface were covered with 10% efficient solar cells our energy needs would be filled.²

Conventional solid-state photovoltaic devices that employ the electrochemical properties of a p-n semiconductor junction have dominated the field of solar conversion since the first modern solar cell was produced at Bell Labs in 1954.³ Since then, technology has improved and devices have been produced that exhibit energy conversion efficiencies better than 25%.⁴ The inorganic semiconductors employed in these devices, typically highly doped crystalline or amorphous silicon, require expensive high temperature and high vacuum fabrication processes and the materials must be of the highest purity. Recently, the increased use of high purity silicon has led to rising prices as refineries are not able to keep up with demand.⁵

It is often forgotten that Becquerel's pioneering research, motivated by photography, was conducted in the solution phase.² Nearly 45 years later, in 1883, German photochemist Hermann Carl Vogel extended the sensitivity of photographic emulsions to longer wavelengths by adding dyes.⁶ Soon thereafter James Moser, another

German photochemist, expanded the concept to photoelectrochemical cells by dyeing silver halide electrodes.⁷ Almost a century later, in 1965 at The Institute of Physical and Chemical Research in Tokyo, Namba and Hishiki reported on the sensitization of zinc oxide semiconductor electrodes with cyanine dyes.⁸ It soon became clear that transition metal complexes chemisorbed to semiconductor substrates transferred electrons efficiently by a metal-to-ligand charge transfer mechanism, and that titanium dioxide (TiO₂) was the preferred semiconductor.⁹⁻¹¹ TiO₂, one of the main ingredients in many paints, is plentiful, non-toxic, and inexpensive.⁴ In 1991 Grätzel and coworkers announced the first operational dye sensitized solar cell (DSSC), with an efficiency of approximately 7%, as an alternative to p-n junction devices.¹² Since then, DSSCs have garnered a great deal of attention as a low-cost alternative to solid state solar conversion devices.^{2, 13}

1.2 Components of DSSCs

Dye-sensitized solar cells are wet photoelectrochemical cells. As such the DSSCs consists of a photoanode, a cathode, and an electrolyte, or mediator, solution. The photoanode is the heart of the DSSC, consisting of a mesoporous layer of nanometer sized TiO₂ particles that is deposited onto a transparent conducting oxide (TCO) glass substrate.⁴ Typically fluorine doped tin oxide (FTO) is the TCO of choice. This deposited mesoporous semiconductor layer is highly structured, resulting in an actual surface area that is 2 to 3 orders of magnitude larger than the geometric surface area.² A scanning electron microscopy (SEM) image of the mesoporous TiO₂ semiconductor at 100,000x magnification is shown in Figure 1.

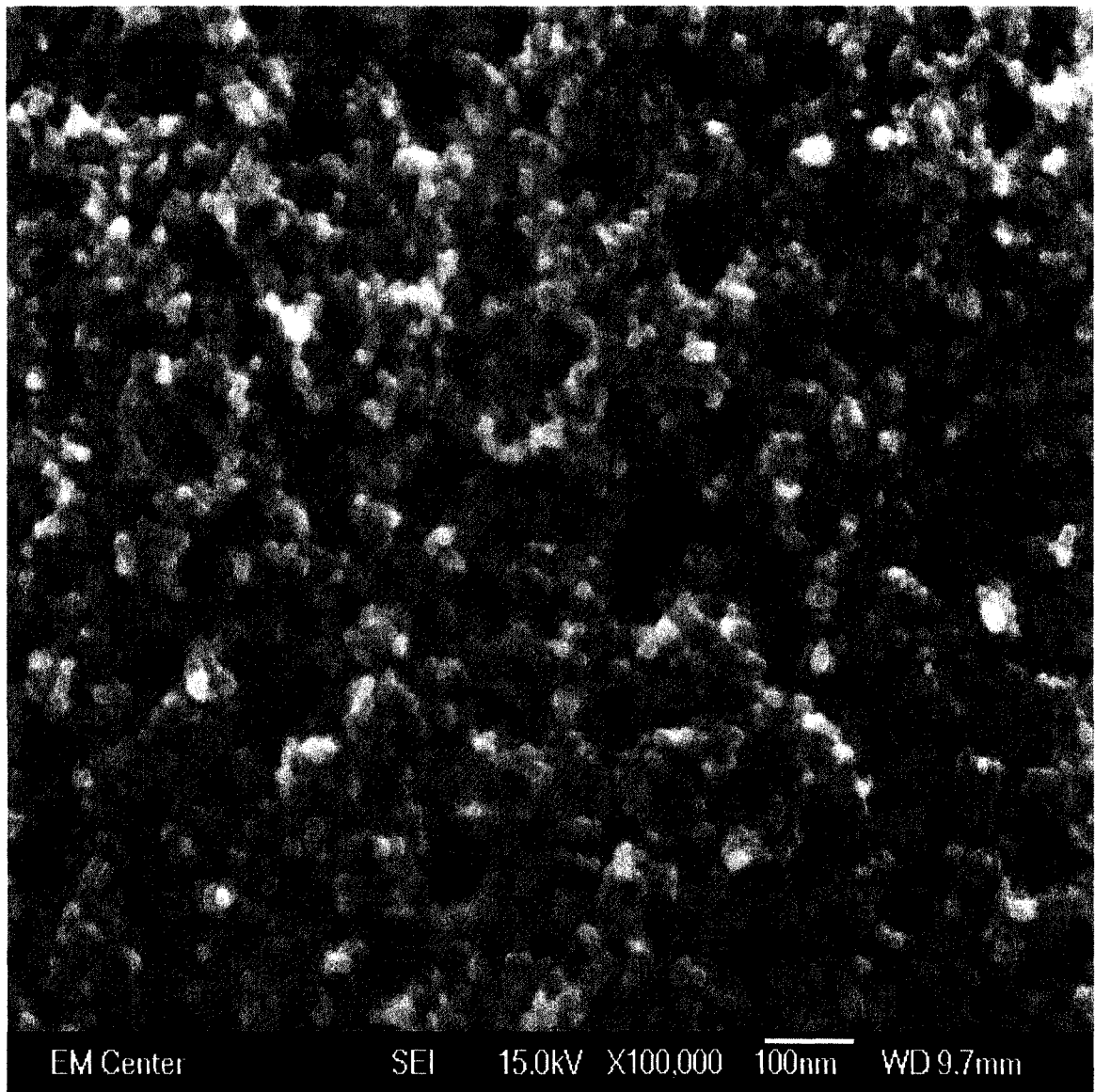


Figure 1. SEM image of mesoporous TiO₂ at 100,000x magnification.

The mesoporous TiO₂ is sensitized by immersing the electrode in a saturated dye solution for 12 to 18 hours to allow for dye adsorption. The huge surface area is what allows a monolayer of sensitizing dye to absorb an appreciable amount of sunlight for conversion to electricity.⁴ The dye that is typically employed as a sensitizer in DSSCs is *cis*-di(thiocyanato)-bis(2,2'-bipyridyl-4,4'-dicarboxylate)ruthenium(II), usually referred to as the N3 dye.¹⁴ The dye is chemi-adsorbed to the mesoporous TiO₂ semiconductor

via the carboxylate functions on the bipyridyl ligands. The structure of the N3 dye is shown in Figure 2.

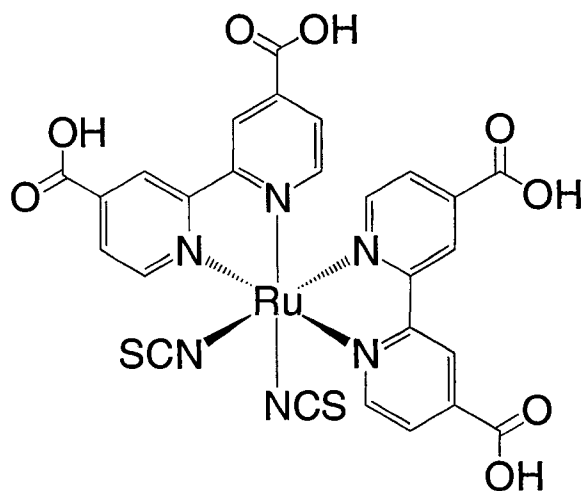


Figure 2. Structure of the N3 dye.

The cathode employed in typical DSSCs is a platinum electrode fabricated by depositing platinum as either a thin reflective layer, or dispersed as nanoparticles, onto a TCO substrate.¹⁵ As will be discussed in Chapters 3 and 4, other electrode materials may be used as cathodes in DSSCs. The function of the cathode is to reduce the electron transport redox couple that is present in the mediator solution.

If the mesoporous TiO_2 is the heart of the DSSC, the mediator solution is the blood. The mediator solution consists of a redox couple that is dissolved in a low viscosity, low vapor pressure solvent.¹⁶ The function of the redox mediator is to reduce the photo-oxidized dye and shuttle the resulting 'hole' (the oxidized form of the mediator) to the cathode. Typical DSSCs utilize the iodide/tri-iodide (I^-/I_3^-) redox couple due to the convergence of necessary kinetics (*vide infra*). Unfortunately, the I^-/I_3^- redox couple possesses some undesirable chemical properties that make it less than ideal for use in DSSCs.¹⁷ I_2 in equilibrium with I_3^- is volatile; most electrode materials do not efficiently catalyze reduction of I_3^- reduction, requiring that cathodes be constructed from

platinum-group metals; cell sealant must be impervious to oxidation by I_3^- ; I_3^- is darkly colored and absorbs visible light that could be absorbed by the sensitizing dye; and the redox potential of the I^-/I_3^- couple is more negative than optimum (for use with standard dyes, at least)—to name a few.¹⁸

1.3 Operational Principles of DSSCs

DSSCs are assembled by pressing the photoanode and cathode together in the so-called ‘sandwich cell’ configuration (Figure 3). The pores of the mesoporous semiconductor are then filled with mediator solution. For experiments discussed in this work, assembly stops there, however, for long-term studies, or production cells, the two electrodes are sealed together to prevent leakage or evaporation of the mediator solution.

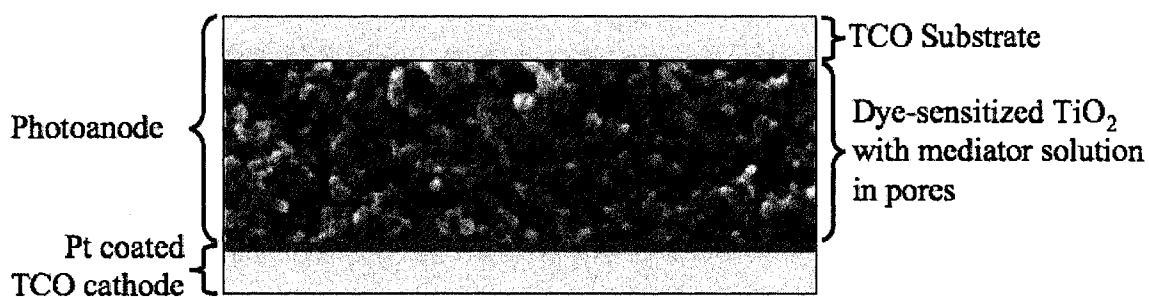


Figure 3. Diagram of DSSC. Dyed TiO₂ layer has been enlarged to show detail. Actual thicknesses of components: TCO substrate ca. 3 mm, Pt coated cathode ca. 3 mm, mesoporous TiO₂ layer ca. 4 μm.

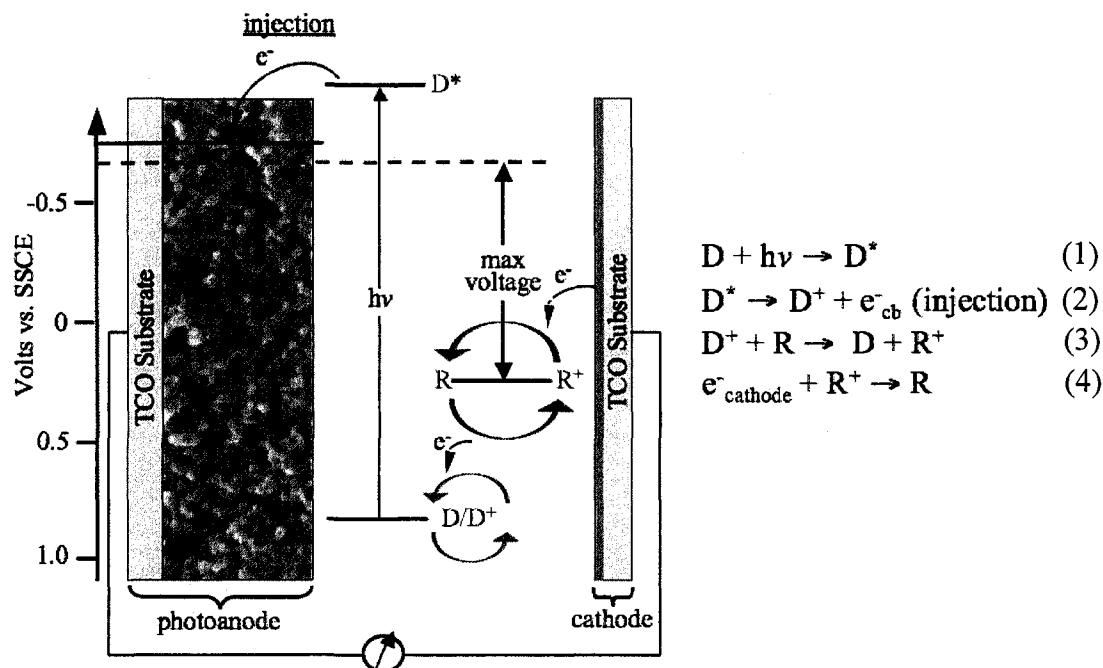


Figure 4. Schematic diagram of the current producing processes in a DSSC. The photoanode accepts electrons from the photoexcited dye (D^*) which is photo-oxidized during the injection process. The oxidized dye, in turn, oxidizes the mediator (R) and is returned to the ground state. The oxidized mediator is reduced at the cathode by the electrons that have flowed through the external circuit.

Current producing processes in a DSSC are described schematically in Figure 4.

Absorption of light by the N3 dye results in a metal-to-ligand charge transfer (MLCT) to ligand centered π^* orbitals (Figure 4, reaction 1). The chemi-adsorption of the dye generates excellent electronic coupling of the ligand π^* orbitals and the 3d orbital manifold of the TiO_2 conduction band. This results in electron injection which is very fast (picosecond or less timescale) from the dye to the semiconductor (Figure 4, reaction 2).¹⁹ Due to this excellent electronic coupling, dye excitation and electron injection, reactions 1 and 2 in Figure 4 occur essentially simultaneously.

The photo-oxidized dye is then reduced by the reduced form of the redox couple present in the mediator solution (Figure 4, reaction 3). Electrons that have been injected into the TiO_2 conduction band travel to the underlying TCO substrate via a diffusional

random walk pathway.²⁰ Once collected in the TCO substrate electrons can flow through an external circuit, creating an electrical current capable of doing useful work. Finally, the oxidized mediator diffuses to the cathode where it is reduced by electrons returning from the external circuit (Figure 4, reaction 4). The maximum theoretical voltage of a DSSC is given by the difference between the quasi-Fermi level of the TiO₂ under illumination, and the redox potential of the mediator system employed in the cell.¹²

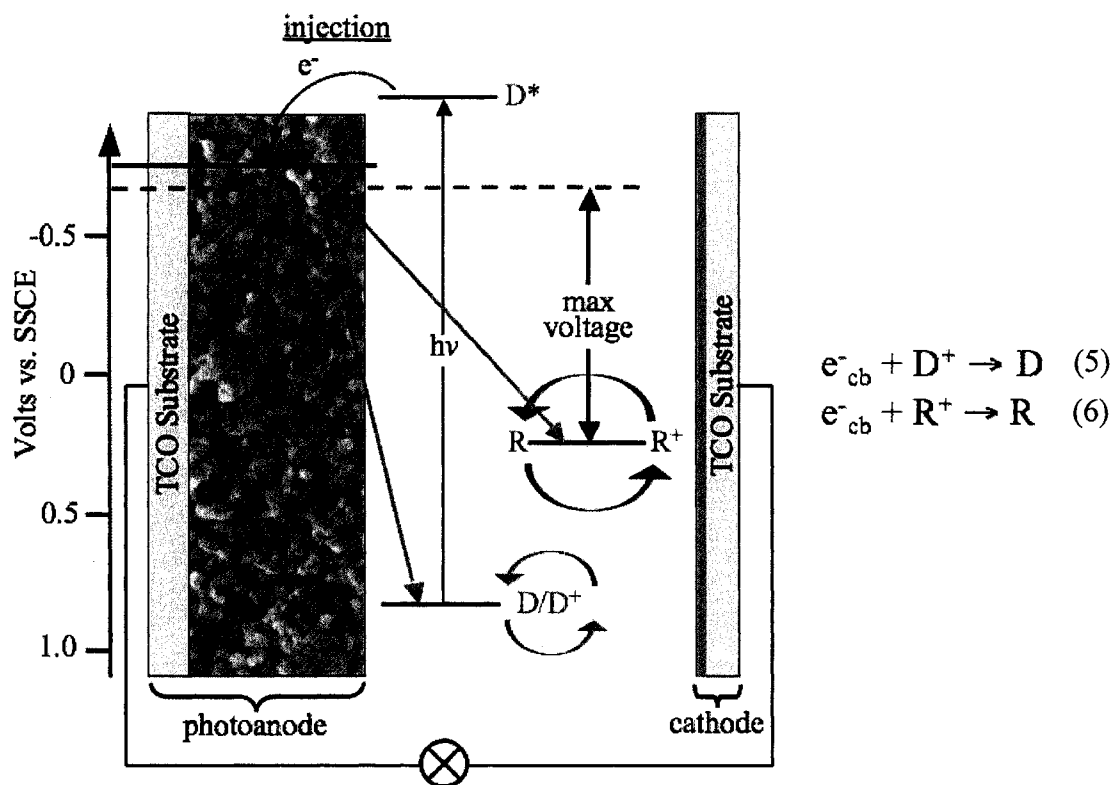


Figure 5. Schematic diagram of current inhibiting processes in a DSSC. Electrons that are injected into the semiconductor conduction band can recombine with the photo-oxidized dye, or reduce the oxidized form of the mediator at the photoanode.

There are electron transfer pathways that can reduce the overall current output of DSSCs. These processes are shown schematically in Figure 5. When the photo-excited dye injects an electron into the semiconductor conduction band there is the possibility that the injected electron will recombine with the photo-oxidized dye (Figure 5, reaction

5). The rate of this recombination reaction is slow since it requires electron transfer from the TiO_2 conduction band to ruthenium centered d orbitals, the two of which have poor electronic overlap.¹⁹ Another inhibiting reaction is reduction of the oxidized form of the mediator by the conduction band electron (Figure 5 reaction 6). The rate of this reaction is slow as well due to slow electron transfer between the mediator and metal oxide electrodes.¹⁷

As mentioned above, the I^-/I_3^- redox couple is the prevailing mediator system employed in DSSCs. This is the result of three kinetic qualities: (1) I^- rapidly reduces the photo-oxidized dye (Figure 4, reaction 3), (2) I_3^- is rapidly reduced at the cathode (Figure 4, reaction 4), and (3) I_3^- reduction on TiO_2 is slow (Figure 5, reaction 6). However, due to the numerous undesirable properties of the I^-/I_3^- mediator system there has been much research into finding alternative redox mediator systems for use in DSSCs.^{16, 21, 22} Previous work in the Elliott group has shown that certain polypyridyl complexes of cobalt function reasonably well as redox mediators in DSSCs.^{16, 18, 23} These cobalt mediators enjoy the benefit of not being corrosive to components of the cell, being less darkly colored so more incident sunlight is absorbed by the sensitizing dye, and allowing a greater choice of cathode materials. Most of the research presented in this body of work will deal with the investigation of the cobalt mediator complexes.

1.4 References

1. Bequerel, E., Recherches sur les effets de la radiation chimique de la lumiere solaire, au moyen des courants electriques. *Les Comptes rendus de l'Académie des sciences* **1839**, 9, 145-149.
2. Grätzel, M., Photoelectrochemical cells. *Nature* **2001**, 414, 338.
3. Chapin, D. M.; Fuller, C. S.; Pearson, G. L., A New Silicon P-N Junction Photocell for Converting Solar Radiation into Electrical Power. *Journal of Applied Physics* **1954**, 25, (5), 676-677.
4. Hagfeldt, A.; Grätzel, M., Molecular Photovoltaics. *Accounts of Chemical Research* **2000**, 33, 269-277.
5. Abboud, L., The Silicon Shake-Up. *Wall Street Journal* September 21, 2007, 2007.
6. West, W., First Hundred Years of Spectral Sensitization. *Photographic Science and Engineering* **1974**, 18, (1), 35-48.
7. Moser, J., Notiz uber die Verstarkung photoelectrischer Strome durch optische Sensibilisierung. *Monatshefte für Chemie* **1887**, 8, 373.
8. Namba, S.; Hishiki, Y., Color Sensitization of Zinc Oxide with Cyanine Dyes. *Journal of Physical Chemistry* **1965**, 69, (3), 774.
9. Dare-Edwards, M. P.; Goodenough, J. B.; Hamnett, A.; Seddon, K. R.; Wright, R. D., Sensitization of Semiconducting Electrodes with Ruthenium-Based Dyes. *Faraday Discussions* **1980**, 285-298.
10. Hamnett, A.; Dare-Edwards, M. P.; Wright, R. D.; Seddon, K. R.; Goodenough, J. B., Photosensitization of Titanium(IV) Oxide with Tris(2,2'-Bipyridine)Ruthenium(II) Chloride - Surface-States of Titanium(IV) Oxide. *Journal of Physical Chemistry* **1979**, 83, (25), 3280-3290.
11. Anderson, S.; Constable, E. C.; Dare-Edwards, M. P.; Goodenough, J. B.; Hamnett, A.; Seddon, K. R.; Wright, R. D., Chemical Modification of a Titanium(IV) Oxide Electrode to Give Stable Dye Sensitization without a Supersensitizer. *Nature* **1979**, 280, (5723), 571-573.
12. Oregan, B.; Grätzel, M., A Low-Cost, High-Efficiency Solar-Cell Based on Dye-Sensitized Colloidal TiO₂ Films. *Nature* **1991**, 353, (6346), 737-740.

13. Bisquert, J.; Cahen, D.; Hodes, G.; Rühle, S.; Zaban, A., Physical Chemical Principles of Photovoltaic Conversion with Nanoparticulate, Mesoporous Dye-Sensitized Solar Cells. *Journal of Physical Chemistry B* **2004**, 108, 8106-8118.
14. Nazeeruddin, M. K.; Kay, A.; Rodicio, I.; Humphry-Baker, R.; Mueller, E.; Liska, P.; Vlachopoulos, N.; Grätzel, M., Conversion of light to electricity by *cis*-X₂bis(2,2'-bipyridyl-4,4'-dicarboxylate)ruthenium(II) charge-transfer sensitizers (X = Cl⁻, Br⁻, I⁻, CN⁻, and SCN⁻) on nanocrystalline titanium dioxide electrodes. *Journal of the American Chemical Society* **1993**, 115, (14), 6382-90.
15. Papageorgiou, N., Counter-electrode function in nanocrystalline photoelectrochemical cell configurations. *Coordination Chemistry Reviews* **2004**, 248, 1421-1446.
16. Sapp, S. A.; Elliott, C. M.; Contado, C.; Caramori, S.; Bignozzi, C. A., Substituted Polypyridine Complexes of Cobalt(II/III) as Efficient Electron-Transfer Mediators in Dye-Sensitized Solar Cells. *Journal of the American Chemical Society* **2002**, 124, (37), 11215-11222.
17. Gregg, B. A.; Pichot, F.; Ferrere, S.; Fields, C. L., Interfacial Recombination Processes in Dye-Sensitized Solar Cells and Methods To Passivate the Interfaces. *Journal of Physical Chemistry B* **2001**, 105, 1422-1429.
18. Scott, M. J.; Nelson, J. J.; Caramori, S.; Bignozzi, C. A.; Elliott, C. M., *cis*-Dichloro-bis(4,4'-dicarboxy-2,2'-bipyridine)osmium(II)-Modified Optically Transparent Electrodes: Application as Cathodes in Stacked Dye Sensitized Solar Cells. *Inorganic Chemistry* **2007**, 46, (24), 10071-10078.
19. Hagfeldt, A.; Grätzel, M., Light-Induced Redox Reactions in Nanocrystalline Systems. *Chemical Reviews* **1995**, 95, (1), 49-68.
20. Nelson, J.; Chandler, R. E., Random walk models of charge transfer and transport in dye sensitized systems. *Coordination Chemistry Reviews* **2004**, 248, (13-14), 1181-1194.
21. Nusbaumer, H.; Moser, J.-E.; Zakeeruddin, S. M.; Nazeeruddin, M. K.; Grätzel, M., Co^{II}(dbbip)₂²⁺ Complex Rivals Tri-iodide/Iodide Redox Mediator in Dye-Sensitized Photovoltaic Cells. *Journal of Physical Chemistry B* **2001**, 105, 10461-10464.
22. Oskam, G.; Bergeron, B. V.; Meyer, G. J.; Searson, P. C., Pseudohalogens for Dye-Sensitized TiO₂ Photoelectrochemical Cells. *Journal of Physical Chemistry B* **2001**, 105, 6867-6873.

23. Elliott, C. M.; Caramori, S.; Bigozzi, C. A., Indium tin oxide electrodes modified with tris(2,2'-bipyridine-4,4'-dicarboxylic acid) iron(II) and the catalytic oxidation of tris(4,4'-di-*tert*-butyl-2,2'-bipyridine) cobalt(II). *Langmuir* **2005**, 21, (7), 3022-3027.

CHAPTER 2

EXPERIMENTAL METHODS

This dissertation chapter is divided into three parts: The first part describes all of the materials used in this dissertation. The second part describes preparation of all electrodes/samples used in this dissertation. The third part describes all of the experimental techniques used to collect the data discussed in this dissertation. All LabView Virtual Instruments were written by Jeremy Nelson.

2.1 MATERIALS

Titanium(IV) isopropoxide (97%) was obtained from Aldrich and purified by vacuum distillation.

Concentrated nitric acid (ACS grade) was obtained from Mallinckrodt and used as received.

Concentrated hydrochloric acid (ACS grade) was obtained from EMD Chemicals and used as received

Poly(ethylene glycol) (MW = 2000) was obtained from Aldrich and used without further purification.

Titanium(IV) chloride (97%) (TiCl₄) was obtained from Acros and stored in a N₂ atmosphere glove box. The TiCl₄ was purified by running through several short alumina columns until colorless in N₂ atmosphere.

Titanium dioxide colloid (TiO₂) was either obtained from Solaronix SA and used as received, or synthesized using a modified literature procedure.¹ Briefly, titanium(IV) isopropoxide was added dropwise to an aqueous, dilute (ca. 75 mM) nitric acid solution. A milky white precipitate formed and the solution was heated at 80 °C for ca. 8 hours. During the heating process the volume was carefully reduced to ca. 1/3 the starting

volume. The solution was transferred to a high-pressure reaction vessel (bomb) with a Teflon® liner and placed in an oven at 220 °C for 12 hours. Upon cooling the sol-gel was transferred to a beaker and 40 weight percent poly(ethylene glycol) was added. After stirring for an additional 8 hours the colloid solution was transferred to a scintillation vial for storage.

Nitrosonium tetrafluoroborate (99%) (NOBF₄) was obtained from Aldrich and stored in the dark in a refrigerator. The bottle was transferred to a N₂ atmosphere glove box before being opened. After weighing out the desired amount of NOBF₄ the bottle was closed, removed from the glove box, and placed back in the refrigerator.

4-*tert*-butylpyridine (99%) was obtained from Aldrich and used without further purification.

Lithium trifluoromethanesulfonate (99%) (lithium triflate) was obtained from Aldrich and used without further purification.

γ-butyrolactone (99%) (γBL) was obtained from Aldrich and used without further purification.

***cis*-di(thiocyanato)-bis(2,2'-bipyridyl-4,4'-dicarboxylate)ruthenium(II) (N3 dye)** was synthesized by Professor Elliott using a modified literature procedure.¹

3-(carboxymethyl)-2-((1*E*,3*E*,5*Z*)-5-(3-(carboxymethyl)benzo[*d*]thiazol-2(3*H*)-ylidene)penta-1,3-dienyl)benzo[*d*]thiazol-3-ium bromide (R8 dye) was obtained from Professor Bruce A. Parkinson's laboratory.

Photoresist AZ 1512 was obtained from Kodak and stored in the dark in a refrigerator. The photoresist was used as received.

Zinc powder (6-9 μm particle size, 97.5%) was obtained from Alfa Aesar and used as received.

Fluorine doped tin oxide (FTO) and indium doped tin oxide (ITO) conducting glass (collectively TCO) were obtained from Delta Technologies and vigorously cleaned before use. For preparation of photoanodes, FTO glass was soaked in a saturated KOH in isopropanol base bath for at least 30 minutes. The FTO glass was then rinsed with tap water, de-ionized water, and 95% ethanol before drying in a N_2 stream. For modification of TCO electrodes, FTO and ITO glass were soaked in a saturated KOH rinsed and dried as above. After the base bath the TCO glass was sonicated in a solution of Alconox ® in de-ionized water for 15 minutes, rinsed with de-ionized water and dried in a N_2 stream. Next the TCO glass was sonicated in neat isopropanol for 15 minutes, rinsed with isopropanol, and dried in a N_2 stream. Finally, the TCO glass was placed in an air plasma for 45 minutes.

Diammonium hexachloroosmate(IV) (99%) was obtained from Acros and used without further purification.

2,2'-bipyridyl-4,4'-dicarboxylic acid (DCB) was prepared according to a previously published procedure.²

cis-dichloro-bis(2,2'-bipyridyl-4,4'-dicarboxylic acid)osmium(II) (Os(DCB)₂Cl₂) was synthesized using a modified literature procedure.³ Briefly, one equivalent (60 mg) of diammonium hexachloroosmate(IV) was suspended in ca. 50 mL of N,N-dimethyl formamide (DMF) yielding a purple-brown solution. Two equivalents (100 mg) of 2,2'-bipyridyl-4,4'-dicarboxylic acid was added and the solution turned yellow as the reaction approached reflux. The reaction was allowed to reflux overnight yielding a deep violet solution. The DMF was removed by rotary evaporation, followed by the addition of 50 mL of 2M HCl, resulting in the formation of a violet precipitate. The solution was filtered and the Os(DCB)₂Cl₂ was used without further purification (73 mg, 72% yield).

Cobalt(II) perchlorate hexahydrate (Co(ClO₄)₂•6H₂O) was obtained from GFS Chemicals and used without further purification.

2,2'-bipyridyl-4,4'-di-*tert*-butyl (DTB) was obtained from Aldrich and used without further purification.

2,2'-bipyridyl-4,4'-di-tert-butoxyester- (DTBEST) was prepared according to a previously published procedure.⁴

2,2'-bipyridyl-4,4'-bis(di-n-butylamide) (DBA) was prepared according to a previously published procedure.⁴

2,2'-bipyridyl-4,4'-diisopropyl (DIP) was prepared by refluxing 4-isopropylpyridine in the presence of palladium on activated carbon for several days. The reaction mixture was allowed to cool to room temperature before the solids were filtered and washed with CH₂Cl₂. Unreacted 4-isopropylpyridine was removed by vacuum distillation resulting in an oily viscous liquid that was subjected to column chromatography using silica gel. The product containing fractions were combined and the solvent was removed *en vacuo* resulting in a white crystalline powder.

H NMR (300 MHz, CDCl₃) δ ppm: 1.20 (12H, d, 6x isopropyl CH₃), 2.87 (2H, h, 2x isopropyl H), 7.19 (2H, d, 2x H5), 8.42 (2H, d, 2x H6), 8.92 (2H, s, 2x H3).

[Co(L)₃](ClO₄)₂ (L = any one of bipyridyl ligands above) were prepared as previously reported.⁴ Briefly, three equivalents of the bipyridyl ligand and one equivalent of cobalt(II) perchlorate hexahydrate were added to a round bottom flask containing methanol. The reaction mixture was allowed to reflux for several hours to ensure completion of the reaction. After cooling the volume of solvent was reduced by ca. 80% *en vacuo*. Addition of excess diethyl ether caused precipitation of the cobalt complex product as a yellow to brown solid, depending on the bipyridyl ligand used, which was

filtered and dried in a vacuum oven. The resulting cobalt complexes were used without further purification

Mediator solutions for cell evaluation (current-voltage) experiments were prepared as 0.15 M $[\text{Co}(\text{L})_3](\text{ClO}_4)_2$, 0.015 M nitrosonium tetrafluoroborate, 0.2 M 4-*tert*-butylpyridine, and 0.2 M lithium trifluoromethanesulfonate in γBL . Addition of NOBF_4 stoichiometrically oxidized the $\text{Co}(\text{L})_3^{2+}$ to $\text{Co}(\text{L})_3^{3+}$ resulting in a 10% oxidized mediator solution. When present, the concentration of PTZ moieties was 0.05 M. γBL was chosen for its low vapor pressure and relatively low viscosity.

Mediator solutions for transient laser spectroscopy experiments were prepared as above with the exclusion of NOBF_4 .

10-Methylphenothiazine (N-MePTZ) was obtained from Aldrich and recrystallized three times from 10:1 toluene-hexanes yielding a colorless crystalline solid.⁶

Lithium 4-(10*H*-phenothiazin-10-yl)butane-1-sulfonate (LiPTZ4S) was prepared according to a previously published procedure.⁷

***N,N,N*-trimethyl-3-(10*H*-phenothiazin-10-yl)propan-1-aminium**

hexafluorophosphate (PTZ3QPF₆) was prepared according to a previously published procedure.⁷

2.2 Electrode Preparation

Photoanodes – Deposition of TiO₂

A rectangular piece of FTO glass was scored (dashed lines in Figure 1) on the non-conducting side to provide individual electrodes that were ca. 1.2 cm x 2.5 cm which were later broken apart. Sacrificial space on the long edges facilitated breaking individual electrodes from the full piece. After scoring, the FTO conducting

glass was thoroughly cleaned by soaking in a saturated KOH in isopropanol base bath for a minimum of 30 minutes. After removal from the base bath the glass was rinsed successively with tap water, de-ionized water, and 95% ethanol before drying in a nitrogen stream.

The 3 cm x 5 cm FTO glass plank was held to the bench top by a piece of Scotch[®] tape (gray in figure). The tape not only held the FTO glass blank in place, but also provided a spacer (ca. 70 μm) for deposition of TiO₂. Alternatively, thinner layers of TiO₂ were deposited using a custom made rig where stretched Parafilm[®] was the spacer.

The rig was constructed by taking a piece of Parafilm[®] (6 cm wide by 2 cm long) and sandwiching each 6 cm end between 2 microscope slides (4 slides total) with Super Glue[®] so there was ca. 0.5 cm separating the slide/Parafilm[®] sandwiches (Figure 2a). After the glue had dried the Parafilm[®] was carefully and evenly stretched to 8 times its original length (ca. 4 cm separating slide/Parafilm[®] sandwiches, Figure 2b). Stabilizing slides were glued in place to maintain the ca. 4 cm separation. After the glue had completely dried and the frame was rigid, 2.5 cm of the stretched Parafilm[®] was

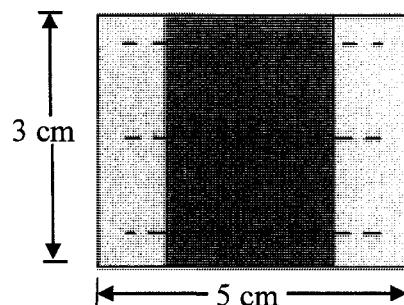


Figure 1. Layout of FTO glass for typical fabrication of photo-anodes. Dashed lines represent edges of individual photo-anodes. Gray area represents scotch tape or stretched Parafilm. Blue area represents deposited TiO₂.

removed from the middle of the frame, leaving two thin strips of stretched Parafilm® (ca. 30 μm thick) on either side that functioned as spacers (Figure 2c). For TiO_2 deposition the rig was then pressed down on the FTO glass blank.

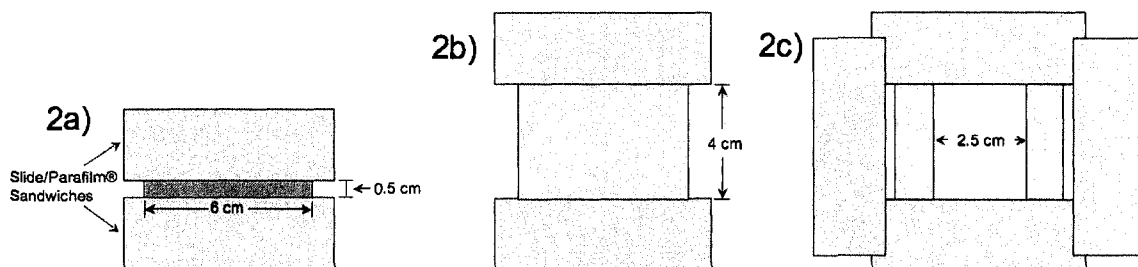


Figure 2. Parafilm® rig before stretching (2a), after stretching (2b), with middle of Parafilm® removed and stabilizing slides glued in place (2c).

Titania layers attained using a single strip of tape as a spacer were termed “one-scotch” layers and titania layers attained using the stretched Parafilm® rig were termed “half-scotch” layers. The thickness of deposited TiO_2 layers was determined with a Datatek Profilometer. Half-scotch layers were $2.4(\pm 0.1)$ μm thick, and one-scotch layers were $4.4(\pm 0.1)$ μm thick.

Mesoporous TiO_2 layers were deposited using the Doctor Blade technique.⁸ The FTO glass blanks, held down either by tape or the custom rig (*vide supra*), had a bead of TiO_2 colloidal paste applied at one end, between the spacers on each side (Figure 3). This bead was then spread with a smooth stroke of a glass rod.

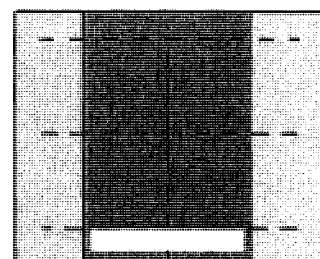


Figure 3. FTO glass blank with spacers (gray) and bead of colloidal TiO_2 (thick white line).

When depositing half-scotch layers with the stretched Parafilm rig a custom made hook shaped glass rod was used to spread the colloidal paste. Care must be exercised when spreading the TiO_2 as the thin layer of colloid dries quickly and repeated passes with the glass rod results in a very uneven layer. After the applied TiO_2 layer dried in air, the coated glass was baked at

450 °C for one hour to sinter the TiO₂ nanoparticles together and ensure electrical conductivity.⁸

Photoanodes – TiCl₄ Treatment

An additional step in photoanode preparation, which has been shown to improve DSSC performance, is the so-called TiCl₄ treatment.^{1,9} After the TiO₂ layer had been applied, baked, and cooled to room temperature, the individual photoanodes were broken from the FTO glass blank. A 0.2 M aqueous solution of TiCl₄ was applied to the TiO₂ layer (ca. 100 μL with a syringe) and left overnight in a high humidity chamber.¹ After being rinsed with de-ionized water and dried in a nitrogen stream, the photoanode was re-fired at 450 °C for one hour. This TiCl₄ treatment was used in all photoanodes and pseudo-photoanodes discussed in this work.

Pseudo-photoanodes

Transient absorption spectroscopy experiments were completed on pseudo-photoanodes that were prepared using the same method as “one-scotch” photoanodes (*vide supra*). The only exceptions were that non-conducting glass was used in the form of microscope slides, the area of TiO₂ on each slide was ca. 2 cm², and one microscope slide constituted one sample.¹¹

Photoanodes – Dye-Sensitization

Dye-sensitization was accomplished by soaking the photoanodes (or pseudo-photoanodes) in a saturated dye solution in dry ethanol. The N3 dye chemisorbs to the

TiO₂ through the carboxylate functions of the bipyridyl ligands. This results in excellent orbital overlap of the ligand π^* orbitals and the 3d orbital manifold of the TiO₂ conduction band.¹⁰

After the TiO₂ layer was applied and baked, the individual photoanodes were broken apart and placed in the dye solution while they were still hot (ca. 100 °C). This ensured that water would not adsorb to the mesoporous TiO₂ and occupy dye adsorption sites. The photoanodes were left in the dye solution for 12-18 hours, while stored in the dark. The dye-sensitized photoanodes were rinsed with ethanol to remove any excess dye, and dried in a nitrogen stream. For best results, dye-sensitized photoanodes were used immediately.

Gold-plated Cathodes

Gold electrodes used as DSSC cathodes and as stock for patterned electrodes (*vide infra*) were prepared by depositing 15 nm of chromium, followed by 200 nm of gold, onto FTO glass in a vacuum deposition chamber.

Glassy Carbon Cathode

A Type 2 Glassy carbon electrode was purchased from Alfa Aesar and cut into 1 cm x 2 cm pieces. The surface of the glassy carbon electrode was roughened with 600 grit Emory paper prior to use in a DSSC.

Patterned Electrodes

To attain patterned electrodes each of the same shape and area, 1 cm x 2 cm rectangles of the gold-plated FTO (*vide supra*), bare FTO, and bare ITO were vigorously cleaned by soaking in a saturated KOH base bath for a minimum of 30 minutes. A layer of Photoresist AZ 1512 was deposited by spin coating at 2500 rpm. The photoresist was cured in a 90 °C oven for 20 minutes. After curing, opaque masks of the desired area were placed over the electrodes before exposing them to UV light for two minutes. The UV exposed photoresist was removed by immersing the electrode in 0.5% NaOH for 30 to 60 seconds. The unexposed photoresist remains intact, protecting the underlying conductive substrate. For the patterned ITO electrodes, the layer of ITO not covered by photoresist was removed by immersing the electrode in a dilute aqua regia solution (45% HCl, 5% HNO₃, 50% de-ionized H₂O) for 15 to 20 minutes.¹² For the patterned FTO electrodes, a slurry of zinc powder (6-9 μm) in de-ionized water was spread on the FTO coated glass. This was then immersed in concentrated HCl for 20 to 30 seconds. The solution bubbled vigorously as H₂ was produced reducing the tin(IV) to tin metal, which dissolved in the acid. For the patterned gold electrodes, the gold layer was removed in the dilute aqua regia solution before the FTO layer was removed by the Zn/HCl reaction. To ensure that the conducting layer had been completely removed, the resistance was measured with a digital multi-meter. When the two probe resistance measured between points separated by ca. 0.5 cm was greater than 20 MΩ the removal was considered complete and the protective photoresist was rinsed off with acetone.

Transparent Cathodes

Transparent conducting oxide electrodes modified with $\text{Os}(\text{DCB})_2\text{Cl}_2$ were prepared by first soaking TCO electrodes in a KOH base bath for 20 minutes. The electrodes were rinsed with tap water, de-ionized water, and 95% ethanol before drying under a nitrogen stream. The electrodes were then placed in a solution of Alconox[®] in de-ionized water in an ultrasonic cleaner for 15 minutes, rinsed, dried, and then sonicated in electronics grade isopropanol for 15 minutes. Following this treatment, the dried electrodes were transferred to a plasma cleaner and exposed to an air plasma for 45 minutes.¹³ A monolayer of a $\text{Os}(\text{DCB})_2\text{Cl}_2$ was adsorbed onto the TCO surface by soaking the electrode overnight in a saturated dry-ethanol solution of $\text{Os}(\text{DCB})_2\text{Cl}_2$. The $\text{Os}(\text{DCB})_2\text{Cl}_2$ modified electrodes were then rinsed with dry ethanol and dried under a nitrogen stream.

2.3 Experimental Techniques

Cell performance evaluation

Cell performance was evaluated by assembling a DSSC and measuring its current output when exposed to simulated sunlight. The photoanode and cathode were clamped together in a custom cell holder with a 0.4 cm^2 optical aperture. The clamps were tightened to 14 mN m with a torque driver (Precision Instruments) unless otherwise stated (cf. Chapter 5). Redox mediator solution (ca. 10 μL) was introduced to the interface of the photoanode and cathode with a Pasteur pipette and capillary forces pulled the solution into the spaces of the mesoporous semiconductor. Electrical leads were connected and the cell was illuminated with a 100 W xenon arc lamp calibrated to 100

mW cm^{-2} with a Molectron PowerMax 500A power meter. A 400 nm cutoff filter was placed between the lamp and the cell to prevent direct excitation of the TiO_2 semiconductor. Output current was measured by a Keithley Sourcemeter run by a LabView virtual instrument while the potential was scanned from 700 mV to -100 mV at 50 mV s^{-1} . The resulting current-voltage curves were assessed on the basis of open circuit voltage (V_{oc}), short circuit current density (J_{sc}), fill factor (FF), and efficiency (η) (determined by dividing the power at the maximum power point by the incident light power, 100 mW cm^{-2}). Dye-sensitized solar cells used in cell performance evaluation experiments consisted of photoanodes that were fabricated by depositing thin layers of TiO_2 on FTO conducting glass. The cathodes were either gold coated FTO glass (*vide supra*), catalyst-modified FTO (cf. Chapter 4), or roughened glassy carbon (*vide supra*).

UV-Vis Spectroscopy

To compare the light absorbing ability of the dyed TiO_2 layers, UV-Vis spectra were recorded with a HP 8452A diode array spectrometer. The dyed photoanodes were held to the instrument sample holder with double-sided tape. A clean piece of FTO substrate was used as a blank and several positions on the photoanode were averaged for each spectrum.

Incident Photon to Current Conversion Efficiency

Photoaction spectra, incident photon to current conversion efficiency (IPCE) versus wavelength, were acquired by assembling a DSSC (*vide supra*) in the path of a 75 W tungsten lamp coupled to a Jarrel Ashe 0.25 m monochromator. The wavelength was

scanned from 800 to 400 nm while the short circuit current was recorded by PAR 174 polarographic analyzer linked to a computerized control and data acquisition system.¹⁴

Electrochemistry

Cyclic voltammetry (CV) was used to ascertain the stability of the cobalt complex mediator solutions with time (Chapter 3), to determine the electrode material dependence of the cobalt mediator solutions (Chapter 3), to compare the osmium modified and gold electrodes' ability to catalyze the reduction of $\text{Co}(\text{DTB})_3^{3+}$ (Chapter 4), and to determine the catalytic efficiency of phenothiazine mediator additives (Chapter 6). A standard three-electrode cell was used with a BAS 100B Potentiostat-Galvanostat run by BAS 100W software on a personal computer. All cyclic voltammograms were recorded using tetramethylammonium perchlorate (0.1 M in γBL) as the supporting electrolyte, a sodium saturated calomel electrode (SSCE) reference, and a large area platinum counter electrode. Electrochemical data are reported relative to the ferrocene/ferrocinium redox couple.

For mediator-solution stability experiments in Chapter 3, the working electrode was glassy carbon (GC, area = 0.07 cm²). Mediator solutions of each of the three cobalt complexes investigated were prepared in γBL in four varieties:

- 1) 0.15 M $[\text{Co}(\text{L})_3](\text{ClO}_4)_2$.
- 2) 0.15 M $[\text{Co}(\text{L})_3](\text{ClO}_4)_2$ and 0.2 M lithium triflate.
- 3) 0.15 M $[\text{Co}(\text{L})_3](\text{ClO}_4)_2$ and 0.2 M 4-*tert*-butylpyridine.
- 4) 0.15 M $[\text{Co}(\text{L})_3](\text{ClO}_4)_2$, 0.2 M lithium triflate, and 0.2 M 4-*tert*-butylpyridine.

A 100 μL aliquot of each of these solutions was diluted with the supporting electrolyte solution (0.1 M tetramethylammonium perchlorate in γBL) to a final volume of 5 mL. This resulted in concentrations of 3 mM $[\text{Co}(\text{L})_3](\text{ClO}_4)_2$, 4 mM lithium triflate, and 4 mM 4-*tert*-butylpyridine. CV experiments were performed on the solutions immediately after they were prepared. For CV experiments with the $[\text{Co}(\text{DTB})_3](\text{ClO}_4)_2$ mediator solutions, the potential window was -200 mV to 500 mV at a scan rate of 50 mV/s. For CV experiments with the $[\text{Co}(\text{DTBEST})_3](\text{ClO}_4)_2$ mediator solutions the potential window was -200 mV to 1200 mV at a scan rate of 50 mV/s. For CV experiments with the $[\text{Co}(\text{DBA})_3](\text{ClO}_4)_2$ mediator solutions the potential window was -200 mV to 1300 mV at a scan rate of 50 mV/s. After storage in scintillation vials for one week, a new 100 μL aliquot of the concentrated mediator solutions was diluted to 5 mL with electrolyte solution and the CV experiments were repeated. The potential window for the $[\text{Co}(\text{DTB})_3](\text{ClO}_4)_2$ mediator solutions was increased to -200 mV to 1200 mV.

For electrode dependence experiments in Chapter 3, the working electrode was either gold (Au, area = 0.007 cm^2), platinum (Pt, area = 0.007 cm^2), glassy carbon (GC, area = 0.07 cm^2), FTO modified by adsorption of *cis*-dichloro-bis(2,2'-bipyridyl-4,4'-dicarboxylate)osmium(II) (OsFTO, cf. Chapter 4, area = 0.5 cm^2), or unmodified FTO (area = 0.5 cm^2) as indicated. Cyclic voltammograms were recorded using solutions prepared and diluted as described in the stability experiments (*vide supra*).

For working electrode comparisons in Chapter 4 the electrodes were all 0.5 cm^2 and either ITO, FTO, (unmodified or osmium modified as indicated), or gold. Voltammograms were recorded with a potential window of -200 mV to 400 mV and a scan rate of 50 mV/s.

For catalytic efficiency experiments in Chapter 6 the working electrode was unmodified FTO (area = 0.5 cm²). CVs were recorded with a potential window of 0 mV to 1200 mV at a scan rate 50 mV/s. After obtaining a background CV of the electrolyte solution, LiPTZ4S was added to a concentration of 0.05 mM and a CV was recorded. Subsequent CVs were recorded after adding [Co(L)₃](ClO₄)₂ to concentrations of 0.5 mM, 1.0 mM, 2.5 mM, and 5.0 mM, respectively.

Three-dimensional Current Imaging

Instrumentation developed in Professor Bruce A. Parkinson's research laboratory was employed to obtain three-dimensional current images.¹⁵ An assembled DSSC was mounted in the cell holder (*vide supra*) and connected in a two-electrode configuration to a Princeton Applied Research 174A Potentiostat held at short circuit. The cell was illuminated by a frequency doubled Nd:YAG laser (532 nm) that had a beam diameter of ca. 1 mm and power of ca. 80 mW cm². The beam was rastered by a Labview virtual instrument that applied stepwise voltages to a two-mirror galvanometer. The resulting photocurrent of the cell was recorded at each step of the laser beam by the same Labview virtual instrument¹⁵ producing a two dimensional current image of the cell. Results are presented as 3D plots where the surface of the cell is in the xy plane and the current is plotted in the z dimension (cf. chapter 5 figure).

Thin Film Transient Laser Spectroscopy

Pseudo-photoanodes, samples of dyed TiO₂ films deposited on non-conducting microscope slides (*vide supra*) were investigated using a modified pump-probe laser

setup. Because the samples were thin films, the typical perpendicular alignment of the pump and probe beams was unsuited. For this reason, the pump beam was brought to the sample coincident with the probe beam at an angle of ca. 5 degrees. The 532 nm pump beam was provided by an optical parametric oscillator (Opotek) and was defocused to a diameter of ca. 1 cm. The probe beam was provided by a 100 W xenon arc lamp (Oriel) and the thin film sample was placed past the focal point where the probe beam diameter was ca. 1 cm, overlapping the area excited by the pump beam. To prevent direct excitation of the TiO_2 by the UV portion of the probe beam, a 450 nm cutoff filter was placed between the lamp and the sample. After passing through the thin film sample the probe beam was focused onto the entrance slit of a Jarrell Ash model 84-210 monochromator set to 480 nm and detected using a Hamamatsu R2496 fast photomultiplier connected to a Tektronix oscilloscope. Scatter from the excitation beam was filtered with a bandpass filter. Data acquisition was accomplished with a Labview virtual instrument. A diagram of the laser setup is shown in Figure 3.

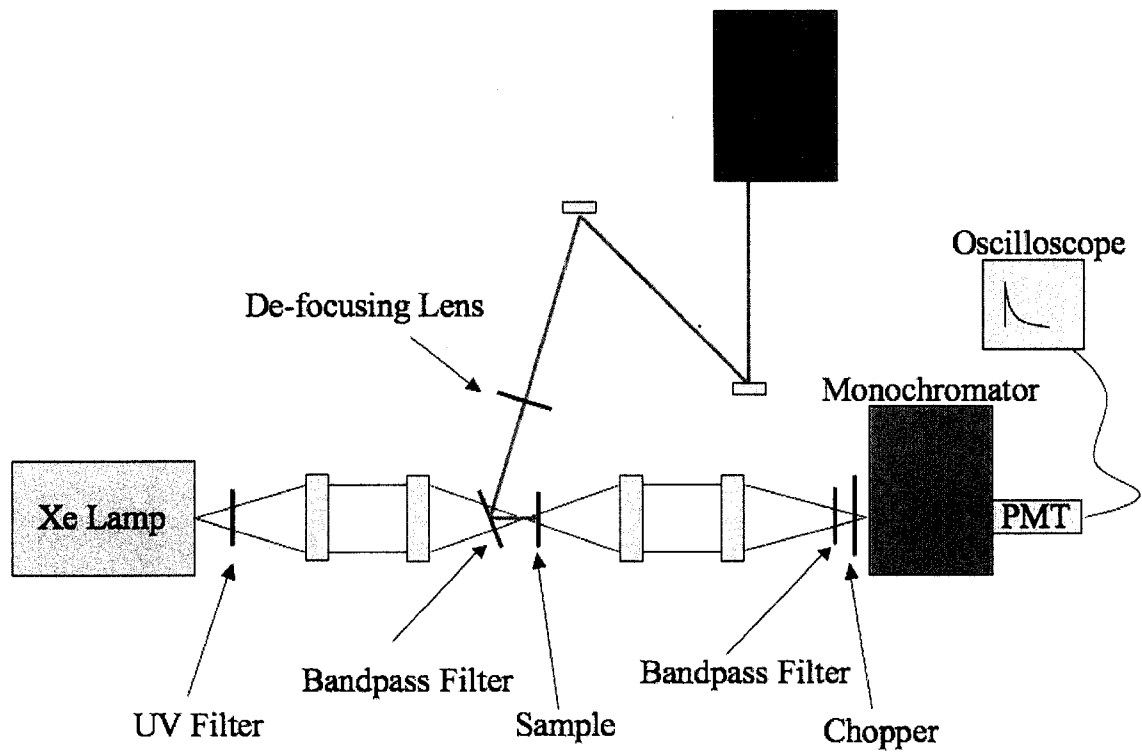


Figure 3. Schematic diagram of laser setup for thin-film transient absorption experiments. Excitation beam (532 nm) is shown in green.

2.4 References

1. Nazeeruddin, M. K.; Kay, A.; Rodicio, I.; Humphry-Baker, R.; Mueller, E.; Liska, P.; Vlachopoulos, N.; Graetzel, M., Conversion of light to electricity by *cis*-X₂bis(2,2'-bipyridyl-4,4'-dicarboxylate)ruthenium(II) charge-transfer sensitizers (X = Cl⁻, Br⁻, I⁻, CN⁻, and SCN⁻) on nanocrystalline titanium dioxide electrodes. *Journal of the American Chemical Society* **1993**, 115, (14), 6382-90.
2. Nazeeruddin, K.; Kalyanasundaram, K.; Graetzel, M., A One-Pot Synthesis of Tetrahydronium tris(4,4'-dicarboxylato-2,2'-bipyridine)-Ruthenium(II) Dihydrate. In *Inorganic Syntheses*, 1998; Vol. 32, pp 181-186.
3. Buckingham, D. A.; Dwyer, F. P.; Goodwin, H. A.; Sargeson, A. M., Mono- and bis-(2,2'-bipyridine) and (1,10-phenanthroline) chelates of Ruthenium and Osmium IV. Bis chelates of bivalent and trivalent Osmium. *Australian Journal of Chemistry* **1964**, 17, (3), 325-336.
4. Sapp, S. A.; Elliott, C. M.; Contado, C.; Caramori, S.; Bignozzi, C. A., Substituted Polypyridine Complexes of Cobalt(II/III) as Efficient Electron-Transfer Mediators in Dye-Sensitized Solar Cells. *Journal of the American Chemical Society* **2002**, 124, (37), 11215-11222.
5. Sasse, W. H.; Whittle, C. P., Synthetical Applications of Activated Metal Catalysts .12. Preparation of Symmetrically Substituted 2,2'-Bipyridyls. *Journal of the Chemical Society* **1961**, (83), 1347.
6. Rawls, M. T. Charge Separation in Covalently Bound and Self-Assembled Donor Chromophore Acceptor System. Ph. D. Dissertation, Colorado State University, Fort Collins, Colorado, 2007.
7. Sapp, S. A. Materials Synthesis Strategies for: Microstructure Self-Assembly, Polymer-Encapsulated Reverse Micelles, Ionic Donors in Bimolecular Photosystems, and Efficient Mediators in Dye-Sensitized Solar Cells. Ph. D. Dissertation, Colorado State University, Fort Collins, Colorado, 2001.
8. Zaban, A.; Ferrere, S.; Sprague, J.; Gregg, B. A., pH-Dependent Redox Potential Induced in a Sensitizing Dye by Adsorption onto TiO₂. *Journal of Physical Chemistry B* **1997**, 101, 55-57.
9. Scott, M. J.; Nelson, J. J.; Caramori, S.; Bignozzi, C. A.; Elliott, C. M., Cis-Dichloro-bis(4,4'-dicarboxy-2,2'-bipyridine)osmium(II)-Modified Optically Transparent Electrodes: Application as Cathodes in Stacked Dye Sensitized Solar Cells. *Inorganic Chemistry* **2007**, 46, (24), 10071-10078.
10. Hagfeldt, A.; Grätzel, M., Light-Induced Redox Reactions in Nanocrystalline Systems. *Chemical Reviews* **1995**, 95, (1), 49-68.

11. Nusbaumer, H.; Moser, J.-E.; Zakeeruddin, S. M.; Nazeeruddin, M. K.; Grätzel, M., $\text{Co}^{\text{II}}(\text{dbbip})_2^{2+}$ Complex Rivals Tri-iodide/Iodide Redox Mediator in Dye-Sensitized Photovoltaic Cells. *Journal of Physical Chemistry B* **2001**, 105, 10461-10464.
12. Elliott, C. M.; Caramori, S.; Bignozzi, C. A., Indium tin oxide electrodes modified with tris(2,2'-bipyridine-4,4'-dicarboxylic acid) iron(II) and the catalytic oxidation of tris(4,4'-di-tert-butyl-2,2'-bipyridine) cobalt(II). *Langmuir* **2005**, 21, (7), 3022-3027.
13. Xue, D.; Elliott, C. M.; Gong, P.; Grainger, D. W.; Bignozzi, C. A.; Caramori, S., Indirect electrochemical sensing of DNA hybridization based on the catalytic oxidation of cobalt (II). *Journal of the American Chemical Society* **2007**, 129, (7), 1854-1855.
14. Fillinger, A.; Soltz, D.; Parkinson, B. A., Dye Sensitization of Natural Anatase Crystals with a Ruthenium-Based Dye. *Journal of the Electrochemical Society* **2002**, 149, (9), A1146-A1156.
15. Woodhouse, M.; Herman, G. S.; Parkinson, B. A., Combinatorial approach to identification of catalysts for the photoelectrolysis of water. *Chemistry of Materials* **2005**, 17, (17), 4318-4324.

CHAPTER 3

Stability and Electrode Dependence of Cobalt Mediator Solutions

This dissertation chapter describes the stability with time and electrode dependence of three cobalt complex mediator systems. All data collection, manipulation, and manuscript preparation were completed by Michael Scott.

3.1 Introduction

As described in Chapter 1, bipyridyl-cobalt complexes have been shown to function well as substitute redox mediators in DSSCs.¹ These cobalt(II) complexes have the benefit of being less injurious to cell components, and are not as darkly colored as the I^-/I_3^- mediator solutions typically employed¹. A further disadvantage of the I^-/I_3^- redox couple is that it is monolithic; it is what it is and cannot be modified. Bipyridyl-cobalt complexes have the advantage of being chemically modifiable. By substitution of electron withdrawing groups in the 4 and 4' positions of the bipyridyl ligands, the redox potential of the complex may be tuned in such a way as to increase the DSSCs overall maximum voltage.¹

Optimum performance in DSSCs employing cobalt complex mediator systems is achieved by including additives in the redox mediator solution.¹ Lithium trifluoromethanesulfonate (lithium triflate) increases the thermodynamic driving force for electron injection of the photo-excited electron from the sensitizing dye into the TiO_2 conduction band. This is a result of the adsorbed Li^+ ions decreasing (making more positive) the energy of the lower edge of the TiO_2 conduction band.² The addition of 4-*tert*-butylpyridine inhibits the reaction of electrons in the TiO_2 and FTO conduction bands with the oxidized form of the mediator (Co^{3+}) by adsorbing to vacancy sites on both of the metal oxides, resulting in increased open circuit voltage (V_{oc})^{3,4} and short circuit current density (J_{sc}).¹ Due to the presence of these compounds in the mediator solutions, metathesis reactions might occur, replacing the bipyridyl ligands of the cobalt complex and rendering the mediators ineffective.

The three cobalt complexes discussed in this work, tris(2,2'-bipyridyl-4,4'-di-*tert*-butyl)cobalt(II) perchlorate ($[\text{Co}(\text{DTB})_3](\text{ClO}_4)_2$), tris(2,2'-bipyridyl-4,4'-di-*tert*-butylester)cobalt(II) perchlorate ($[\text{Co}(\text{DTBEST})_3](\text{ClO}_4)_2$), and tris(2,2'-bipyridyl-4,4'-di-(bis-*N,N*-butylamide))cobalt(II) perchlorate ($[\text{Co}(\text{DBA})_3](\text{ClO}_4)_2$), are shown in Figure 1.

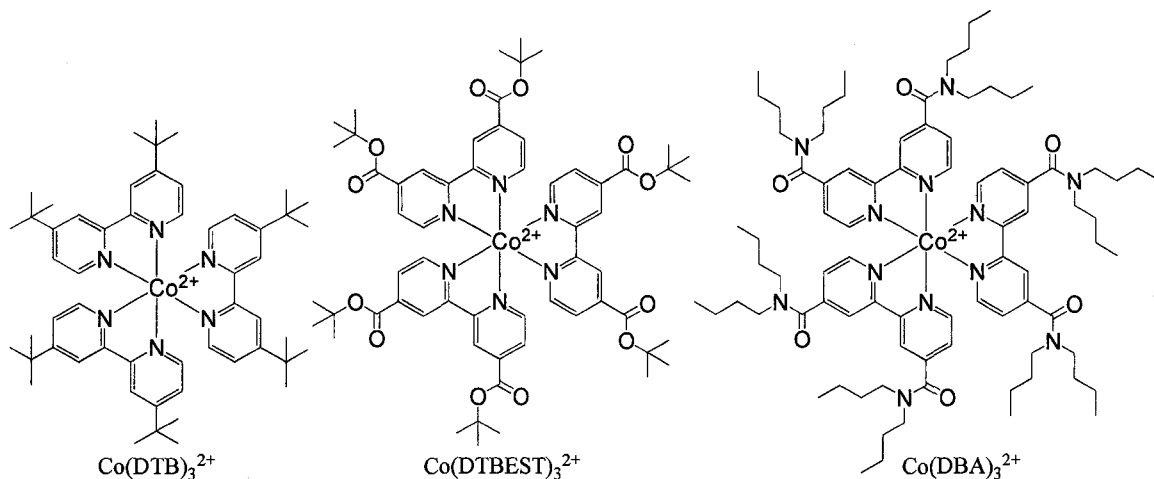


Figure 1. Structure of the 3 cobalt complexes considered.

The complexes $[\text{Co}(\text{DTBEST})_3](\text{ClO}_4)_2$ and $[\text{Co}(\text{DBA})_3](\text{ClO}_4)_2$ in Figure 1 contain, respectively, electron withdrawing ester and amide functional groups that shift the redox potential of the complexes to a more positive value. The half wave potentials ($E_{1/2}$) of the complexes, determined by cyclic voltammetry are given in Table 1.

Complex	$E_{1/2}$
$\text{Co}(\text{DTB})_3(\text{ClO}_4)_2$	-250 mV vs. ferrocene
$\text{Co}(\text{DTBEST})_3(\text{ClO}_4)_2$	20 mV vs. ferrocene
$\text{Co}(\text{DBA})_3(\text{ClO}_4)_2$	75 mV vs. ferrocene

Table 1. Cobalt complex redox potentials determined by cyclic voltammetry. 0.1 M tetramethylammonium perchlorate in γ BL supporting electrolyte, GC working electrode, Pt counter electrode, and SSCE reference electrode. 50 mV/s scan rate, 0.001 M $[\text{Co}(\text{L})_3](\text{ClO}_4)_2$.

The maximum voltage in a DSSC is given by the difference between the quasi-Fermi level of the illuminated TiO₂ and the redox potential of the mediator present.⁵ The shift in redox potential due to the electron withdrawing functional groups increases this difference, thereby increasing the maximum voltage of the DSSC.¹

In order to ascertain whether the cobalt complex mediator solutions are stable with respect to time, the electrochemical behavior of three different cobalt complexes was investigated initially and after storage for one week in the presence and absence of mediator solution additives. Mediator solutions of each of the three cobalt complexes investigated were prepared in γ BL in four varieties:

- 1) 0.15 M [Co(L)₃](ClO₄)₂.
- 2) 0.15 M [Co(L)₃] (ClO₄)₂ and 0.2 M lithium triflate.
- 3) 0.15 M [Co(L)₃] (ClO₄)₂ and 0.2 M 4-*tert*-butylpyridine.
- 4) 0.15 M [Co(L)₃] (ClO₄)₂, 0.2 M lithium triflate, and 0.2 M 4-*tert*-butylpyridine.

100 μ L of each of these solutions was diluted with the supporting electrolyte solution (0.1 M tetramethylammonium perchlorate in γ BL) to a final volume of 5 mL. This resulted in concentrations of 3 mM [Co(L)₃] (ClO₄)₂, 4 mM lithium triflate, and 4 mM 4-*tert*-butylpyridine. CV experiments were performed on the solutions immediately after they were prepared. After a period of one week, a new 100 μ L aliquot of the concentrated mediator solution was diluted with electrolyte solution and the CV experiments were repeated.

Previous work in the Elliott Group has shown that these different cobalt complexes display widely varying electrochemical activity on different electrode

materials¹. In other words, an electrode material that functions well with one cobalt complex may not function well with another. In a previous study, the cobalt complexes alone in solution, without lithium triflate and 4-*tert*-butylpyridine additives, were considered with gold, platinum, and carbon electrodes.¹ The ideality of solution phase electrochemistry of a particular cobalt complex/electrode combination did not necessarily relate to good performance in an assembled DSSC. Of interest in this study is the electrochemical behavior of the three cobalt complexes with different working electrodes with the mediator solution additives lithium triflate and 4-*tert*-butylpyridine (*vide supra*).

For these electrode dependence experiments the working electrode was either gold (Au, area = 0.007 cm²), platinum (Pt, area = 0.007 cm²), glassy carbon (GC, area = 0.07 cm²), FTO modified by adsorption of *cis*-dichloro-bis(2,2'-bipyridyl-4,4'-dicarboxylate)osmium(II) (OsFTO, cf. Chapter 4, area = 0.5 cm²), or unmodified FTO (area = 0.5 cm²) as indicated. Cyclic voltammograms were recorded using solutions prepared and diluted as described in the stability experiments (*vide supra*).

3.2 Results and Discussion

Time Dependence of Mediator Solutions

The results of the CV experiments for the [Co(DTB)₃](ClO₄)₂, [Co(DTBEST)₃](ClO₄)₂, and [Co(DBA)₃](ClO₄)₂ with mediator solution age are presented in Figures 2, 3, and 4, respectively. Experiments were conducted on a BAS 100B Potentiostat-Galvanostat run by BAS 100W software on a personal computer. All cyclic voltammograms were recorded at scan rate of 50 mV/s using tetramethylammonium perchlorate (0.1 M in γ BL) as the supporting electrolyte, GC

working electrode, SSCE reference electrode, and a large area platinum counter electrode. The GC working electrode was polished with a slurry of 0.15 μm alumina in de-ionized water, rinsed with de-ionized water, and dried with a KimWipe[®] before each CV experiment. Sample solutions had concentrations of 3 mM $[\text{Co}(\text{L})_3](\text{ClO}_4)_2$, 4 mM lithium triflate, and 4 mM 4-*tert*-butylpyridine as indicated in the Figures. CV experiments were performed on the solutions immediately after they were prepared, and again after a period of one week. Electrochemical data are reported relative to the ferrocene/ferrocinium redox couple.

A sign that the redox mediator solutions are not stable over the time period in question is the growth of new peaks in the voltammograms. For this reason the potential window of the CVs with the $[\text{Co}(\text{DTB})_3](\text{ClO}_4)_2$ mediator solutions were increased from -200 mV to 500 mV for the initial experiments, to -200 mV to 1200 mV for the experiments performed after one week. CV experiments with the $[\text{Co}(\text{DTBEST})_3](\text{ClO}_4)_2$ mediator solutions had a potential window of -200 mV to 1200 mV, and CV experiments with the $[\text{Co}(\text{DBA})_3](\text{ClO}_4)_2$ mediator solutions had a potential window of -200 mV to 1300 mV.

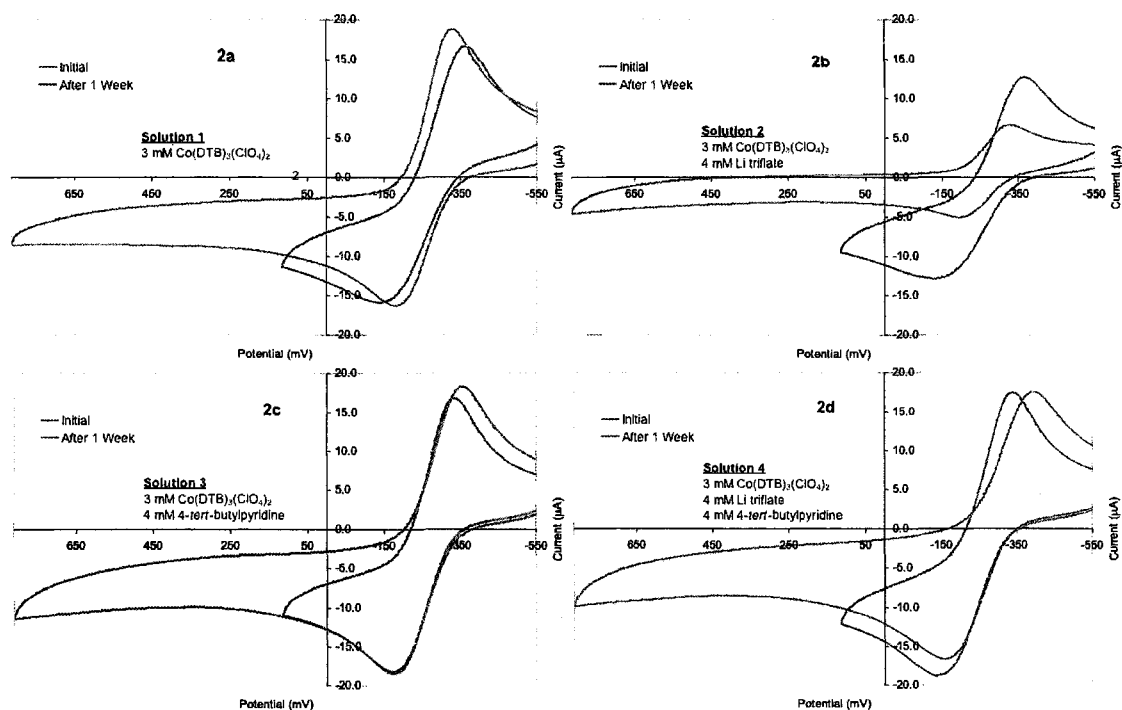


Figure 2. Time dependence of $[\text{Co}(\text{DTB})_3](\text{ClO}_4)_2$ mediator solutions. 2a: $[\text{Co}(\text{DTB})_3](\text{ClO}_4)_2$ only. 2b: $[\text{Co}(\text{DTB})_3](\text{ClO}_4)_2$ and lithium triflate. 2c: $[\text{Co}(\text{DTB})_3](\text{ClO}_4)_2$ and 4-*tert*-butylpyridine. 2d: $[\text{Co}(\text{DTB})_3](\text{ClO}_4)_2$, lithium triflate, and 4-*tert*-butylpyridine. In all 4 panes the blue trace is the initial CV collected immediately after preparing the solutions and the red trace is the CV collected after one week. 0.1 M tetramethylammonium perchlorate in γ BL supporting electrolyte, GC working electrode, SSCE reference electrode, Pt counter electrode, 50 mV/s scan rate. CVs are shown referenced to ferrocene.

It is evident in Figure 2 that all four varieties of the $[\text{Co}(\text{DTB})_3](\text{ClO}_4)_2$ solutions are stable for the time period in question. The ca. ± 30 mV shift in peak positions is within experimental error for the instrumentation. In Figure 2b, the peak currents after 1 week are reduced to approximately half of the magnitude of the initial voltammograms. This was due to a loss of sample between experiments resulting in only ca. 50 μL of the concentrated $[\text{Co}(\text{DTB})_3](\text{ClO}_4)_2$ /lithium triflate solution being available for dilution. Nevertheless, the peak positions have not changed significantly and no new peaks have appeared in the voltammogram that was recorded after a one-week interval.

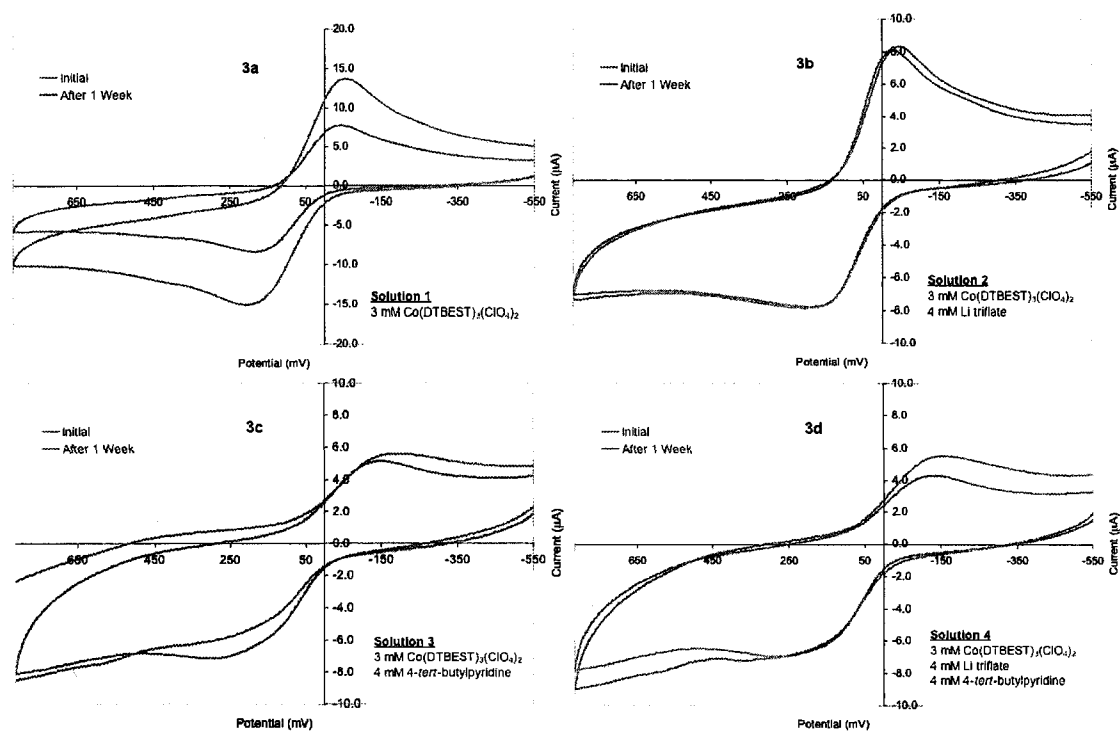


Figure 3. Time dependence of $[\text{Co}(\text{DTBEST})_3](\text{ClO}_4)_2$ mediator solutions. 3a: $[\text{Co}(\text{DTBEST})_3](\text{ClO}_4)_2$ only. 3b: $[\text{Co}(\text{DTBEST})_3](\text{ClO}_4)_2$ and lithium triflate. 3c: $[\text{Co}(\text{DTBEST})_3](\text{ClO}_4)_2$ and 4-*tert*-butylpyridine. 3d: $[\text{Co}(\text{DTBEST})_3](\text{ClO}_4)_2$, lithium triflate, and 4-*tert*-butylpyridine. In all 4 panes the blue trace is the initial CV collected immediately after preparing the solution and the red trace is the CV collected after one week. 0.1 M tetramethylammonium perchlorate in γBL supporting electrolyte, GC working electrode, SSCE reference electrode, Pt counter electrode, 50 mV/s scan rate. CVs are shown referenced to ferrocene.

Figure 3 shows that the $[\text{Co}(\text{DTBEST})_3](\text{ClO}_4)_2$ mediator solutions are also stable for the time period considered. Peak potentials remained constant and no new peaks formed in the voltammograms. The reduced current in Figure 3a for the voltammogram collected after one week is the result of an inadequate amount of the concentrated $[\text{Co}(\text{DTBEST})_3](\text{ClO}_4)_2$ solution available for dilution. Figures 3c and 3d reveal that the presence of 4-*tert*-butylpyridine with the $[\text{Co}(\text{DTBEST})_3](\text{ClO}_4)_2$ complex results in slower electron transfer, evidenced by the increased peak separation and the broadness of the oxidation and reduction peaks.⁶ However, these differences are not time dependent—i.e., they occur immediately upon addition of 4-*tert*-butylpyridine to the solution.

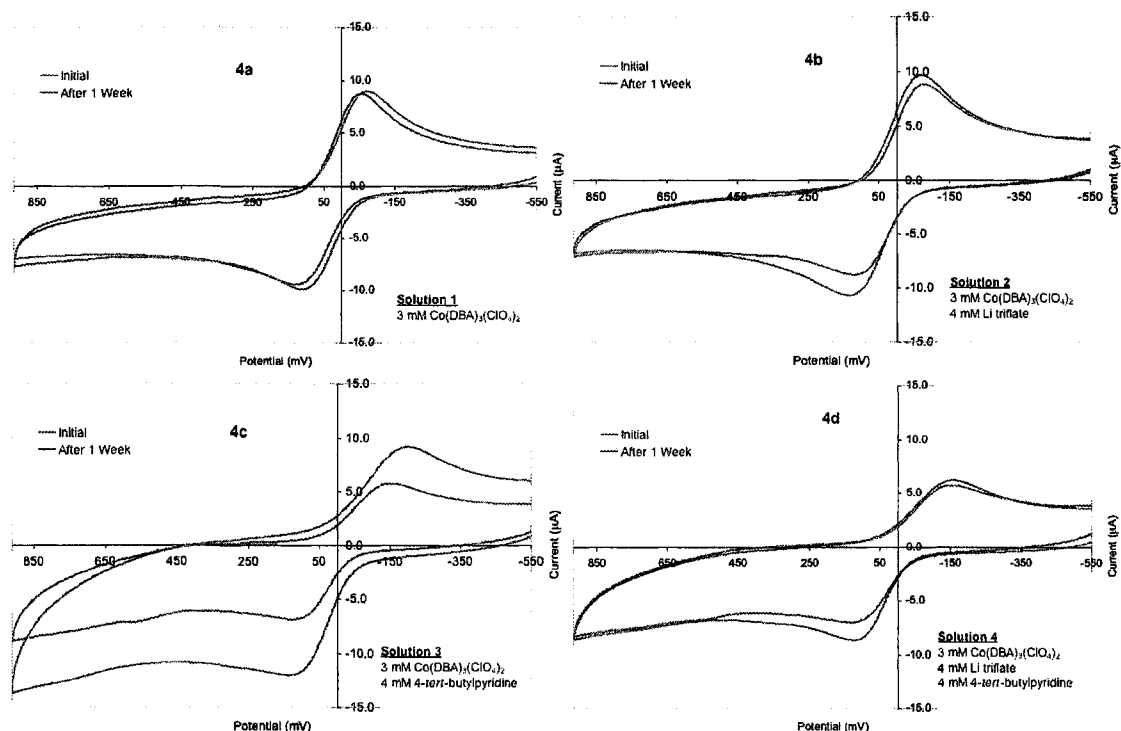


Figure 4. Time dependence of $[\text{Co}(\text{DBA})_3](\text{ClO}_4)_2$ mediator solutions. 4a: $[\text{Co}(\text{DBA})_3](\text{ClO}_4)_2$ only. 4b: $[\text{Co}(\text{DBA})_3](\text{ClO}_4)_2$ and lithium triflate. 4c: $[\text{Co}(\text{DBA})_3](\text{ClO}_4)_2$ and 4-*tert*-butylpyridine. 4d: $[\text{Co}(\text{DBA})_3](\text{ClO}_4)_2$, lithium triflate, and 4-*tert*-butylpyridine. In all 4 panes the blue trace is the initial CV collected immediately after preparing the solution and the red trace is the CV collected after one week. 0.1 M tetramethylammonium perchlorate in γBL supporting electrolyte, GC working electrode, SSCE reference electrode, Pt counter electrode, 50 mV/s scan rate. CVs are shown referenced to ferrocene.

Figure 4 shows that the $[\text{Co}(\text{DBA})_3](\text{ClO}_4)_2$ mediator solutions are also stable for the time period in question. In all four cases, peak potentials do not shift significantly and no new peaks appear in the voltammograms. As is the case with the $[\text{Co}(\text{DTBEST})_3](\text{ClO}_4)_2$ mediator solutions, the presence of 4-*tert*-butylpyridine with the $[\text{Co}(\text{DBA})_3](\text{ClO}_4)_2$ complex causes a time independent slowing of electron transfer, shown in the increased peak separation and broadness of oxidation and reduction peaks.

Mediator Solution Electrode Dependence

CV experiments were performed to compare the cobalt complexes redox activity on different electrode materials. Results for the $[\text{Co}(\text{DTB})_3](\text{ClO}_4)_2$, $[\text{Co}(\text{DTBEST})_3](\text{ClO}_4)_2$, and $[\text{Co}(\text{DBA})_3](\text{ClO}_4)_2$ mediator solutions are presented in Figure 5, 6, and 7, with electrochemical data summarized in Tables 2, 3, and 4, respectively. All cyclic voltammograms were recorded at scan rate of 50 mV/s using tetramethylammonium perchlorate (0.1 M in γBL) as the supporting electrolyte, SSCE reference electrode, and a large area platinum counter electrode. Au, Pt, and GC working electrodes were polished with a slurry of 0.15 μm alumina in de-ionized water, rinsed with de-ionized water, and dried with a KimWipe[®] before each CV experiment. OsFTO and FTO working electrodes were rinsed with acetonitrile and dried in a nitrogen stream before each CV experiment. Current densities (mA/cm^2) are reported in Figures 5, 6, and 7 to account for different working electrode areas. Sample solutions had concentrations of 3 mM $\text{Co}(\text{L})_3(\text{ClO}_4)_2$, 4 mM lithium triflate, and 4 mM 4-*tert*-butylpyridine as indicated in the Figures. Electrochemical data are reported relative to the ferrocene/ferrocinium redox couple.

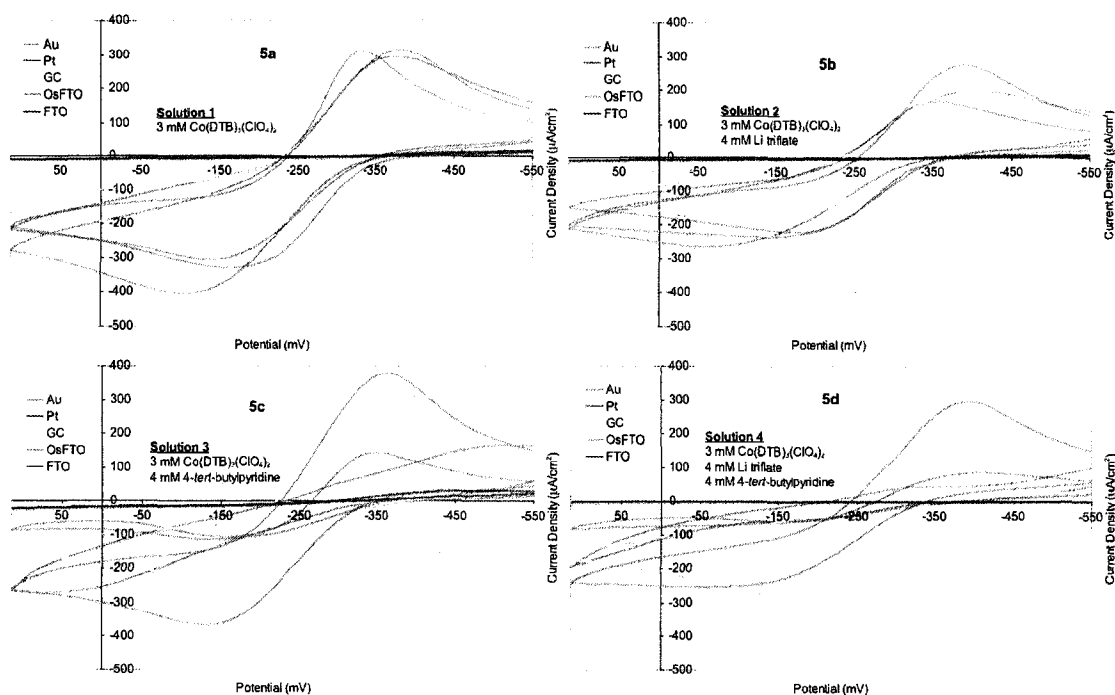


Figure 5. Electrode dependence of $[\text{Co}(\text{DTB})_3](\text{ClO}_4)_2$ mediator solutions. 5a: $[\text{Co}(\text{DTB})_3](\text{ClO}_4)_2$ only. 5b: $[\text{Co}(\text{DTB})_3](\text{ClO}_4)_2$ and lithium triflate. 5c: $[\text{Co}(\text{DTB})_3](\text{ClO}_4)_2$ and 4-tert-butylpyridine. 5d: $[\text{Co}(\text{DTB})_3](\text{ClO}_4)_2$, lithium triflate, and 4-tert-butylpyridine. 0.1 M tetramethylammonium perchlorate in γBL supporting electrolyte, 50 mV/s scan rate, SSCE reference electrode, Pt counter electrode. Working electrodes are indicated in figure legends. CVs are shown referenced to ferrocene.

Electrode	$[\text{Co}(\text{DTB})_3](\text{ClO}_4)_2$ Solution 1	$[\text{Co}(\text{DTB})_3](\text{ClO}_4)_2$ Solution 2	$[\text{Co}(\text{DTB})_3](\text{ClO}_4)_2$ Solution 3	$[\text{Co}(\text{DTB})_3](\text{ClO}_4)_2$ Solution 4
Au	$E_{p,c} = -330 \text{ mV}$ $J_{p,c} = 315 \mu\text{A}/\text{cm}^2$ $E_{p,a} = -160 \text{ mV}$ $J_{p,a} = -325 \mu\text{A}/\text{cm}^2$	$E_{p,c} = -355 \text{ mV}$ $J_{p,c} = 170 \mu\text{A}/\text{cm}^2$ $E_{p,a} = -180 \text{ mV}$ $J_{p,a} = -220 \mu\text{A}/\text{cm}^2$	$E_{p,c} = -350 \text{ mV}$ $J_{p,c} = 145 \mu\text{A}/\text{cm}^2$ $E_{p,a} = -140 \text{ mV}$ $J_{p,a} = -115 \mu\text{A}/\text{cm}^2$	$E_{p,c} = -410 \text{ mV}$ $J_{p,c} = 90 \mu\text{A}/\text{cm}^2$ $E_{p,a} = \text{-----}$ $J_{p,a} = \text{-----}$
Pt	$E_{p,c} = -380 \text{ mV}$ $J_{p,c} = 295 \mu\text{A}/\text{cm}^2$ $E_{p,a} = -100 \text{ mV}$ $J_{p,a} = -405 \mu\text{A}/\text{cm}^2$	$E_{p,c} = -410 \text{ mV}$ $J_{p,c} = 195 \mu\text{A}/\text{cm}^2$ $E_{p,a} = -55 \text{ mV}$ $J_{p,a} = -265 \mu\text{A}/\text{cm}^2$	$E_{p,c} = \text{-----}$ $J_{p,c} = \text{-----}$ $E_{p,a} = \text{-----}$ $J_{p,a} = \text{-----}$	$E_{p,c} = \text{-----}$ $J_{p,c} = \text{-----}$ $E_{p,a} = \text{-----}$ $J_{p,a} = \text{-----}$
GC	$E_{p,c} = -370 \text{ mV}$ $J_{p,c} = 240 \mu\text{A}/\text{cm}^2$ $E_{p,a} = -125 \text{ mV}$ $J_{p,a} = -235 \mu\text{A}/\text{cm}^2$	$E_{p,c} = -370 \text{ mV}$ $J_{p,c} = 180 \mu\text{A}/\text{cm}^2$ $E_{p,a} = -130 \text{ mV}$ $J_{p,a} = -235 \mu\text{A}/\text{cm}^2$	$E_{p,c} = -340 \text{ mV}$ $J_{p,c} = 240 \mu\text{A}/\text{cm}^2$ $E_{p,a} = -170 \text{ mV}$ $J_{p,a} = -260 \mu\text{A}/\text{cm}^2$	$E_{p,c} = -340 \text{ mV}$ $J_{p,c} = 250 \mu\text{A}/\text{cm}^2$ $E_{p,a} = \text{-----}$ $J_{p,a} = \text{-----}$
OsFTO	$E_{p,c} = -385 \text{ mV}$ $J_{p,c} = 315 \mu\text{A}/\text{cm}^2$ $E_{p,a} = -135 \text{ mV}$ $J_{p,a} = -305 \mu\text{A}/\text{cm}^2$	$E_{p,c} = -395 \text{ mV}$ $J_{p,c} = 275 \mu\text{A}/\text{cm}^2$ $E_{p,a} = -120 \text{ mV}$ $J_{p,a} = -180 \mu\text{A}/\text{cm}^2$	$E_{p,c} = -365 \text{ mV}$ $J_{p,c} = 380 \mu\text{A}/\text{cm}^2$ $E_{p,a} = -130 \text{ mV}$ $J_{p,a} = -365 \mu\text{A}/\text{cm}^2$	$E_{p,c} = -395 \text{ mV}$ $J_{p,c} = 295 \mu\text{A}/\text{cm}^2$ $E_{p,a} = \text{-----}$ $J_{p,a} = \text{-----}$

Table 2. Electrochemical data from CVs of $[\text{Co}(\text{DTB})_3](\text{ClO}_4)_2$ mediator solutions shown in Figure 5. Subscript 'c' denotes cathodic peak, subscript 'a' denotes anodic peak, dashes indicate no distinct peak present.

What is most obvious in Figure 5 is that unmodified FTO is a poor electrode for redox chemistry with the $[\text{Co}(\text{DTB})_3](\text{ClO}_4)_2$ mediator solutions, showing almost no

current. This is also the case for the $[\text{Co}(\text{DTBEST})_3](\text{ClO}_4)_2$ and $[\text{Co}(\text{DBA})_3](\text{ClO}_4)_2$ mediator solutions (cf. Figures 6 and 7). For this reason the FTO data are omitted from Tables 2 through 4. With only $[\text{Co}(\text{DTB})_3](\text{ClO}_4)_2$ present (Figure 5a), Au, Pt, GC, and OsFTO electrodes behave similarly, with quasi-reversible voltammograms. When lithium triflate is present in solution (Figure 5b), Au, Pt, and GC undergo slower electron transfer, shown by broad anodic and cathodic peaks, and increased peak separation.⁶ This is most likely due to the adsorption of Li^+ ions making the surface more positive, decreasing the driving force for $\text{Co}(\text{DTB})_3^{3+}$ reduction.² This effect has been observed on photoanodes of assembled DSSCs where Li^+ ions adsorbed to the TiO_2 surface decreases the rate of I_3^- reduction (a current reducing recombination reaction) resulting in increased short circuit current.¹ In Figure 5c, when 4-*tert*-butylpyridine is present in solution, the Pt electrode is essentially redox inactive. The Au electrode shows decreased current while the GC electrode shows similar performance to the Figure 5a where only $[\text{Co}(\text{DTB})_3](\text{ClO}_4)_2$ is present. The decreased current with the Au electrode is most likely due to adsorption of 4-*tert*-butylpyridine reducing the heterogeneous electron transfer rate for $\text{Co}(\text{DTB})_3^{3+}$ reduction.³ Figure 5d shows the cyclic voltammograms when both lithium triflate and 4-*tert*-butylpyridine are present in the mediator solution. As is the case in Figures 5b and 5c, the Au electrode shows slow electron transfer and the Pt electrode is essentially redox inactive. However, the GC electrode once again shows similar voltammetry to the situation where only $[\text{Co}(\text{DTB})_3](\text{ClO}_4)_2$ is present in solution. Throughout the series of experiments, the OsFTO electrode's performance is unchanged. This is most likely because electron transfer occurs between adsorbed osmium complex and cobalt complex in solution. The effects of Li^+ and 4-*tert*-butylpyridine occur through

modification of the electrode surface by adsorption. Li^+ and 4-*tert*-butylpyridine will not adsorb to the osmium complex and the underlying FTO, already having a monolayer of osmium complex adsorbed, does not undergo further surface modification by adsorption of Li^+ and/or 4-*tert*-butylpyridine. Furthermore, even if Li^+ or 4-*tert*-butylpyridine did adsorb to the FTO surface, it would not affect the electrochemistry. Overall, the data in Figure 5 demonstrate that the four $[\text{Co}(\text{DTB})_3](\text{ClO}_4)_2$ mediator solutions exhibit quasi-reversible voltammetry with Au, GC, and OsFTO working electrodes. Also, the Pt electrode exhibits extremely slow electron transfer kinetics, and un-modified FTO is essentially redox inactive with $[\text{Co}(\text{DTB})_3](\text{ClO}_4)_2$ mediator solutions.

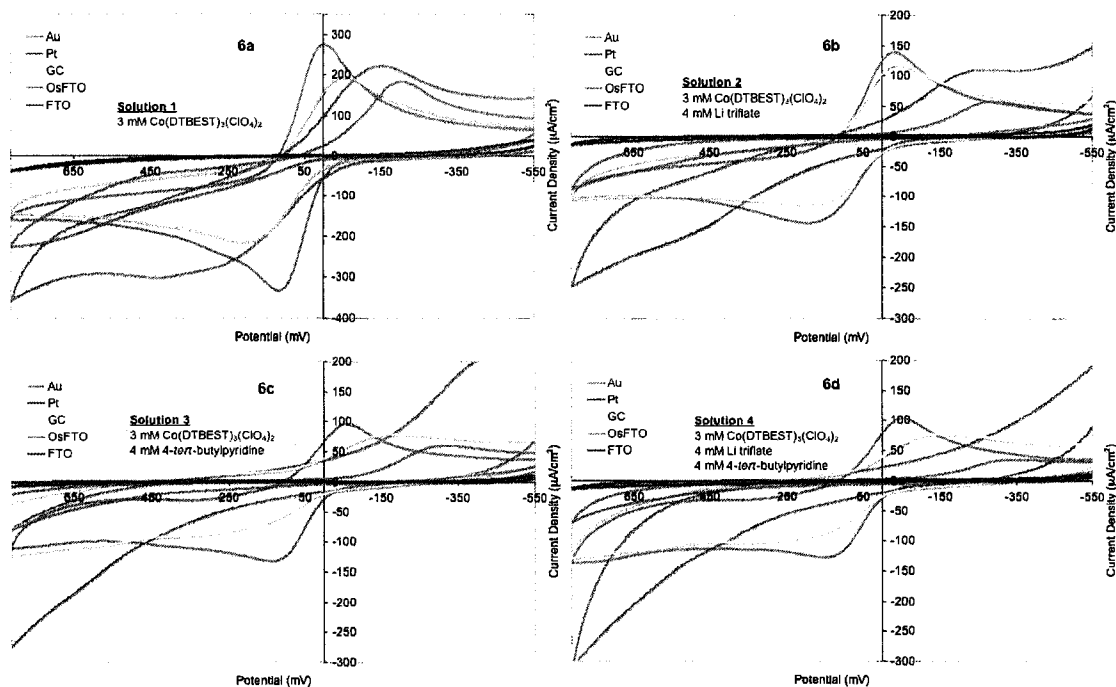


Figure 6. Electrode dependence of $[\text{Co}(\text{DTBEST})_3](\text{ClO}_4)_2$ mediator solutions. 6a: $[\text{Co}(\text{DTBEST})_3](\text{ClO}_4)_2$ only. 6b: $[\text{Co}(\text{DTBEST})_3](\text{ClO}_4)_2$ and lithium triflate. 6c: $[\text{Co}(\text{DTBEST})_3](\text{ClO}_4)_2$ and 4-*tert*-butylpyridine. 6d: $[\text{Co}(\text{DTBEST})_3](\text{ClO}_4)_2$, lithium triflate, and 4-*tert*-butylpyridine. 0.1 M tetramethylammonium perchlorate in γ BL supporting electrolyte, 50 mV/s scan rate, SSCE reference electrode, Pt counter electrode. Working electrodes are indicated in figure legends. CVs are shown referenced to ferrocene.

Electrode	[Co(DTBEST) ₃] (ClO ₄) ₂ Solution 1	[Co(DTBEST) ₃] (ClO ₄) ₂ Solution 2	[Co(DTBEST) ₃] (ClO ₄) ₂ Solution 3	[Co(DTBEST) ₃] (ClO ₄) ₂ Solution 4
Au	E _{p,c} = -10 mV J _{p,c} = 275 μA/cm ² E _{p,a} = 125 mV J _{p,a} = -330 μA/cm ²	E _{p,c} = -40 mV J _{p,c} = 140 μA/cm ² E _{p,a} = 200 mV J _{p,a} = -145 μA/cm ²	E _{p,c} = -70 mV J _{p,c} = 100 μA/cm ² E _{p,a} = 140 mV J _{p,a} = -130 μA/cm ²	E _{p,c} = -60 mV J _{p,c} = 100 μA/cm ² E _{p,a} = 160 mV J _{p,a} = -125 μA/cm ²
Pt	E _{p,c} = -160 mV J _{p,c} = 220 μA/cm ² E _{p,a} = 445 mV J _{p,a} = -300 μA/cm ²	E _{p,c} = ---- J _{p,c} = ---- E _{p,a} = ---- J _{p,a} = ----	E _{p,c} = ---- J _{p,c} = ---- E _{p,a} = ---- J _{p,a} = ----	E _{p,c} = ---- J _{p,c} = ---- E _{p,a} = ---- J _{p,a} = ----
GC	E _{p,c} = -60 mV J _{p,c} = 195 μA/cm ² E _{p,a} = 215 mV J _{p,a} = -215 μA/cm ²	E _{p,c} = -50 mV J _{p,c} = 120 μA/cm ² E _{p,a} = 210 mV J _{p,a} = -110 μA/cm ²	E _{p,c} = -180 mV J _{p,c} = 80 μA/cm ² E _{p,a} = ---- J _{p,a} = ----	E _{p,c} = -170 mV J _{p,c} = 80 μA/cm ² E _{p,a} = ---- J _{p,a} = ----
OsFTO	E _{p,c} = -215 mV J _{p,c} = 185 μA/cm ² E _{p,a} = ---- J _{p,a} = ----	E _{p,c} = -315 mV J _{p,c} = 60 μA/cm ² E _{p,a} = ---- J _{p,a} = ----	E _{p,c} = -335 mV J _{p,c} = 60 μA/cm ² E _{p,a} = ---- J _{p,a} = ----	E _{p,c} = -370 mV J _{p,c} = 35 μA/cm ² E _{p,a} = ---- J _{p,a} = ----

Table 3. Electrochemical data from CVs of [Co(DTBEST)₃](ClO₄)₂ mediator solutions shown in Figure 6. Subscript 'c' denotes cathodic peak, subscript 'a' denotes anodic peak, dashes indicate no distinct peak present.

Figure 6 shows that once lithium triflate or 4-*tert*-butylpyridine are added to the [Co(DTBEST)₃](ClO₄)₂ solutions the Pt electrode becomes essentially redox inactive. Also apparent in Figure 6 is that the cathodic peaks potentials show greater electrode dependence than was observed with the [Co(DTB)₃](ClO₄)₂ mediator solutions with up to a 300 mV shift in peak position when lithium triflate and 4-*tert*-butylpyridine are present. Similar to what was observed with the [Co(DTB)₃](ClO₄)₂ mediator solutions, addition of lithium triflate and 4-*tert*-butylpyridine resulted in lower cathodic peak currents due to decreased heterogeneous electron transfer rate. Unlike the [Co(DTB)₃](ClO₄)₂ mediator solutions, none of the four [Co(DTBEST)₃](ClO₄)₂ mediator solutions display quasi-reversible voltammetry with the OsFTO working electrode. This most results from mismatch of the E_{1/2} of the surface bound [Os(DCB)₂]Cl₂ and the E_{1/2} of the Co(DTBEST)₃^{2+/3+} in solution. As will be discussed in Chapter 4, the surface E_{1/2} of [Os(DCB)₂]Cl₂ is slightly negative of the solution E_{1/2} of [Co(DTB)₃](ClO₄)₂, making the

catalyzed oxidation and reduction of $[\text{Co}(\text{DTB})_3](\text{ClO}_4)_2$ possible. The solution $E_{1/2}$ of $[\text{Co}(\text{DTBEST})_3](\text{ClO}_4)_2$ is ca. 300 mV positive of the surface $E_{1/2}$ of $[\text{Os}(\text{DCB})_2]\text{Cl}_2$, resulting in little catalytic redox activity. The data in Figure 6 show that $[\text{Co}(\text{DTBEST})_3](\text{ClO}_4)_2$ mediator solutions exhibit quasi-reversible voltammetry with Au or GC working electrodes, whereas Pt and OsFTO electrodes exhibit slow electron transfer kinetics.

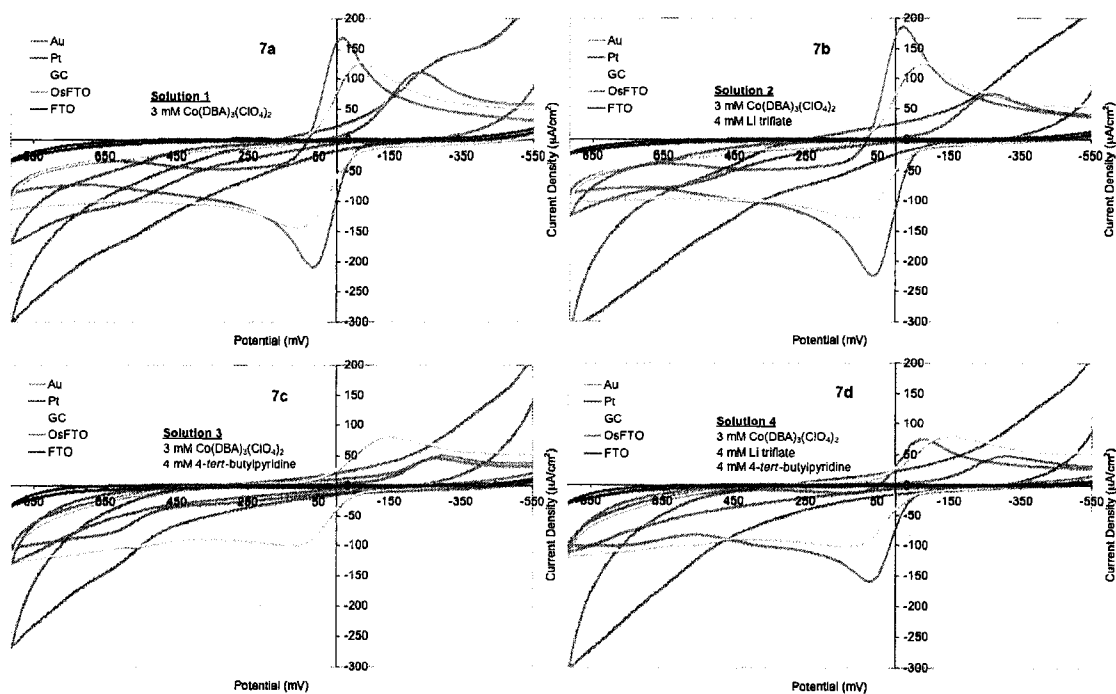


Figure 7. Electrode dependence of $[\text{Co}(\text{DBA})_3](\text{ClO}_4)_2$ mediator solutions. 7a: $[\text{Co}(\text{DBA})_3](\text{ClO}_4)_2$ only. 7b: $[\text{Co}(\text{DBA})_3](\text{ClO}_4)_2$ and lithium triflate. 7c: $[\text{Co}(\text{DBA})_3](\text{ClO}_4)_2$ and 4-tert-butylpyridine. 7d: $[\text{Co}(\text{DBA})_3](\text{ClO}_4)_2$, lithium triflate, and 4-tert-butylpyridine. 0.1 M tetramethylammonium perchlorate in γ BL supporting electrolyte, 50 mV/s scan rate, SSCE reference electrode, Pt counter electrode. Working electrodes are indicated in figure legends. CVs are shown referenced to ferrocene.

Electrode	[Co(DBA) ₃](ClO ₄) ₂ Solution 1	[Co(DBA) ₃](ClO ₄) ₂ Solution 2	[Co(DBA) ₃](ClO ₄) ₂ Solution 3	[Co(DBA) ₃](ClO ₄) ₂ Solution 4
Au	E _{p,c} = -30 mV J _{p,c} = 165 μA/cm ² E _{p,a} = 70 mV J _{p,a} = -210 μA/cm ²	E _{p,c} = -30 mV J _{p,c} = 185 μA/cm ² E _{p,a} = 70 mV J _{p,a} = -220 μA/cm ²	E _{p,c} = -290 mV J _{p,c} = 45 μA/cm ² E _{p,a} = ----- J _{p,a} = -----	E _{p,c} = -85 mV J _{p,c} = 75 μA/cm ² E _{p,a} = 75 mV J _{p,a} = -160 μA/cm ²
Pt	E _{p,c} = ----- J _{p,c} = ----- E _{p,a} = ----- J _{p,a} = -----	E _{p,c} = ----- J _{p,c} = ----- E _{p,a} = ----- J _{p,a} = -----	E _{p,c} = ----- J _{p,c} = ----- E _{p,a} = ----- J _{p,a} = -----	E _{p,c} = ----- J _{p,c} = ----- E _{p,a} = ----- J _{p,a} = -----
GC	E _{p,c} = -80 mV J _{p,c} = 130 μA/cm ² E _{p,a} = 120 mV J _{p,a} = -140 μA/cm ²	E _{p,c} = -85 mV J _{p,c} = 125 μA/cm ² E _{p,a} = 130 mV J _{p,a} = -125 μA/cm ²	E _{p,c} = -155 mV J _{p,c} = 80 μA/cm ² E _{p,a} = 130 mV J _{p,a} = -100 μA/cm ²	E _{p,c} = -160 mV J _{p,c} = 85 μA/cm ² E _{p,a} = 145 mV J _{p,a} = -100 μA/cm ²
OsFTO	E _{p,c} = -235 mV J _{p,c} = 110 μA/cm ² E _{p,a} = ----- J _{p,a} = -----	E _{p,c} = -275 mV J _{p,c} = 75 μA/cm ² E _{p,a} = ----- J _{p,a} = -----	E _{p,c} = -300 mV J _{p,c} = 50 μA/cm ² E _{p,a} = ----- J _{p,a} = -----	E _{p,c} = -310 mV J _{p,c} = 50 μA/cm ² E _{p,a} = ----- J _{p,a} = -----

Table 4. Electrochemical data from CVs of [Co(DBA)₃](ClO₄)₂ mediator solutions shown in Figure 7. Subscript 'c' denotes cathodic peak, subscript 'a' denotes anodic peak, dashes indicate no distinct peak present.

Figure 7 shows Pt is a poor working electrode for all four varieties of the [Co(DBA)₃](ClO₄)₂ mediator solutions with no discernable anodic or cathodic peaks. Figure 7 also suggests that, with the [Co(DBA)₃](ClO₄)₂ mediator and Au or GC working electrodes, the presence of 4-*tert*-butylpyridine slows electron transfer significantly, whereas the presence of lithium triflate does not. This is again due to absorbed 4-*tert*-butylpyridine decreasing the rate of heterogeneous electron transfer. Similar to the results for the [Co(DTBEST)₃](ClO₄)₂ mediator solutions, the [Co(DBA)₃](ClO₄)₂ mediator solutions do not display quasi-reversible voltammetry with the OsFTO working electrode, once again a result mismatched solution E_{1/2} for the [Co(DBA)₃](ClO₄)₂ and surface E_{1/2} of the adsorbed [Os(DCB)₂]Cl₂. Figure 7 demonstrates that with Au and GC working electrodes the [Co(DBA)₃](ClO₄)₂ mediator solutions alone, and with lithium triflate, exhibit quasi-reversible voltammetry, while showing slow electron transfer when 4-*tert*-butylpyridine is present. Additionally, that Pt and OsFTO working electrodes

experience very slow electron transfer with all four varieties of the $[\text{Co}(\text{DBA})_3](\text{ClO}_4)_2$ mediator solutions.

Cell Evaluation

Current-voltage experiments were performed on the cobalt complex mediated DSSCs employing Au and GC cathodes. Au cathodes were prepared by depositing 15 nm of chromium, followed by 200 nm of gold, onto FTO glass in a vacuum deposition chamber. GC cathodes were cut from ca. one inch squares of Type 2 Glassy Carbon purchased from Alfa Aesar into ca. 1 cm x 2 cm pieces. The surface of the glassy carbon electrode was roughened with 600 grit Emory paper prior to use in DSSCs. A different photoanode was used for each of the three cobalt mediator complexes. Mediator solutions were prepared as 0.15 M $[\text{Co}(\text{L})_3](\text{ClO}_4)_2$, 0.015 M NOBF_4 , 0.2 M lithium triflate, and 0.2 M 4-*tert*-butylpyridine in γBL . DSSCs were assembled in a custom cell holder with a 0.4 cm² optical aperture. Clamps holding the photoanode and cathode together were tightened to 14 mN m with a torque driver (Precision Instruments). Redox mediator solution (ca. 10 μL) was introduced to the interface of the photoanode and cathode with a Pasteur pipette and capillary forces pulled the solution into the spaces of the mesoporous semiconductor. The resulting current-voltage curves were assessed on the basis of open circuit voltage (V_{oc}), short circuit current density (J_{sc}), and fill factor (FF) and efficiency (η).

Figure 8 presents the combined results of all three cobalt complexes coupled with a Au cathode. The cell parameters for the current voltage curves are summarized in Table 5. Figure 8 demonstrates how the presence of the electron withdrawing groups on

the ligands of the $[\text{Co}(\text{DTBEST})_3](\text{ClO}_4)_2$ and $[\text{Co}(\text{DBA})_3](\text{ClO}_4)_2$ complexes increases the voltage in their respective DSSCs. Current-voltage experiments that are plotted together for comparison in Figures 9 through 11 represent results from a single photoanode coupled with the cathode indicated in the figure.

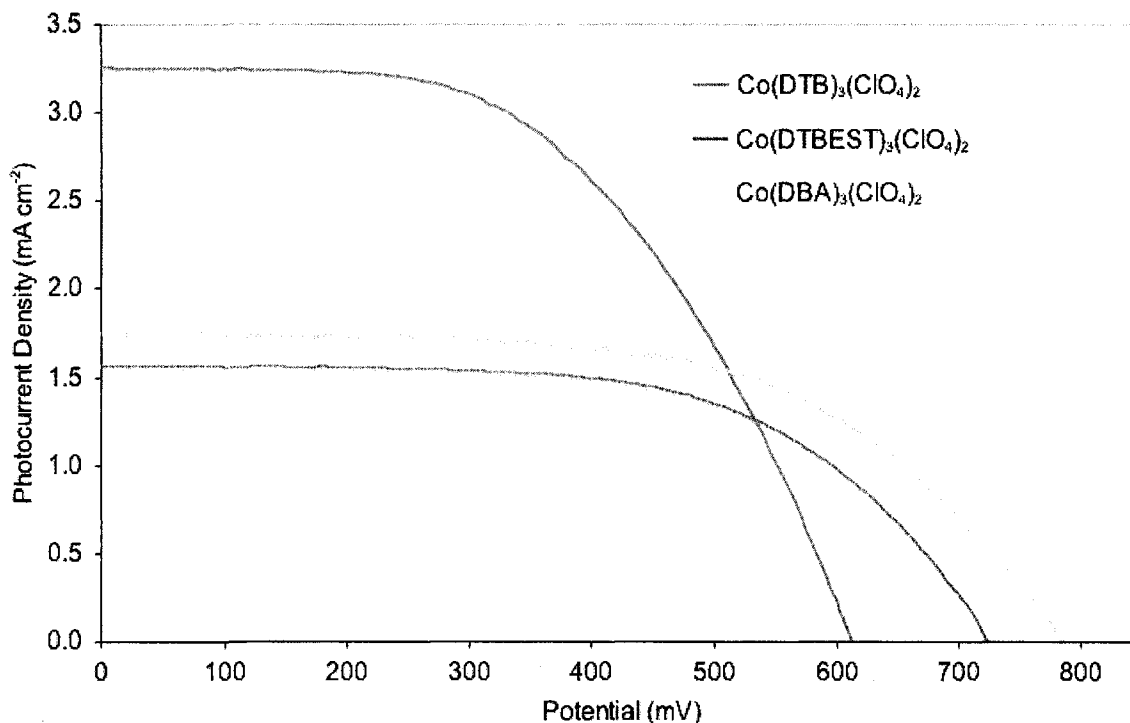


Figure 8. Current-Voltage results of DSSCs mediated with $[\text{Co}(\text{DTB})_3](\text{ClO}_4)_2$ (blue trace), $[\text{Co}(\text{DTBEST})_3](\text{ClO}_4)_2$ (red trace), and $[\text{Co}(\text{DBA})_3](\text{ClO}_4)_2$ (orange trace). All 3 cells employed an Au cathode.

Mediator	V_{oc}	J_{sc}	Fill Factor	Efficiency
$[\text{Co}(\text{DTB})_3](\text{ClO}_4)_2$	615 mV	3.26 mA/cm ²	52.4%	1.05%
$[\text{Co}(\text{DTBEST})_3](\text{ClO}_4)_2$	725 mV	1.56 mA/cm ²	59.8%	0.68%
$[\text{Co}(\text{DBA})_3](\text{ClO}_4)_2$	785 mV	1.75 mA/cm ²	58.2%	0.80%

Table 5. Cell parameters for current-voltage curves shown in Figure 8.

CV results in Figure 5 demonstrated that the $[\text{Co}(\text{DTB})_3](\text{ClO}_4)_2$ mediator solutions exhibited quasi-reversible voltammetry with Au, GC, and OsFTO working electrodes. The OsFTO electrode will be discussed in detail in Chapter 4. Current-

voltage results for $[\text{Co}(\text{DTB})_3](\text{ClO}_4)_2$ mediated DSSCs with Au and GC electrodes are presented in Figure 9 with cell parameters summarized in Table 6.

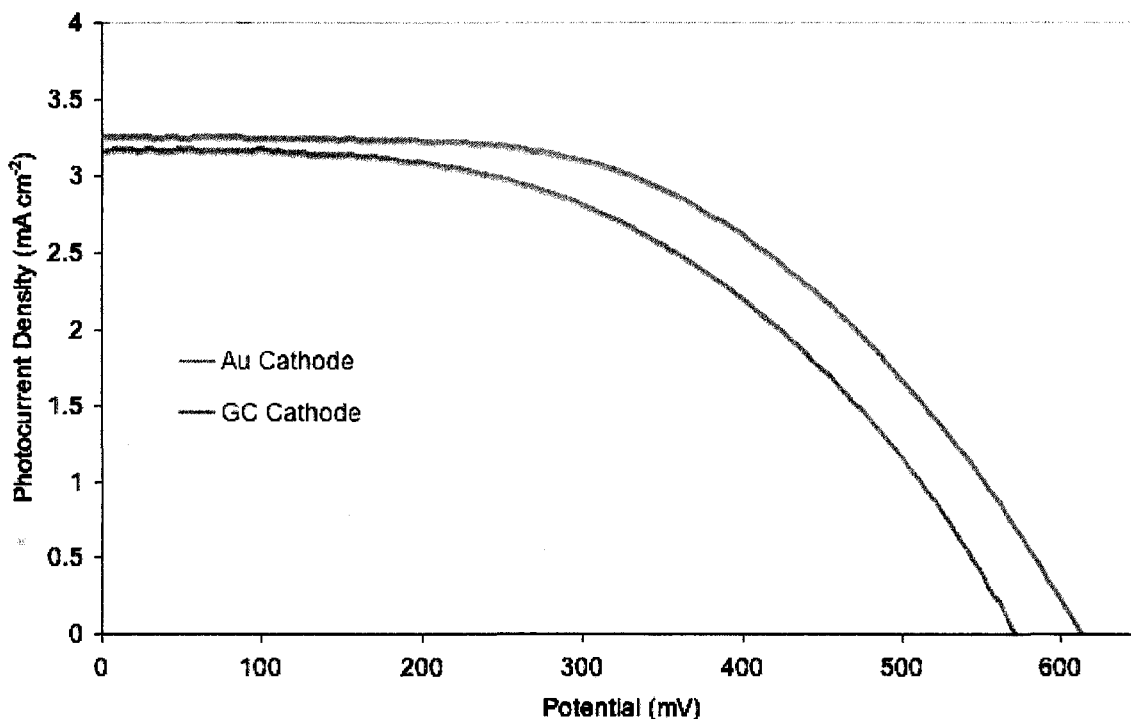


Figure 9. Current-Voltage results of DSSCs mediated with $[\text{Co}(\text{DTB})_3](\text{ClO}_4)_2$ using an Au cathode (blue trace) and a GC cathode (red trace) with the same photoanode.

Cathode	V_{oc}	J_{sc}	Fill Factor	Efficiency
Au	615 mV	3.26 mA/cm ²	52.4%	1.05%
GC	570 mV	3.17 mA/cm ²	49.8%	0.90%

Table 6. Cell parameters for current-voltage curves shown in Figure 9.

The results presented in Figure 9 demonstrate that the GC cathode works just as well as the Au cathode in a DSSC employing the $[\text{Co}(\text{DTB})_3](\text{ClO}_4)_2$ mediator solution. The difference in V_{oc} between the two cells is typical of DSSCs mediated by cobalt complexes. Thousands of experiments conducted over several years have shown that cells assembled with similar photoanodes, or even the same photoanodes, exhibit an inherent variability of ca. ± 60 mV in V_{oc} whereas the J_{sc} is typically more reproducible

with a variability of ca. $\pm 0.2 \text{ mA cm}^{-2}$. Bearing this in mind, the two current-voltage curves shown in Figure 9 are equivalent, within experimental error.

CV results in Figure 6 demonstrated that the $[\text{Co}(\text{DTBEST})_3](\text{ClO}_4)_2$ mediator solutions had quasi-reversible voltammetry with Au and GC working electrodes.

Current-voltage results for $[\text{Co}(\text{DTBEST})_3](\text{ClO}_4)_2$ mediated DSSCs with Au and GC electrodes are presented in Figure 10 with cell parameters summarized in Table 7.

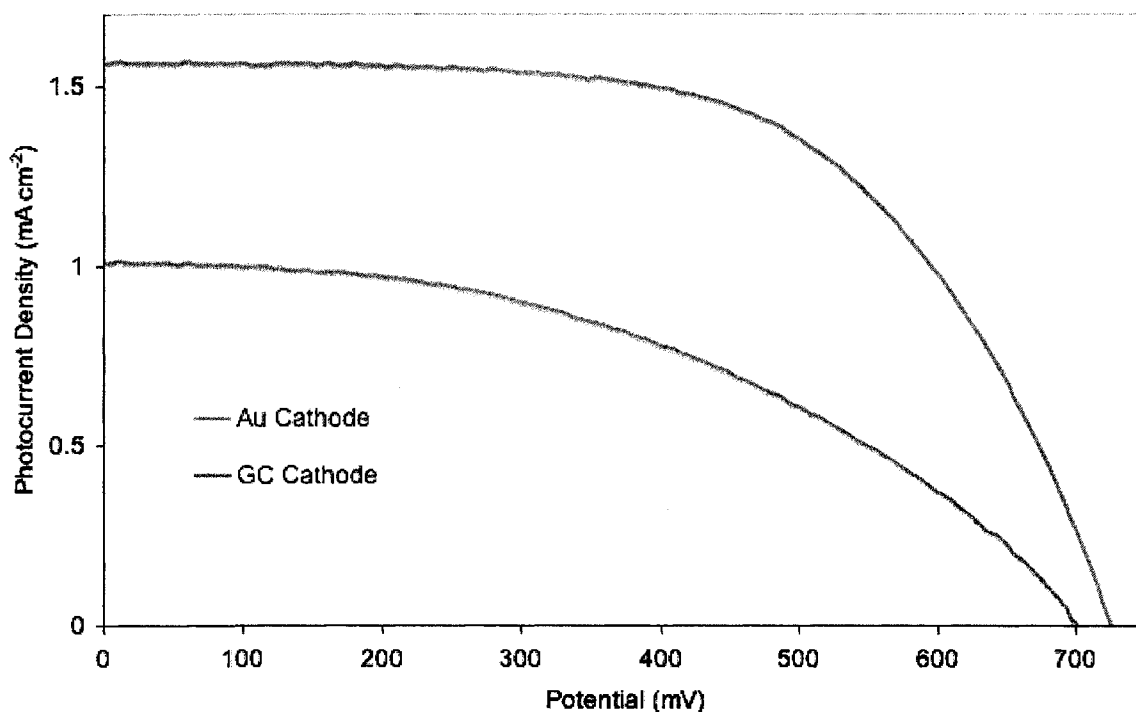


Figure 10. Current-voltage results of DSSCs mediated with $[\text{Co}(\text{DTBEST})_3](\text{ClO}_4)_2$ using an Au cathode (blue trace) and a GC cathode (red trace).

Cathode	V_{oc}	J_{sc}	Fill Factor	Efficiency
Au	725 mV	1.56 mA/cm^2	59.8%	0.68%
GC	700 mV	1.01 mA/cm^2	44.6%	0.32%

Table 7. Cell parameters for current-voltage curves shown in Figure 10.

In the case of the $[\text{Co}(\text{DTBEST})_3](\text{ClO}_4)_2$ mediator, the CV data (cf. Figure 6) and current-voltage data agree. In Figure 6d the Au electrode yields a more reversible

CV for $\text{Co}(\text{DTBEST})_3^{2+/3+}$ than the GC electrode. This manifests in a significantly higher J_{sc} and better FF from the DSSC with Au cathode shown in Figure 10. The difference in V_{oc} between the Au and GC electrodes is within experimental error (*vide supra*).

CV results in Figure 7 demonstrated that the $[\text{Co}(\text{DBA})_3](\text{ClO}_4)_2$ mediator solutions had quasi-reversible voltammetry with Au and GC working electrodes. Current-voltage results for $[\text{Co}(\text{DBA})_3](\text{ClO}_4)_2$ mediated DSSCs with Au and GC electrodes are presented in Figure 11 with cell parameters summarized in Table 8.

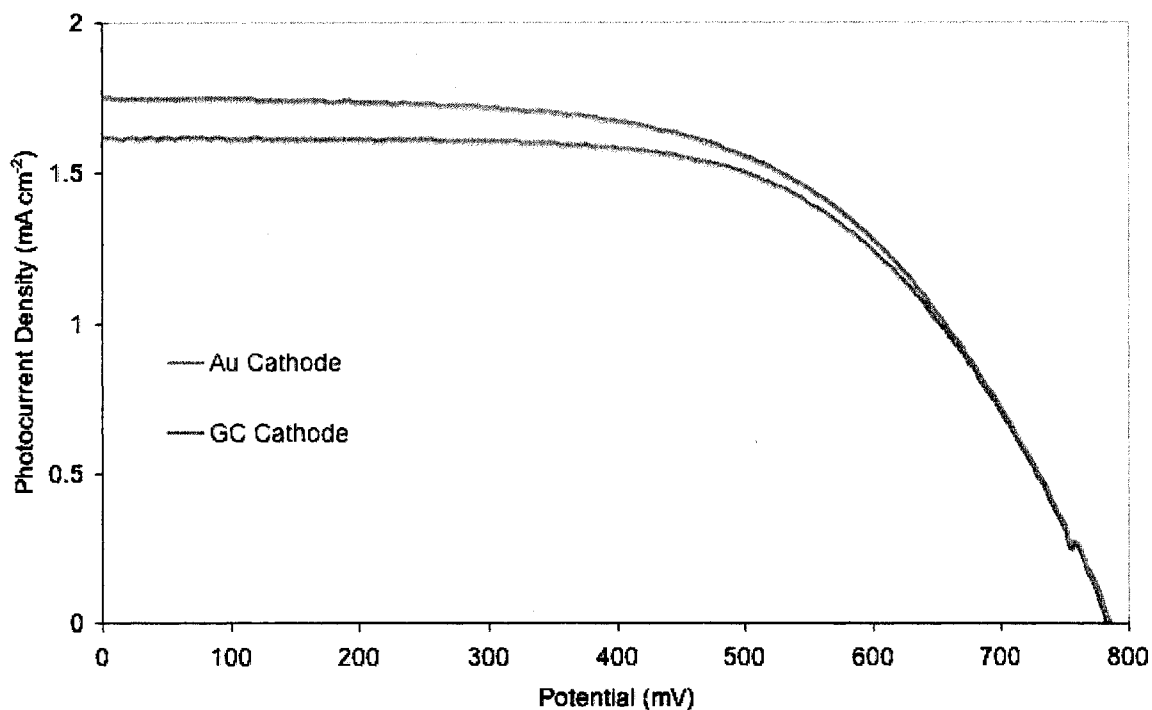


Figure 11. Current-Voltage results of DSSCs mediated with $[\text{Co}(\text{DBA})_3](\text{ClO}_4)_2$ using an Au cathode (blue trace) and a GC cathode (red trace).

Cathode	V_{oc}	J_{sc}	Fill Factor	Efficiency
Au	785 mV	1.75 mA/cm ²	58.2%	0.80%
GC	785 mV	1.62 mA/cm ²	61.0%	0.77%

Table 8. Cell parameters for DSSCs shown in Figure 11.

As was the case with $[\text{Co}(\text{DTBEST})_3](\text{ClO}_4)_2$ mediated DSSCs, the current-voltage results and CV results (cf. Figure 7) for the $[\text{Co}(\text{DBA})_3](\text{ClO}_4)_2$ mediator agree.

Figure 7d shows that the Au and GC electrodes both yield quasi-reversible CVs for $\text{Co}(\text{DBA})_3^{2+/3+}$. This is reflected in current-voltage curves that are the same within experimental error for DSSCs mediated with $\text{Co}(\text{DBA})_3(\text{ClO}_4)_2$ coupled with Au and GC cathodes, shown in Figure 11.

3.3 Conclusions

This chapter has shown that the three cobalt complex mediator solutions investigated show no signs of being unstable over a one week time period when γBL is the solvent. It must be noted that these experiments were not intended to state anything about mediator solution stability in an assembled and functioning DSSC. The issue in question was if the presence of the additives discussed, which enhance the performance of cobalt mediated DSSCs, would displace the bipyridyl ligands or otherwise react with the cobalt complexes to render the mediator solutions ineffective.

The electrode dependence experiments discussed in this chapter suggest that Au and GC electrodes are worthy for use as cathodes in DSSCs employing all three of the cobalt complexes investigated. OsFTO cathodes perform well in DSSCs employing the $[\text{Co}(\text{DTB})_3](\text{ClO}_4)_2$ mediator solution due to catalyzed reduction of $\text{Co}(\text{DTB})_3^{3+}$.⁷

Current-voltage experiments were performed to verify the efficacy of using Au and GC cathodes in operational DSSCs. These experiments revealed that while a GC cathode performed as well as Au with the $[\text{Co}(\text{DTB})_3](\text{ClO}_4)_2$ and $[\text{Co}(\text{DBA})_3](\text{ClO}_4)_2$ mediators, Au is a superior cathode material when considering the $[\text{Co}(\text{DTBEST})_3](\text{ClO}_4)_2$ mediator complex.

3.4 References

1. Sapp, S. A.; Elliott, C. M.; Contado, C.; Caramori, S.; Bignozzi, C. A., Substituted Polypyridine Complexes of Cobalt(II/III) as Efficient Electron-Transfer Mediators in Dye-Sensitized Solar Cells. *Journal of the American Chemical Society* **2002**, 124, (37), 11215-11222.
2. Kelly, C. A.; Farzad, F.; Thompson, D. W.; Stipkala, J. M.; Meyer, G. J., Cation-Controlled Interfacial Charge Injection in Sensitized Nanocrystalline TiO₂. *Langmuir* **1999**, 15, 7047-7054.
3. Boschloo, G.; Haggman, L.; Hagfeldt, A., Quantification of the Effect of 4-*tert*-Butylpyridine Addition to I⁻/I₃⁻ Redox electrolytes in Dye-Sensitized Nanostructured TiO₂ Solar Cells. *Journal of Physical Chemistry B* **2006**, 110, 13144-13150.
4. Huang, S. Y.; Schlichthörl, G.; Nozik, A. J.; Grätzel, M.; Frank, A. J., Charge Recombination in Dye-Sensitized Nanocrystalline TiO₂ Solar Cells. *Journal of Physical Chemistry B* **1997**, 101, 2576-2582.
5. Hagfeldt, A.; Grätzel, M., Molecular Photovoltaics. *Accounts of Chemical Research* **2000**, 33, 269-277.
6. Bard, A. J.; Faulkner, L. R., *Electrochemical Methods: Fundamentals and Applications*. 2nd ed. ed.; John Wiley & Sons, Inc.: New York, 2001.
7. Scott, M. J.; Nelson, J. J.; Caramori, S.; Bignozzi, C. A.; Elliott, C. M., *cis*-Dichloro-bis(4,4'-dicarboxy-2,2'-bipyridine)osmium(II)-Modified Optically Transparent Electrodes: Application as Cathodes in Stacked Dye Sensitized Solar Cells. *Inorganic Chemistry* **2007**, 46, (24), 10071-10078.

This page intentionally left blank.

CHAPTER 4

cis-Dichloro-bis(2,2'-bipyridyl-4,4'-dicarboxylic acid)osmium(II)-Modified Optically Transparent Electrodes: Applications as Cathodes in Stacked Dye-Sensitized Solar Cells

Michael J. Scott, Jeremy J. Nelson, Stefano Caramori,
Carlo A. Bignozzi, and C. Michael Elliott

Published in the journal *Inorganic Chemistry* 2007; 46(24); 10071-10078. Printed here with permission from the authors.

This dissertation chapter contains the results from an article published in the journal *Inorganic Chemistry*. The manuscript was written primarily by Michael Scott and Mike Elliott with assistance from Jeremy Nelson. Three electrode data shown in Figure 2 were collected by Jeremy Nelson. Photoaction spectra shown in Figure 6 were corroborated by repeat experiments completed at the University of Ferrara, Italy by Stefano Caramori.

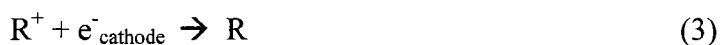
This chapter describes the modification of transparent conducting oxide (TCO) electrodes for use as cathodes in dye-sensitized solar cells. These modified TCO cathodes efficiently reduce the oxidized form of the cobalt mediator complex, allowing DSSCs to be stacked and operated in tandem to increase the amount of light energy converted to electrical energy. Additionally, the concept of stacking DSSCs with spectrally complementary dyes is shown to extend the cell's light absorption to longer wavelengths than with the typical dye employed.

4.1 Abstract

An optically transparent cathode was developed for use in dye sensitized solar cells. Fluorine doped tin oxide conducting glass modified with a monolayer of *cis*-dichloro-bis(2,2'-bipyridyl-4,4'-dicarboxylic acid)osmium(II) efficiently reduces the oxidized form of the redox mediator. This transparent cathode transmits light that is not absorbed by the dyed TiO₂; consequently, more than one cell can operate in optical tandem (i.e., "stacked"). Two types of stacked cells are considered: one where both photoanodes are dyed with the same dye and one where the photoanodes are dyed with different, spectrally complementary dyes. Overall behavior of these tandem cells is compared with single cell analogs.

4.2 Introduction

Since the present-day incarnation of the dye-sensitized solar cell (DSSC) was described by Grätzel and co-workers,¹ much effort has focused on maximizing the energy conversion efficiency and device lifetime while minimizing production costs and environmental impact. Energy conversion in a DSSC is characterized by three processes: (1) photo-oxidation of the sensitizing dye via injection of electrons into the conduction band of, typically, nanocrystalline TiO₂, (2) reduction of the oxidized dye by a redox mediator in solution, and (3) reduction of the oxidized mediator at the cathode.



These processes efficiently separate charge and confine the electrons to the solid semiconductor phase and the holes to the liquid electrolyte phase. The predominant processes that negatively influence cell efficiencies are: (4) recombination of the photo-injected electron with oxidized dye or (5) with oxidized mediator.



The defining feature of the present-day DSSC is the extremely high surface area mesoporous photoanode fabricated from nanometer size TiO₂ crystals. The mesoporous semiconductor is deposited as a thin layer (usually less than 10 μm thick) on a transparent conducting substrate, resulting in a three dimensional structure that has an actual surface area ca. 1000 times greater than the apparent surface area. After dyeing, the pores of this three dimensional structure are typically filled with mediator electrolyte solution. Within

the resulting bicontinuous phase, the domains are small (i.e., less than ca. 50 nm) thus no macroscopic electric field can be sustained in the TiO₂ due to screening by the electrolyte.^{2,3} For this reason, photo-injected electrons travel through the porous TiO₂ structure to the underlying conducting glass substrate via a diffusional walk pathway. Along this course, electrons temporarily reside in trap states for periods of time dependent on the depth of the trap.⁴ Thus the electron can be thought of as moving (diffusing) randomly (i.e., towards or away from the collector electrode) from trap to trap. Because of this diffusional motion, doubling the distance between the collector and the photo-oxidized dye site quadruples the electron's residence time in the TiO₂. Therefore, the probability that the electron will recombine with a photo-oxidized dye molecule or react with the oxidized mediator is also approximately quadrupled. The net consequence is that the photocurrent does not scale linearly with increased light absorption for a thicker TiO₂ layer,⁵ provided that the thickness of the layer is similar to or greater than the average electron diffusion length.

The iodide (I⁻/I₃⁻) redox couple is by far and away the dominant mediator system used in DSSCs. This prevalence is for two kinetic reasons: first, the reduction of the photo-oxidized dye by I⁻ (R in the above reactions) is very fast, and second, the reaction of injected electrons with I₃⁻ (R⁺ in the above reactions) is very slow.⁶ Montanari et al. have shown that, for DSSCs having photoanodes that incorporate the so-called N3 dye (*cis*-di(isothiocyanato)-bis(2,2'-bipyridyl-4,4'-dicarboxylate)ruthenium(II)), and mediated by I⁻/I₃⁻, the reduction of the photo-oxidized sensitizing dye by I⁻ is sufficiently fast that the predominant recombination reaction is that of the conduction-band electron with the oxidized form of the mediator, reaction 5 above.⁷ However, transient laser

spectroscopy experiments completed in our respective laboratories^{8,9} and results published by Nusbaumer et al.¹⁰ have shown that in cobalt mediated DSSCs, reduction of the photo-oxidized sensitizing dye by cobalt(II) is not as efficient as that observed in I^-/I_3^- mediated DSSCs. For this reason the recombination reaction of the conduction-band electron with the photo-oxidized dye, reaction 4 above, cannot be dismissed when considering DSSCs employing alternative redox mediator systems.

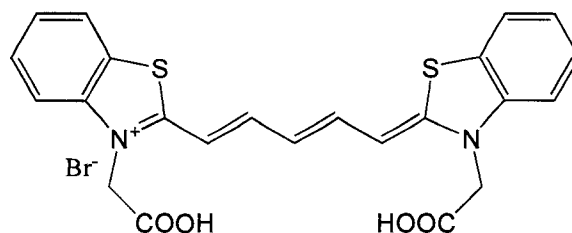
Unfortunately, the I^-/I_3^- redox couple has several negative features within the context of its application as a DSSC mediator: I_2 in equilibrium with I_3^- is volatile, cathodes must be constructed from platinum-group metals, I_3^- is darkly colored and absorbs visible light, and the redox potential of the I^-/I_3^- couple is more negative than optimum (for use with standard dyes, at least)—to name a few. Consequently, there is inherent interest in the discovery of redox couples that avoid some or all of these problems while still functioning efficiently as mediators in the DSSC. Several years ago, we reported that certain polypyridine complexes of cobalt function as reasonable DSSC mediators exhibiting relative efficiencies greater than 80% of a comparable I^-/I_3^- mediated cell without most of the undesirable properties of the I^-/I_3^- couple.¹¹ Of the polypyridine cobalt mediators studied thus far, tris(2,2'-bipyridyl-4,4'-di-*tert*-butyl)cobalt(II/III) ($Co(DTB)_3^{2+/3+}$) is one of the best in our hands.

As mentioned above, increasing the thickness of the absorbing dyed TiO_2 layer does not result in a proportional increase in photocurrent. The I^-/I_3^- couple imposes restrictions on strategies that might be employed to deal with this and other issues. When unbridled from these restrictions by employing the $Co(DTB)_3^{2+/3+}$ mediator system, a number of otherwise unavailable options present themselves. For example, one possible

way to circumvent the problem associated with increasing the photoanode thickness is to run multiple cells in optical tandem (i.e. stack them). Doing this requires, however, that the cathode be optically transparent.

While many electrode materials function at least adequately as cathodes in $\text{Co}(\text{DTB})_3^{2+/3+}$ -mediated cells (gold, carbon, platinum), they are opaque. In contrast, native (unmodified) transparent indium doped tin oxide (ITO) and fluorine doped tin oxide (FTO) electrodes function extremely poorly as cathodes in $\text{Co}(\text{DTB})_3^{2+/3+}$ -mediated cells.¹¹ However, when these optically transparent conducting oxides (collectively TCO) are modified by adsorbing certain metal complexes on their surfaces, they become catalytic to the oxidation of $\text{Co}(\text{DTB})_3^{2+}$.¹² Moreover, when the $E_{1/2}$ of the adsorbed catalyst coincides with that of $\text{Co}(\text{DTB})_3^{2+/3+}$, both the oxidation and reduction of the $\text{Co}(\text{DTB})_3^{2+/3+}$ are catalyzed resulting in quasi-reversible voltammetry. An example of such a catalyst is *cis*-dichloro-bis(2,2'-bipyridyl-4,4'-dicarboxylic acid)osmium(II) ($[\text{Os}(\text{DCB})_2]\text{Cl}_2$).

In the following we describe studies of stacked DSSCs of two types, each employing ($[\text{Os}(\text{DCB})_2]\text{Cl}_2$)-modified transparent FTO cathodes. In the first series of investigations, we consider stacked cells employing only photoanodes dyed with the standard N3 dye.¹³ In the second, we consider stacked cells employing an N3 dyed anode stacked with an anode dyed with a dicarboxylated cyanine dye.⁵ The cyanine dye, R8, has a spectrum complementary to that of N3 and thus has the potential to capture a larger portion of the long wavelength spectrum.



R8

4.3 Results and Discussion

Osmium Modified Transparent Cathodes

As stated in the Introduction, many materials function as cathodes in $\text{Co}(\text{DTB})_3^{2+/3+}$ mediated DSSCs; however, bare TCO electrodes do not. This is not unexpected because, were heterogeneous electron transfer between the $\text{Co}(\text{DTB})_3^{2+/3+}$ couple and FTO rapid, recombination between photo-injected electrons in the FTO conduction band and $\text{Co}(\text{DTB})_3^{3+}$ would also be fast. In an earlier study we demonstrated that, in contrast to bare TCO substrates, FTO and ITO electrodes modified by irreversibly adsorbing a monolayer of $\text{Fe}(\text{DCB})_3^{2+}$ very efficiently oxidized $\text{Co}(\text{DTB})_3^{2+}$.¹² In this case, the oxidized $\text{Fe}(\text{DCB})_3^{3+}$ surface species catalyzes the oxidation of $\text{Co}(\text{DTB})_3^{2+}$ via an EC' (i.e., surface catalytic) mechanism. The $E_{1/2}$ for the $\text{Fe}(\text{DCB})_3^{2+/3+}$ couple is significantly more positive than that of $\text{Co}(\text{DTB})_3^{2+/3+}$; consequently, Fe(III) has more than sufficient oxidizing strength to oxidize Co(II) but Fe(II) is thermodynamically too weak a reductant to reduce Co(III). Because the reaction of interest at the cathode in the DSSC is Co(III) reduction, the $\text{Fe}(\text{DCB})_3^{2+/3+}$ couple is of no value in this regard. However, we have further determined that catalysis of $\text{Co}(\text{DTB})_3^{2+}$ oxidation by surface-bound, redox-active metal complexes is a relatively general phenomenon. It was, therefore, reasonable to believe that, given a metal complex with a sufficiently negative $E_{1/2}$, catalytic reduction of $\text{Co}(\text{DTB})_3^{3+}$ would also be

possible. Based on solution redox potentials, we first considered *cis*-dichloro-bis(4,4'-dicarboxylic acid-2,2'-bipyridine)ruthenium(II). Unfortunately, when adsorbed to TCO substrates, the $E_{1/2}$ of this complex shifts to a potential which is too positive to reduce $\text{Co}(\text{DTB})_3^{3+}$ efficiently. Due to its inherently more negative solution $E_{1/2}$, the corresponding osmium(II) complex, *cis*-dichloro-bis(2,2'-bipyridyl-4,4'-dicarboxylic acid)osmium(II), was synthesized and used to modify the TCO substrate electrodes. When adsorbed on TCO, the surface $E_{1/2}$ of $[\text{Co}(\text{DTB})_3](\text{ClO}_4)_2$ is ca. -310 mV versus ferrocene/ferrocenium, which is slightly negative of the potential for the $\text{Co}(\text{DTB})_3^{2+/3+}$ couple. Consequently, these modified TCO electrodes proved to efficiently catalyze both the oxidation and reduction of $\text{Co}(\text{DTB})_3^{2+/3+}$.

To more quantitatively evaluate the redox activity of $[\text{Os}(\text{DCB})_2]\text{Cl}_2$ -modified TCO electrodes, the CV behavior of $\text{Co}(\text{DTB})_3^{2+}$ in solution was investigated. Working electrodes of vapor deposited gold (i.e., the typical cathode used in $\text{Co}(\text{DTB})_3^{2+/3+}$ mediated DSSCs), FTO and ITO (both $[\text{Os}(\text{DCB})_2]\text{Cl}_2$ -modified and unmodified), all patterned to the same shape and area, were compared. The results are shown in Figure 1.

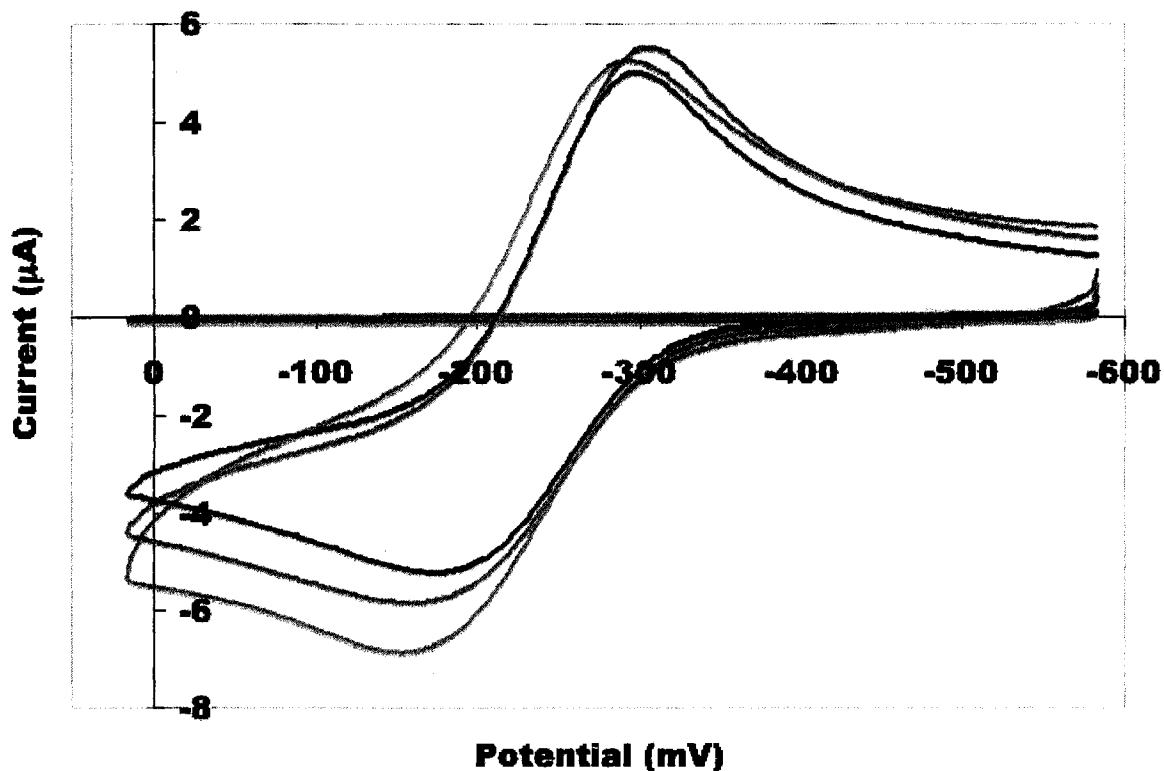


Figure 1. CVs of gold (red), FTO (brown), ITO (violet), $[\text{Os}(\text{DCB})_2]\text{Cl}_2$ modified FTO (green), and $[\text{Os}(\text{DCB})_2]\text{Cl}_2$ modified ITO (blue) working electrodes with ~ 0.1 mM $[\text{Co}(\text{DTB})_3](\text{ClO}_4)_2$ in acetonitrile. The $[\text{Os}(\text{DCB})_2]\text{Cl}_2$ modified electrodes give CVs nearly identical to gold while unmodified TCO electrodes produce no current. Potentials are relative to ferrocene.

Essentially no current is observed on either unmodified ITO or FTO electrodes (Figure 1, brown and violet curves). In contrast TCO electrodes that had been modified with $[\text{Os}(\text{DCB})_2]\text{Cl}_2$ (Figure 1, blue and green curves) give voltammograms nearly identical to those obtained on gold (Figure 1, red curve). It must be noted that the cyclic voltammograms shown in Figure 1 are only quasi-reversible, evidenced by the magnitude of peak separation ($\Delta E_p \approx 140$ mV) and the broadness of the peaks. This is a result of the large inner-sphere reorganization energy typical of cobalt(II/II) redox processes.

Ideally in a DSSC under illumination, there is negligible electron-transfer resistance at the cathode and essentially all of the potential drop across the cell occurs at the photoanode.¹⁸ Based on the results from the CVs in Figure 1, however, one would

expect a large electron-transfer resistance in a photocell employing an unmodified TCO cathode and much smaller resistance upon modification of the TCO cathode with $[\text{Os}(\text{DCB})_2]\text{Cl}_2$. A three-electrode measurement, adapted from two previously reported procedures,^{18, 19} was devised to evaluate the cathode behavior. The cell bias was controlled externally while simultaneously monitoring the potential of the cathode and anode relative to the reference. This approach provides the photoanode potential (E_{an} vs. ref.), cathode potential (E_{cat} vs. ref.), cell potential ($E_{\text{cell}} = E_{\text{cat}} - E_{\text{an}}$), and current throughout a single scan.

The data from three cells employing different cathodes are shown in Figure 2.

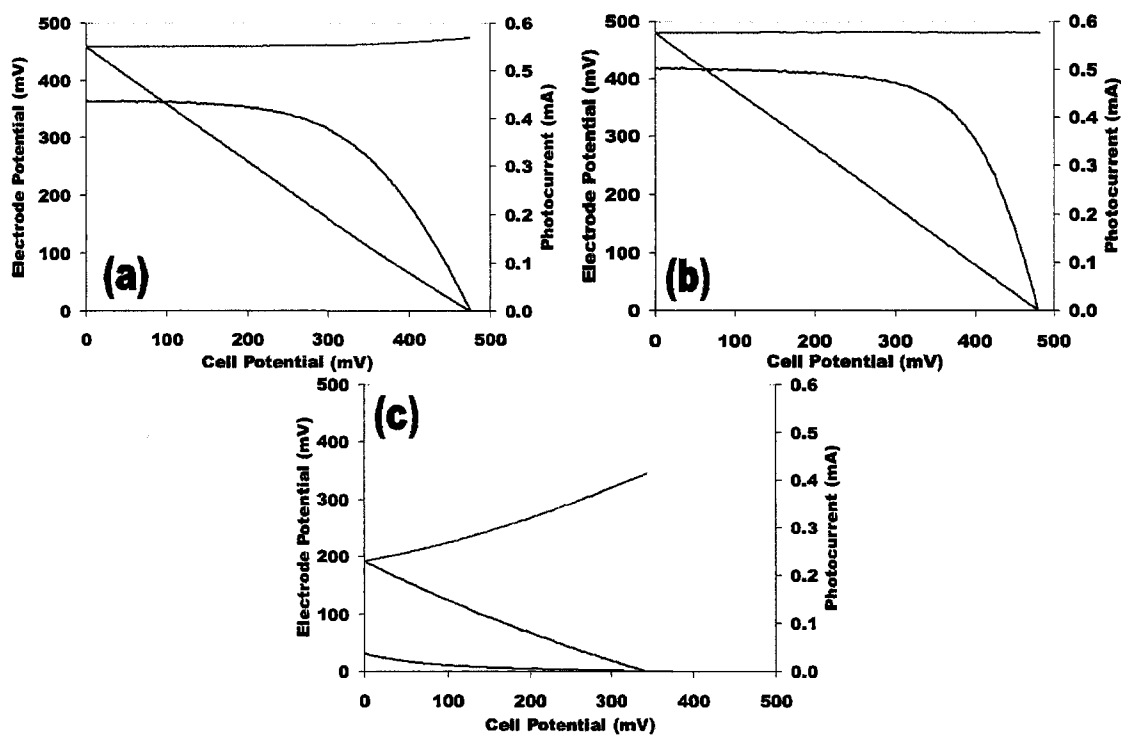


Figure 2. Results from 3-electrode cell experiments with $[\text{Os}(\text{DCB})_2]\text{Cl}_2$ modified FTO cathode (2a), gold cathode (2b), and unmodified FTO (2c). The black curves are current, the red curves are E_{cat} and the blue curves are E_{an} .

The horizontal-axis for all plots is E_{cell} . Electrode potentials (E_{cat} , E_{an}) are plotted using the left vertical-axis and are relative to the photocell's V_{oc} , determined by adjusting the reference potential slightly to account for the slight differences in V_{oc} commonly

observed between the two photoanode halves (*vide supra*). Due to the difficulty of measuring the true illuminated area of the photoanode, cell current rather than the current density is also shown (right vertical-axis). Figure 2A shows results for a cell incorporating an osmium-modified FTO cathode. The V_{oc} of the active cell corresponds to the E_{cell} at which no current flows (475 mV). At V_{oc} there exists a large difference between E_{an} (essentially the quasi-Fermi energy of the FTO) and E_{cat} (the potential of which is determined by the mediator composition in solution). At short circuit, both electrodes are at the same potential ($E_{cell} = 0$), which is slightly negative of the mediator's reduction potential. This small magnitude of overpotential (~ 12 mV at short circuit) is characteristic of cathodes capable of efficiently reducing the redox mediator. Analogous results for a DSSC incorporating a gold cathode are shown in Figure 2B. With this cathode, no experimentally significant overpotential was required over the entire applied potential range, as evidenced by a perfectly constant E_{cat} . The situation is very different for an unmodified FTO cathode shown in Figure 2C. In this case, there is a very large potential drop needed at short circuit just to supply a very modest current. Clearly, both the current-voltage and electrode potential curves indicate that unmodified FTO is ill-suited as a cathode in DSSCs mediated by $Co(DTB)_3^{2+/3+}$.

Stacked Cells

UV-Vis spectra of photoanodes with three different thicknesses of TiO_2 dyed with N3 are shown in Figure 3.

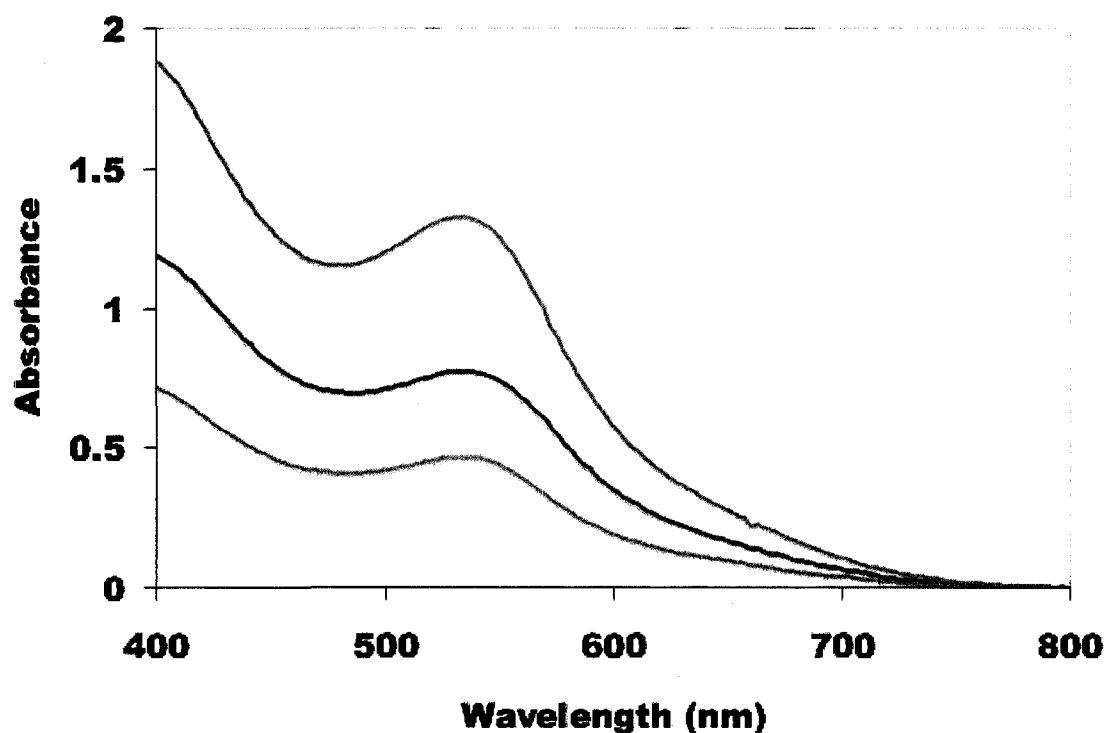


Figure 3. Visible absorption spectra of N3 dyed TiO₂. TiO₂ layers were 2.4 μm (red), 4.4 μm (blue), and 7.8 μm (green).

These absorption spectra are qualitatively similar to the solution spectrum of N3, exhibiting strong broad absorptions in the 400 to 550 nm region of the spectrum. As anticipated, the absorbance scales proportionately with the thickness of the TiO₂ layer. At longer wavelengths the N3 absorbs progressively less light until ca. 650 nm where little of the incident light is absorbed even for the thickest TiO₂ layer. In contrast to N3, the R8 cyanine dye has its maximum absorption at longer wavelengths. Figure 4 demonstrates the spectral complementarity of TiO₂ layers of similar thicknesses (ca. 2.4 μm) sensitized with the two dyes.

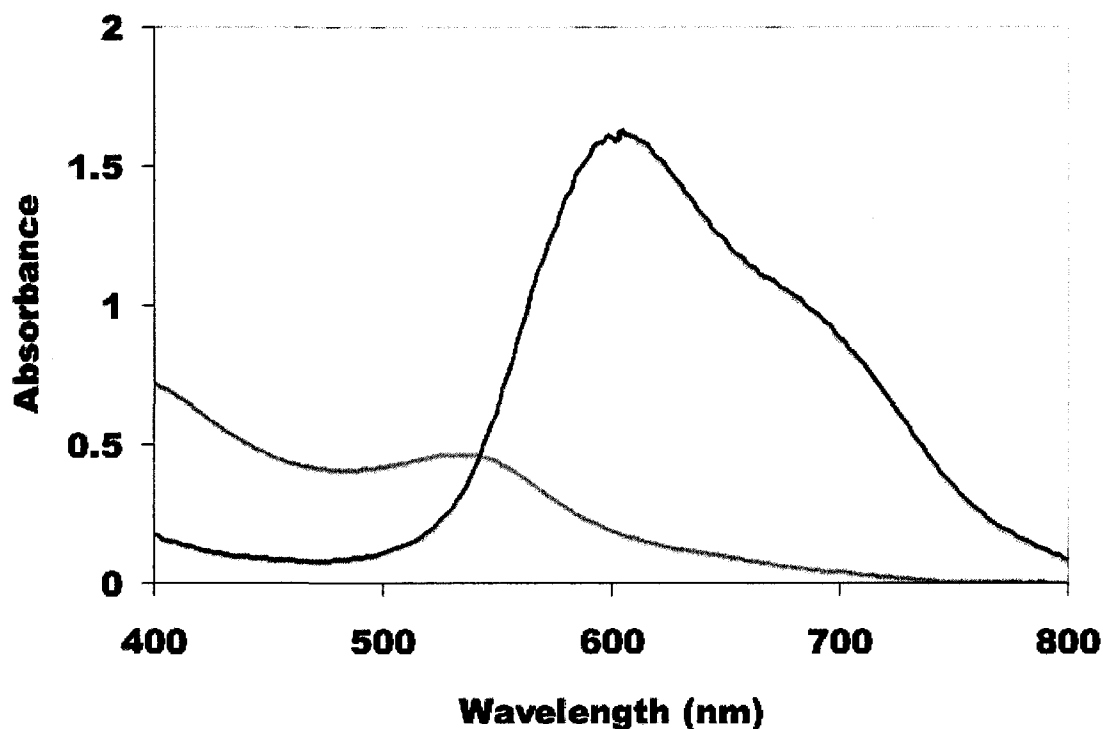


Figure 4. Visible absorption spectra of N3 dyed (red) and R8 dyed (blue) TiO₂. TiO₂ layers were 2.4 μm.

It is clear from Figure 4 that the R8 dye is a much stronger absorber than the N3 dye. In fact, when free in dilute solution the molar extinction coefficient of the R8 dye is ca. 100,000 M⁻¹ cm⁻¹.⁵ It has been observed that when cyanine dyes aggregate into dimers their molar extinction coefficient is reduced by ca. a factor of two.²⁰⁻²² Using the literature molar extinction coefficient value for the N3 dye of 14,200 M⁻¹ cm⁻¹,¹³ and half of the literature value for the R8 dye, one calculates roughly equal surface concentrations of the two dyes. Even with the decreased molar extinction coefficient due to aggregation, the R8 dye is still a stronger absorber than the N3 dye by ca. a factor of 3.5 times and absorbs in a region where the N3 dye does not.

To investigate the potential utility of an optically transparent DSSC cathode, two types of cells were prepared and examined. Each consisted of two individual cells, wired

in parallel and operated in optical tandem (i.e., “stacked”). The top, or front, photoanode (closest to the source of illumination) is paired with an $[\text{Os}(\text{DCB})_2]\text{Cl}_2$ -modified FTO cathode. The second photoanode is paired with a conventional gold cathode.

The first type of cell considered employs two N3-dyed photoanodes of the same thickness (half-scotch, ca. $2.4\ \mu\text{m}$) stacked together. The performance of this cell was compared with a single photoanode of ca. twice the thickness (one-scotch, ca. $4.4\ \mu\text{m}$) paired with a gold cathode. Current voltage curves for these cells are shown in Figure 5.

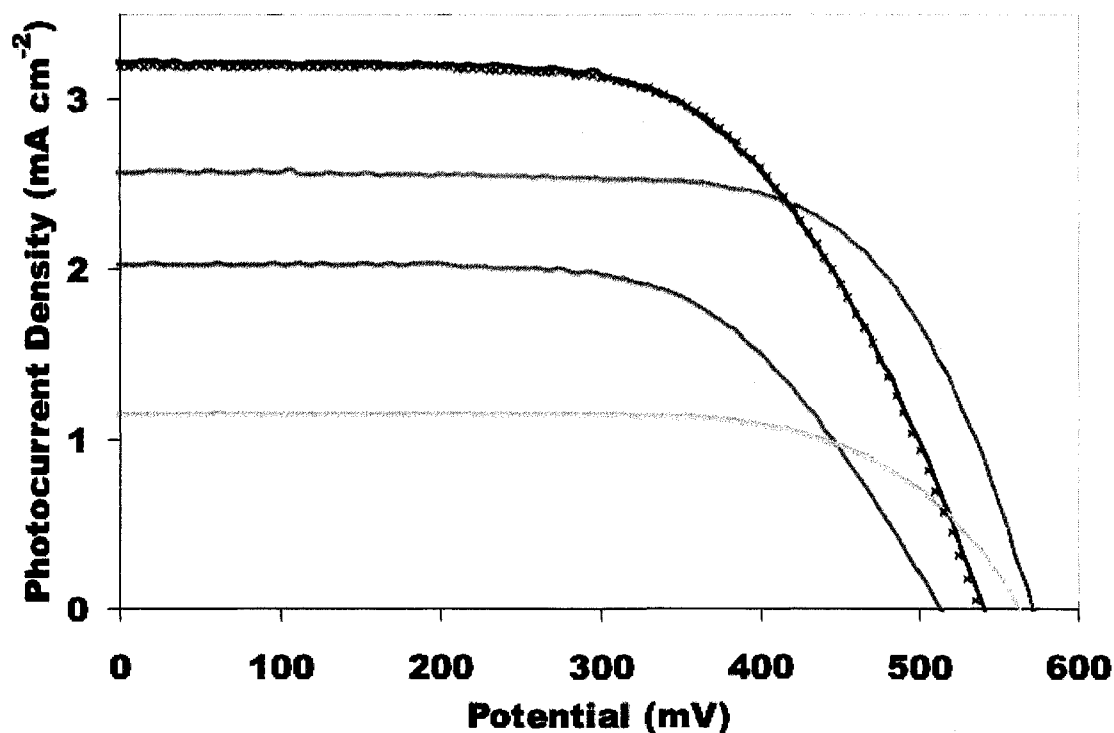


Figure 5. I-V curves for “one-scotch” cell (red), “half-scotch” stacked cell with both cells active (blue), front cell only (green) and back cell only (orange). Green and orange curves sum numerically (\times 's) to overlay the blue curve.

Comparing the half-scotch stack (blue trace) with the one-scotch cell (red trace), the short-circuit current density, J_{sc} , of the half-scotch stack is 25% higher and the efficiency is 10% higher. Also shown in Figure 5 is how the front (green trace) and back (orange trace) cells in the half scotch stack sum numerically to give the total output of the stack

(x's). The overall current densities of the stack are the sum of the current densities of the front and back cells at each potential. Similarly, as would be expected, the overall efficiency of the stack is the sum of the efficiencies for the front and back cells.

Since the absorbance of two half scotch layers roughly adds up to the absorbance of a one scotch layer (*vide infra*), it is reasonable to infer that the increase in current density of the stacked half scotch cells results from a decrease in the number of photo-injected electrons in the TiO₂ that combine with the oxidized form of the mediator and the photo-oxidized dye. The effect of both of these parasitic reactions is mitigated by decreasing the average time between charge separation and charge carrier collection. The decrease in overall V_{oc} of the half-scotch stack is due to the lower V_{oc} of the front cell. We have found over many experiments with cells employing Co(DTB)₃^{2+/3+} as mediator that there is an inherent variability in behavior between photoanodes that are ostensibly identical or even between cells disassembled and reassembled with the same photoanode. In that context, the experimental variability in V_{oc} (ca. ± 60 mV) between the different photoanodes used to gather the data presented in Figure 5 is within typical limits. On the other hand, while identical cells often exhibit variability in the V_{oc}, the J_{sc} is typically more reproducible with a variability of ca. ± 0.2 mA cm⁻². Consequently the differences in J_{sc} and efficiency between the half-scotch stack and one-scotch cell are experimentally significant even after accounting for the ca. 9% difference in absorbance resulting from the small difference in total TiO₂ thickness.

The experiments giving rise to the data in Figure 5 demonstrate that [Os(DCB)₂]Cl₂-modified FTO can serve as a functional cathode in DSSCs mediated with Co(DTB)₃^{2+/3+}. Figure 3 demonstrates that a considerable amount of the long wavelength

portion of the visible solar spectrum will not be absorbed by N3 at any practical photoanode thickness. It is thus reasonable to consider a tandem cell incorporating a second dye that is spectrally complimentary to N3 such as R8 (cf. Figure 4).

Ehret and co-workers examined a collection of dicarboxylated cyanine dyes as TiO₂ sensitizers in I⁻/I₃⁻ mediated DSSCs.⁵ Some of these dyes were reported to produce photoanodes with electron-injection efficiencies comparable to N3. One dye in their study is structurally quite similar to R8. Unfortunately, that particular dye which absorbs strongly in the red (hereafter the “blue dye”), gave only modest photocurrents and monochromatic conversion efficiencies (ca. 8%). Ehret and coworkers suggested that the poor injection efficiency likely results from dye aggregates on the surface that act as non-injecting traps.⁵ This interpretation is consistent with our spectral results for the R8-dyed photoanodes wherein the absorption maximum on TiO₂ ($\lambda_{\text{max}} = 600 \text{ nm}$) is shifted relative to dilute solution ($\lambda_{\text{max}} = 660 \text{ nm}$). Also consistent with dye aggregation, the absorbance is less than expected for a simple adsorbed monolayer of individual dye molecules. Nevertheless, the R8 dye absorbs in a spectral region where photons are largely wasted with an N3-dyed photoanode. Ehret and co-workers also observed that there was an optimum thickness of ca. 4 μm for the dyed TiO₂ layer (with both the N3 dye and cyanine dyes) above which the short circuit photocurrent asymptotically approached a limiting value.⁵ These observations suggest that some of the same issues (*vide supra*) involving loss of electrons from TiO₂/FTO to parasitic reactions are in play with cyanine-dyed photoanodes. Thus, potential advantages could accrue by considering tandem cells incorporating separate photoanodes dyed with N3 and R8 (i.e., in contrast to a single thicker photoanode incorporating both dyes).

The blue dye differs from R8 only in that the latter compound has one fewer methylene group in the alkyl chains of the carboxylic acid moieties. The presence of the carboxylic acid tail was reported to have only a minimal effect on both the absorption spectrum and redox potential (ca. 30 mV),⁵ consequently, it is reasonable to assume that the R8 dye will be similar in these respects to the blue dye. Using the reported redox potential for the D/D⁺ couple, there should be ample thermodynamic driving force for Co(DTB)₃²⁺ to reduce photo-oxidized R8 (ca. 450 mV).⁵ Moreover, their calculated potential for D^{*}/D⁺ indicates electron photo-injection from R8^{*} will occur.⁵

The fact that, relative to the blue dye, R8 has fewer methylene groups in the alkyl chain linking the cyanine and carboxylic acid moieties could affect its coupling to the TiO₂ and thus the efficiency of charge injection. To evaluate R8 in this regard, photoaction spectra were obtained.

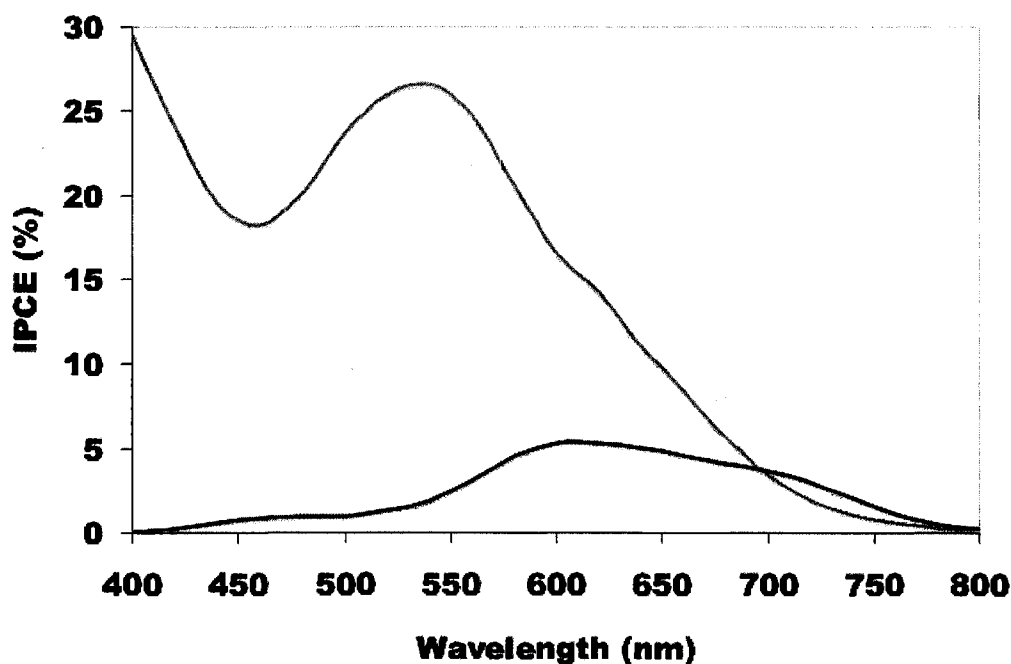


Figure 6. Photoaction spectra of operational DSSCs dyed with N3 (red) and R8 (blue). In both cells Co(DTB)₃^{2+/3+} was the redox mediator and a gold cathode was used. TiO₂ layers were 2.4 μm.

Figure 6 is a plot of incident photon to current efficiency (IPCE) versus wavelength for analogous cells incorporating photoanodes dyed respectively with R8 and N3. Based on these data, R8 appears to exhibit similar electron injection efficiency as the blue dye studied by Ehret even with its shorter linkage.

Despite its low photoelectron injection efficiency, R8 does absorb photons in a wavelength range where N3 does not. A half-scotch stack where the front photoanode was sensitized with N3 and the back photoanode was sensitized with R8 was assembled and evaluated. The resulting current-voltage curves are shown in Figure 7.

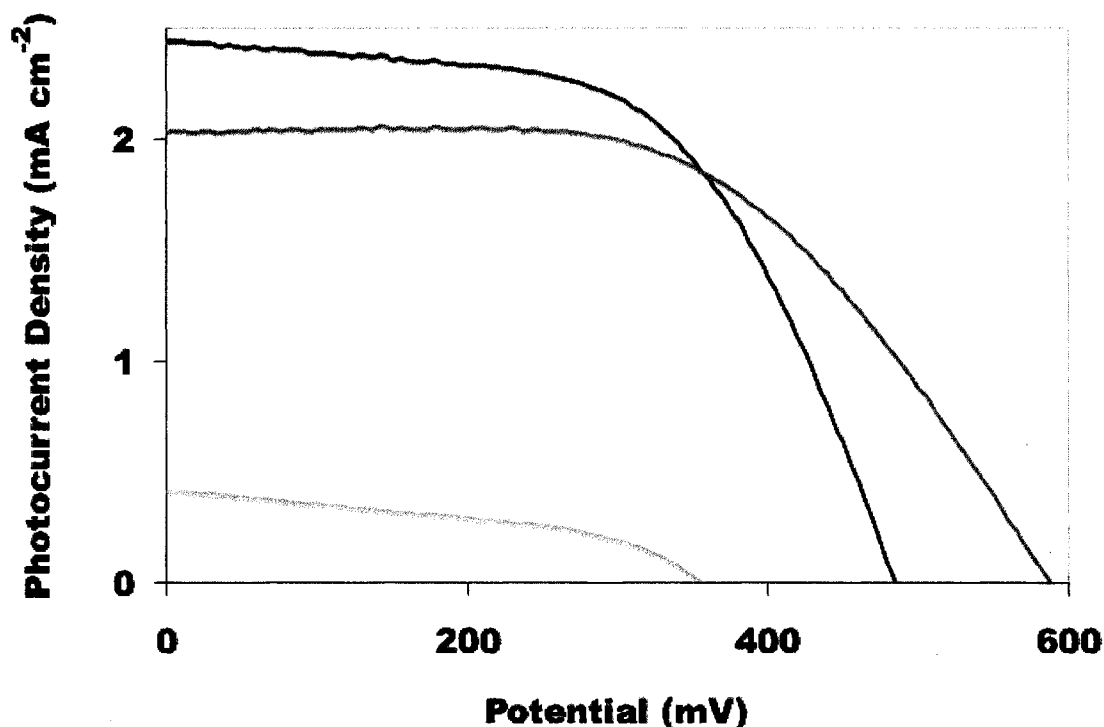


Figure 7. I-V curve for stacked cell employing “half-scotch” photoanodes (blue). Front cell (green) is N3 dyed photoanode with $[\text{Os}(\text{DCB})_2]\text{Cl}_2$ modified FTO cathode, back cell (orange) is R8 dyed photoanode with gold cathode.

The N3/R8 combination performed less well than the two half-scotch N3 stack, yielding a V_{oc} of 485 mV, a J_{sc} of 2.44 mA cm^{-2} , and an efficiency of 0.67%. Additionally, the overall current voltage curve was substantially non-ideal in shape. All of these

imperfections notwithstanding, the J_{sc} and overall power output of the tandem cell were greater than that of the front N3 cell alone, demonstrating proof of concept. With a better performing sensitizer than R8, one could expect a substantial improvement in performance relative to cells having a single photoanode dyed with N3.

4.4 Conclusions

Although DSSCs have great potential as inexpensive alternatives to more conventional solar conversion approaches, there are inherent issues with these cells that must be understood and problems to be overcome. The diffusive nature of charge carrier transport in the solid phase for electrons and the liquid phase for holes makes the distance between charge collecting substrates a significant factor in the cell's performance. By employing electron transfer mediator systems such as $\text{Co}(\text{DTB})_3^{2+/3+}$ it becomes possible to investigate new options for addressing such issues—options that are not open to investigation with the I^-/I_3^- mediator system. We have found that, by proper chemical modification, transparent conducting metal oxide electrodes can perform as transparent cathodes in $\text{Co}(\text{DTB})_3^{2+/3+}$ -mediated DSSCs. By employing these optically transparent cathodes and operating two cells in optical tandem, both the short-circuit current density and the overall cell efficiency can be increased. Relative to cells with a single thicker photoanode, the improved performance from stacked-cells with two photoanodes dyed with the same dye likely arises from the shorter residence time of the electrons in the TiO_2 conduction band. When a second optically complimentary dye is employed with a second photoanode, a broader wavelength range of photon absorption can be realized.

4.5 Acknowledgements

Support of this work through a grant from the U.S. Department of Energy Office of Science (DE-FG02-04ER15591) is acknowledged. Also, the authors wish to thank Professor Bruce A. Parkinson for providing us with samples of the cyanine dye.

4.6 Supplemental Information

TiCl₄ Treatment of Photoanodes

Nazeeruddin et al.¹³ and others have established that the overall performance of photoanodes in I⁻/I₃⁻ mediated cells is substantially improved by treating the as-formed anodes (prior to dyeing) with TiCl₄. Ostensibly, this process does a number of things including coating the FTO with a thin compact layer of TiO₂ which decreases the surface concentration of impurities that can inhibit electron injection, and improving the particle-particle electrical contact in the mesoporous TiO₂ layer. We have observed a similar improvement in performance of Co(DTB)₃^{2+/3+} mediated cells upon TiCl₄ treatment. Scanning electron microscopy of TiO₂ layers before and after TiCl₄ treatment show only very minor changes - specifically, the individual particles appear to have enlarged somewhat (Figure S1). The TiCl₄ treatment nonetheless resulted in a clear increase in the open circuit voltage and short circuit current. In a typical example, the V_{oc} increases by 5%, while the J_{sc} increases by 12%, resulting in an 8% increase in fill factor and a 30% increase in efficiency (Figure S2).

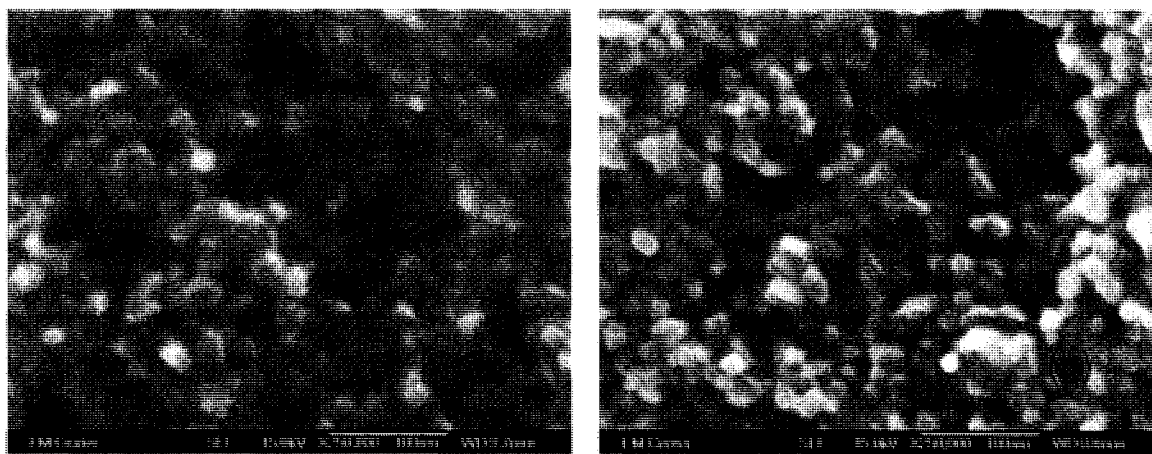


Figure S1. SEM image of mesoporous TiO₂ deposited on FTO conducting glass before (a) and after (b) TiCl₄ treatment.

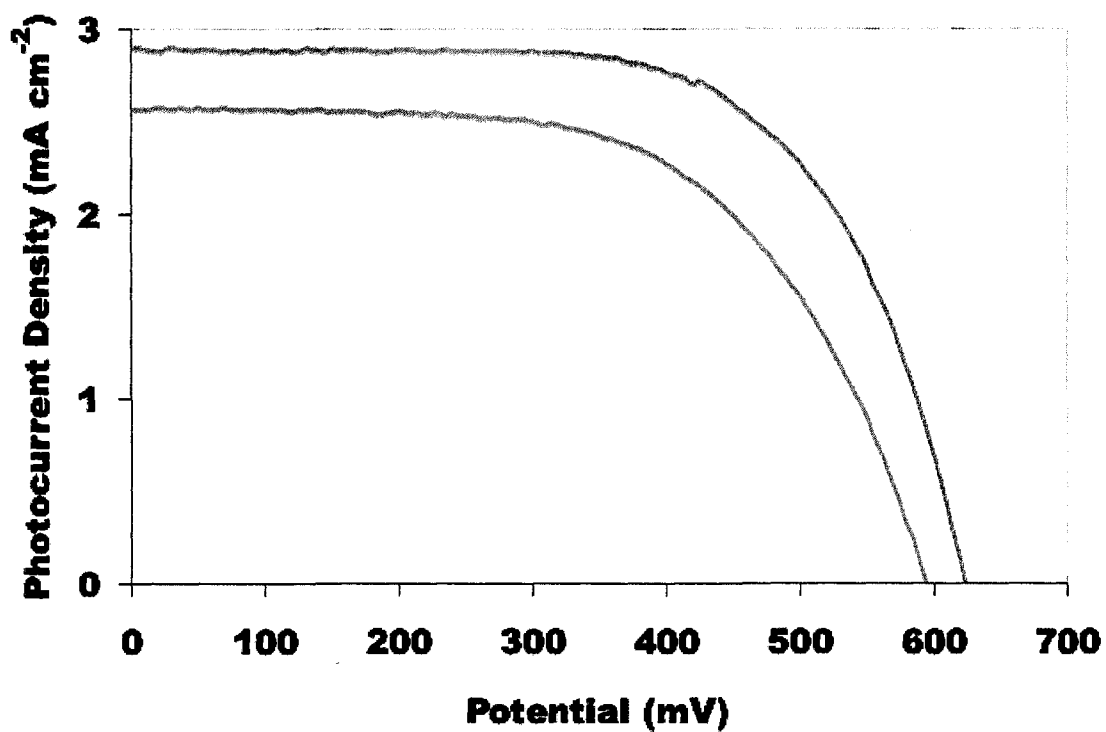


Figure S2. I-V curves comparing DSSCs with untreated (blue) and TiCl₄ treated (red) photoanodes.

Cyclic voltammogram of unmodified FTO electrode and [Os(DCB)₂]Cl₂-modified FTO electrodes relative to E_{1/2} of Co(DTB)₃^{2+/3+}.

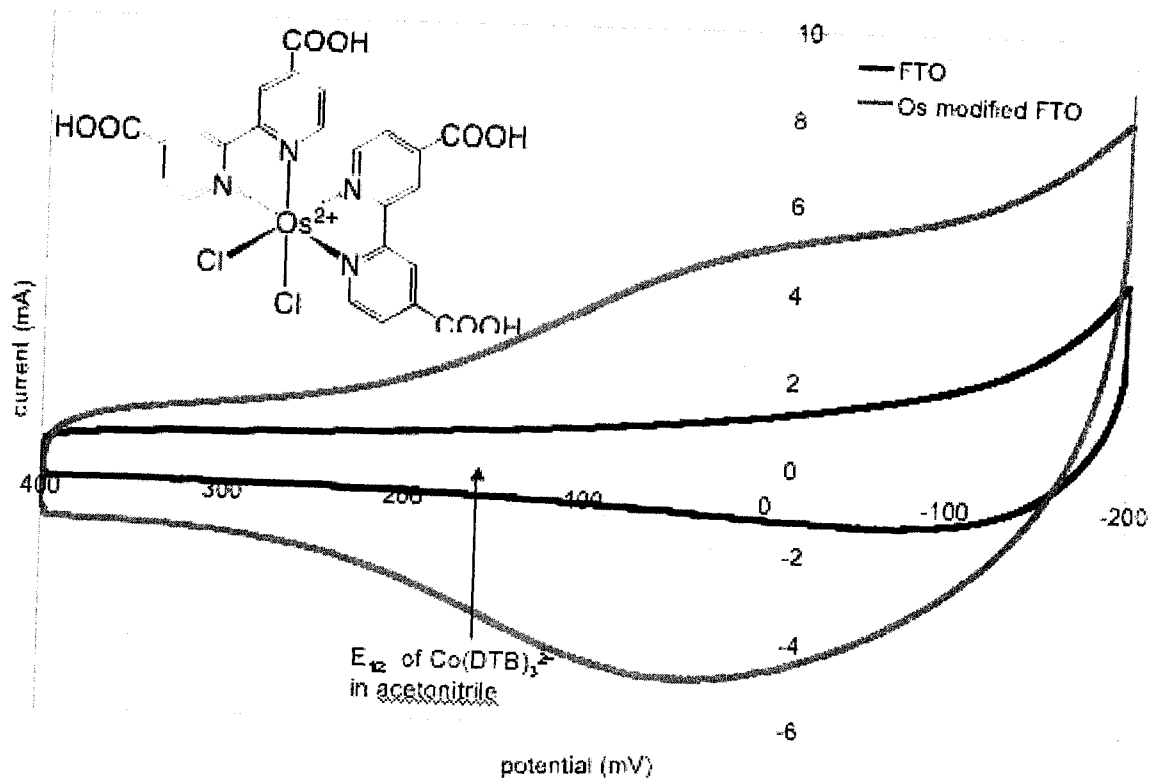


Figure S3. CV of $[\text{Os}(\text{DCB})_2]\text{Cl}_2$ modified FTO electrode (purple) and unmodified FTO electrode (blue) with 0.1 M tetraethyl ammonium perchlorate in acetonitrile. The $E_{1/2}$ of $\text{Co}(\text{DTB})_3^{2+/3+}$ is indicated by the arrow for reference.

4.7 References

1. Oregan, B.; Grätzel, M., A Low-Cost, High-Efficiency Solar-Cell Based on Dye-Sensitized Colloidal TiO₂ Films. *Nature* **1991**, 353, (6346), 737-740.
2. Bisquert, J.; Garcia-Belmonte, G.; Fabregat-Santiago, F., Modelling the electric potential distribution in the dark in nanoporous semiconductor electrodes. *Journal of Solid State Electrochemistry* **1999**, 3, (6), 337-347.
3. Rothenberger, G.; Fitzmaurice, D.; Grätzel, M., Spectroscopy of Conduction-Band Electrons in Transparent Metal-Oxide Semiconductor-Films - Optical Determination of the Flat-Band Potential of Colloidal Titanium-Dioxide Films. *Journal of Physical Chemistry* **1992**, 96, (14), 5983-5986.
4. Nelson, J., Continuous-time random-walk model of electron transport in nanocrystalline TiO₂ electrodes. *Physical Review B* **1999**, 59, (23), 15374-15380.
5. Ehret, A.; Stuhl, L.; Spitler, M. T., Spectral sensitization of TiO₂ nanocrystalline electrodes with aggregated cyanine dyes. *Journal of Physical Chemistry B* **2001**, 105, (41), 9960-9965.
6. Gregg, B. A.; Pichot, F.; Ferrere, S.; Fields, C. L., Interfacial recombination processes in dye-sensitized solar cells and methods to passivate the interfaces. *Journal of Physical Chemistry B* **2001**, 105, (7), 1422-1429.
7. Montanari, I.; Nelson, J.; Durrant, J. R., Iodide electron transfer kinetics in dye-sensitized nanocrystalline TiO₂ films. *Journal of Physical Chemistry B* **2002**, 106, (47), 12203-12210.
8. Cazzanti, S.; Caramori, S.; Argazzi, R.; Elliott, C. M.; Bignozzi, C. A., Efficient non-corrosive electron-transfer mediator mixtures for dye-sensitized solar cells. *Journal of the American Chemical Society* **2006**, 128, (31), 9996-9997.
9. Scott, M. J.; Elliott, C. M., Unpublished Results.
10. Nusbaumer, H.; Moser, J. E.; Zakeeruddin, S. M.; Nazeeruddin, M. K.; Grätzel, M., Co^{II}(dbbip)₂²⁺ complex rivals tri-iodide/iodide redox mediator in dye-sensitized photovoltaic cells. *Journal of Physical Chemistry B* **2001**, 105, (43), 10461-10464.
11. Sapp, S. A.; Elliott, C. M.; Contado, C.; Caramori, S.; Bignozzi, C. A., Substituted Polypyridine Complexes of Cobalt(II/III) as Efficient Electron-Transfer Mediators in Dye-Sensitized Solar Cells. *Journal of the American Chemical Society* **2002**, 124, (37), 11215-11222.

12. Elliott, C. M.; Caramori, S.; Bignozzi, C. A., Indium tin oxide electrodes modified with tris(2,2'-bipyridine-4,4'-dicarboxylic acid) iron(II) and the catalytic oxidation of tris(4,4'-di-*tert*-butyl-2,2'-bipyridine)cobalt(II). *Langmuir* **2005**, 21, (7), 3022-3027.
13. Nazeeruddin, M. K.; Kay, A.; Rodicio, I.; Humphry-Baker, R.; Mueller, E.; Liska, P.; Vlachopoulos, N.; Grätzel, M., Conversion of light to electricity by cis-X₂-bis(2,2'-bipyridyl-4,4'-dicarboxylate)ruthenium(II) charge-transfer sensitizers (X = Cl⁻, Br⁻, I⁻, CN⁻, and SCN⁻) on nanocrystalline titanium dioxide electrodes. *Journal of the American Chemical Society* **1993**, 115, (14), 6382-90.
14. Fillinger, A.; Soltz, D.; Parkinson, B. A., Dye Sensitization of Natural Anatase Crystals with a Ruthenium-Based Dye. *Journal of the Electrochemical Society* **2002**, 149, (9), A1146-A1156.
15. Zaban, A.; Ferrere, S.; Sprague, J.; Gregg, B. A., pH-dependent redox potential induced in a sensitizing dye by adsorption onto TiO₂. *Journal of Physical Chemistry B* **1997**, 101, (1), 55-57.
16. Buckingham, D. A.; Dwyer, F. P.; Goodwin, H. A.; Sargeson, A. M., Mono- and bis-(2,2'-bipyridine) and (1,10-phenanthroline) chelates of Ruthenium and Osmium IV. Bis chelates of bivalent and trivalent Osmium. *Australian Journal of Chemistry* **1964**, 17, (3), 325-336.
17. Xue, D.; Elliott, C. M.; Gong, P.; Grainger, D. W.; Bignozzi, C. A.; Caramori, S., Indirect electrochemical sensing of DNA hybridization based on the catalytic oxidation of cobalt (II). *Journal of the American Chemical Society* **2007**, 129, (7), 1854-1855.
18. Zaban, A.; Zhang, J.; Diamant, Y.; Melemed, O.; Bisquert, J., Internal reference electrode in dye sensitized solar cells for three-electrode electrochemical characterizations. *Journal of Physical Chemistry B* **2003**, 107, (25), 6022-6025.
19. Oskam, G.; Bergeron, B. V.; Meyer, G. J.; Searson, P. C., Pseudohalogens for dye-sensitized TiO₂ photoelectrochemical cells. *Journal of Physical Chemistry B* **2001**, 105, (29), 6867-6873.
20. Lenhard, J. R.; Cameron, A. D., Electrochemistry and Electronic-Spectra of Cyanine Dye Radicals in Acetonitrile. *Journal of Physical Chemistry* **1993**, 97, (19), 4916-4925.
21. Lenhard, J. R.; Parton, R. L., Electrochemical and Spectroscopic Analyses of the Thermodynamics of the Reversible Dimerization of Cyanine Radical Dications. *Journal of the American Chemical Society* **1987**, 109, (19), 5808-5813.

22. Parton, R. L.; Lenhard, J. R., Dimerization Reactions of Cyanine Radical Dications. *Journal of Organic Chemistry* **1990**, *55*, (1), 49-57.

CHAPTER 5

Spatially Resolved Current-Voltage Measurements--Evidence for Non-Uniform Photocurrents in Dye Sensitized Solar Cells

Michael J. Scott, Michael Woodhouse, Bruce A. Parkinson and C. Michael Elliott

Accepted for publication in the *Journal of the Electrochemical Society*. Printed here with permission from the authors.

This dissertation chapter contains the results from an article submitted for publication in the *Journal of the Electrochemical Society*. The manuscript was written primarily by Michael Scott and Mike Elliott. The chapter describes an analytical technique that yields a cross-sectional current profile of a dye-sensitized solar cell. The instrument used to collect this data was built by Michael Woodhouse. Current profile data and current-voltage data collected from the same cells are considered in a discussion of the causes of non-uniform current profiles.

5.1 Abstract

Spatial current distributions of dye-sensitized TiO₂ solar cells (DSSCs) mediated with a bipyridine-cobalt complex are described. By rastering a laser over the surface of a DSSC while measuring the short-circuit current a spatial current image is obtained. Experiments that highlight the potential uses of this technique are discussed. First, intentional damage inflicted on the photoanode and cathode of the DSSC are visualized with the scanning technique and second, the effects of increased pressure of the cell holder clamps are discussed and shown to warrant further investigation. Finally, other variations of the scanning technique are suggested.

5.2 Introduction

Dye sensitized solar cells (DSSCs) offer an inexpensive alternative to conventional solar cells.¹ Energy conversion in DSSCs proceeds by photo-oxidation of the sensitizing dye on the photoanode, reduction of the photo-oxidized dye by the redox mediator in solution, followed by reduction of the redox mediator at the cathode. These processes efficiently separate charge and confine the charge carriers to separate phases in the cell: the electron in the solid semiconductor and the hole in the liquid electrolyte. The operation of DSSCs depends on the very large surface area of the mesoporous TiO₂ semiconductor layer that makes up the photoanode.² This layer consists of nanoscopic TiO₂ particles (ca. 20 nm in diameter) in an irregular arrangement that resembles a sponge. A monolayer of dye adsorbed to this highly textured TiO₂ layer allows these cells to absorb a large portion of incident sunlight.

When considering the irradiated portion of a DSSC, it is typically assumed that the various operative electrochemical processes are uniform within any plane parallel to the photoanode. In other words, all variations in concentration of electrolyte etc. occur perpendicular to the electrode and that the current density over the irradiated region is also uniform.³ It is not clear, as we will demonstrate, that this assumption is always valid, especially in cells where no physical spacer separates the photoanode and cathode. Macht et al. using a related experimental design, showed that the photocurrent across an iodide mediated DSSC follows the thickness profile of the mesoporous TiO₂.⁴ In addition to non-uniform thickness, current variations can arise from the physical condition of the photoanode and cathode and of the pressure applied to hold the electrodes in place.

To further examine the question of lateral cell uniformity, we have employed a method for resolving the photocurrent response as a function of lateral position across the face of the photoanode. This is accomplished by rastering a focused laser across the cell while recording the short-circuit photocurrent (i_{sc}) as a function of beam position and thus producing a three-dimensional map of the cell's current response. The scanning light spot analysis of photocurrent generation has long been used to study the uniformity of response in solar cells⁵ and was first applied to liquid junction cells in 1980.⁶ Related methodologies have been used with I^-/I_3^- mediated DSSCs to determine electron diffusion lengths in nanostructured electrodes⁷ and to monitor long term performance changes under simulated solar irradiation.⁴

In what follows we describe results for two cells. For the first, we examine the effect of (intentional) physical damage to both the cathode and anode. In the second we examine the effects of increased pressure applied across a cell with an “intact” photoanode and cathode. Results from the latter cell show clearly that significant non-uniformities can result along the lateral dimensions, in particular these cells exhibit regions of significantly enhanced current or “hot-spots.”

5.3 Results and Discussion

In the first system examined, a cell was prepared that had intentional scratches across the center of both the photoanode and the cathode. The cell was assembled such that the respective scratches were oriented at approximately right angles to one another to produce a “crosshair” in the spatial current image (Figure 1).

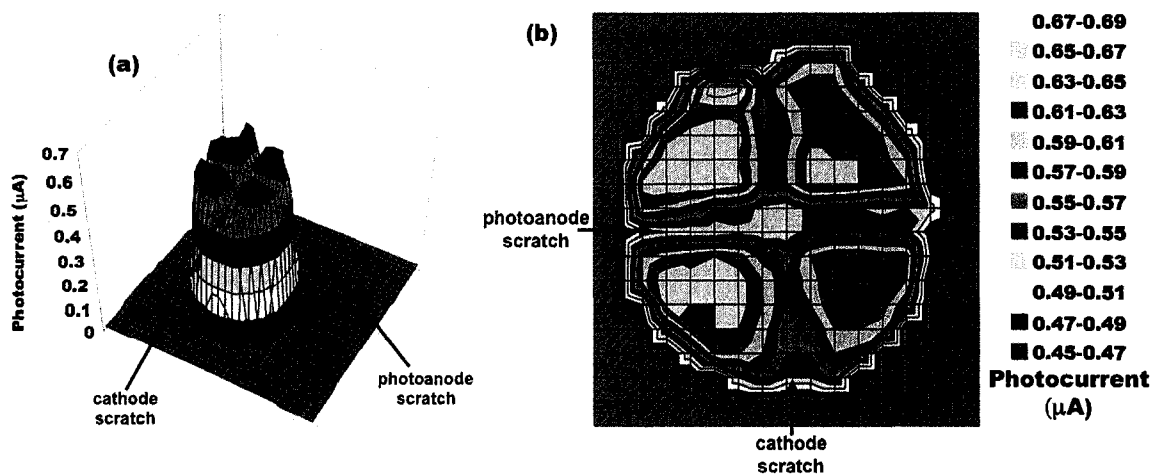


Figure 1. Three-dimensional crosshair image (1a) produced by arranging scratches on the photoanode and cathode perpendicular to one another. The false color image in Figure 1b shows the differences in current for the two scratches more quantitatively.

The current images in Figure 1 were acquired with a laser beam diameter of ca. 1 mm and a step size of ca. 450 μm . Notice that the currents are non-zero in the region of the scratches and that the “depth” of the current decrease is greater for the scratch on the photoanode. As presently configured, the width of each scratch (ca. 500 μm) is less than the spatial resolution of the instrument. Here the resolution is limited by the size of the laser spot, the fact that the step size of the laser was somewhat smaller than the diameter of the beam and scatter of the laser light as it passes through the substrate. These caveats notwithstanding, the effect of each feature on photocurrent is clearly evident. Additionally, it is evident that, in regions of the cell far from either scratch, there is experimentally significant variation in photocurrent over the cell face.

One potential application of this technique is to learn more about local phenomenon, for instance short circuits that can occur between the photoanode and cathode in DSSCs. Figure 2 shows a single DSSC that was characterized through a series of laser scan experiments.

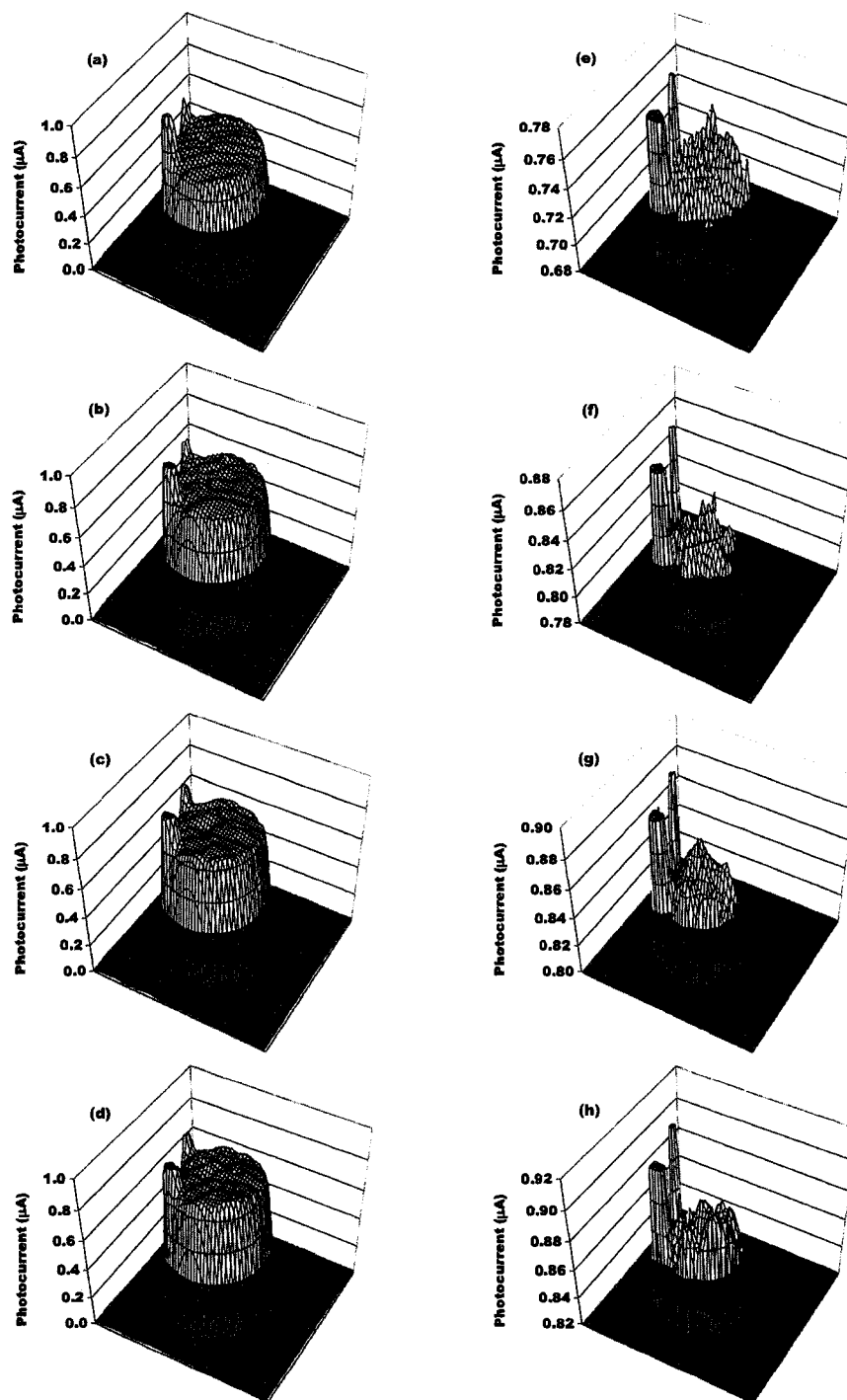


Figure 2. Spatial current image of a DSSC that was scanned with the clamps finger tight (2a,e), with 14.1 mNm of force on the clamps (2b,f), with 28.2 mNm of force on the clamps (2c,g), and with 42.3 mNm of force on the clamps (2d,h). The overall current increases as the pressure increases. The spatial current images shown on the right (2e, 2f, 2g,2h) are the same as those on the left with the exception that the scale of the z-axis has been made more sensitive.

The current images in Figure 2 were acquired with a laser beam diameter of ca. 1 mm and a step size of ca. 200 μm . Initially, the cell was assembled as described above and the clamps holding the electrodes in place were made finger tight. A laser scan experiment was completed, followed by a current-voltage experiment. The clamps were then tightened with a torque driver (Precision Instruments) to, respectively, 14 mN m, 28 mN m), and 42 mN m. A laser scan experiment and current-voltage experiment were again conducted immediately after each increase in tightness. Three things are of note: first, that the average current of the cell increases as the pressure increases, second, that several local current spikes (“hot-spots”) are present throughout the series of experiments and, third, that the localized current, excluding the hot-spots changes appearance as the pressure is increased (*vide infra*). It should be noted, however, that the apparent plateau of the two most intense hot-spots is not real and results from a current limitation of the instrument. Presumably the actual feature is “spike-shaped” and likely increases with pressure (*vide infra*) as does the average current. The increase in the average current with pressure can be rationalized as resulting from the decreased distance that the redox mediator molecules must travel (by diffusion and migration) to transit from the cathode, where the Co^{3+} complex is reduced, to the photoanode where the photo-oxidized dye molecules are reduced by the Co^{2+} complex.

Current-voltage experiments recorded after each laser scan are shown in Figure 3. When the cell was assembled finger tight a fill factor of 63% was attained. When pressure was applied to the clamps the fill factor decreased to 57%. Figure 3 also shows an overall short-circuit photocurrent increase as the pressure on the clamps increases and a small decrease in the open-circuit voltage (V_{OC}).

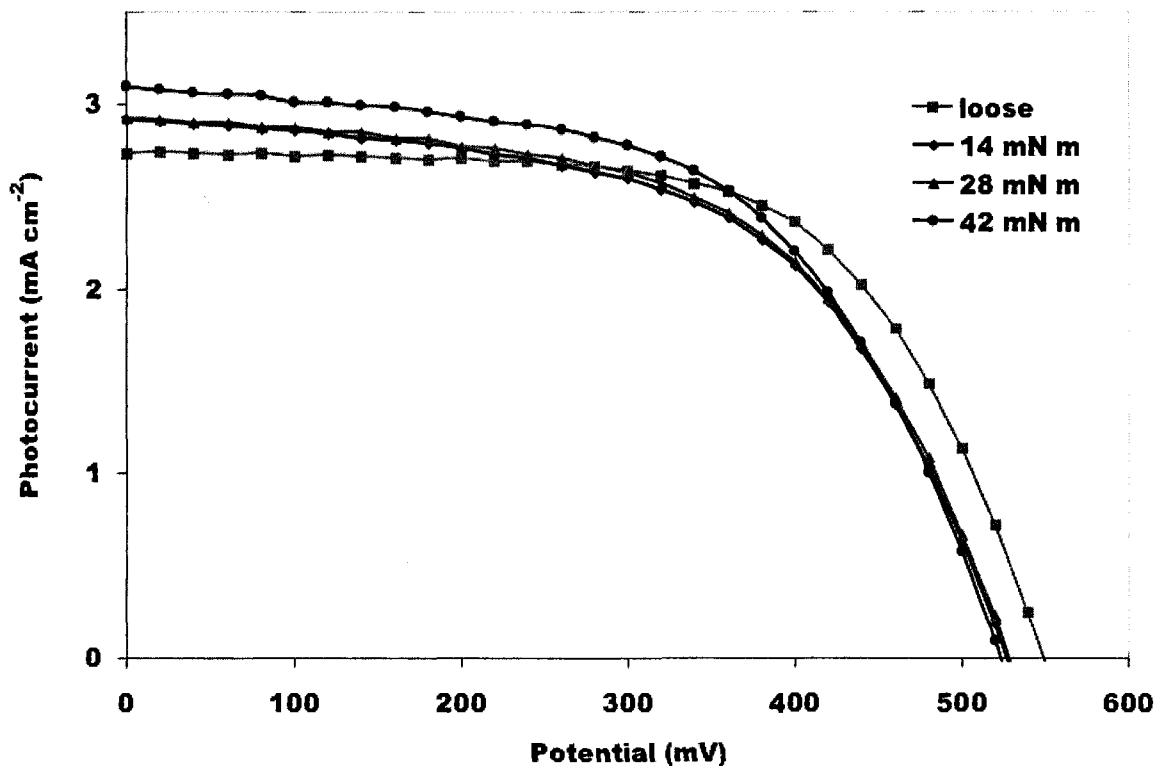


Figure 3. Current voltage scans of the cell shown in figure 2. As the pressure on the cell holder clamps was increased a short circuit caused the fill factor of the current voltage curves to decrease.

It must be stressed that the cell was not disassembled during this series of experiments.

The only change to the cell was that the inter-electrode pressure (and ostensibly distance) was decreased by tightening the cell holder clamps with the torque driver.

It seems unlikely that the hot-spots evident in Figure 2 are the result of shorts between the two electrodes since such a short should *decrease* the photo-current in that region, not increase it. Possibly these current features result from imperfections in either the anode or cathode surface that brings the two electrodes locally and substantially closer together but does not short them—however, this is only speculation. Nonetheless, the result is real and will require further study to develop a credible explanation. On the other hand, if the origin of these features can be understood it might be possible to

intentionally fabricate and exploit them to significantly increase the average photocurrent.

For a cell, such as this, where the photoanode and cathode are nominally in direct contact (i.e., no spacer), with increased pressure short(s) could develop between the two electrodes. It is obvious from Figure 2a-d that as the pressure is increased the qualitative appearance of the main plateau current (i.e. excluding the hot-spots) changes but there is no obvious indication of shorts which again, are expected to result in significant current decreases. However, the decrease in V_{oc} of ca. 20 mV and the decrease in fill factor are consistent with the presence of short circuits. When the cell is initially assembled finger-tight (Figure 2a and e) the plateau region of the current exhibits a regular “ wave pattern” in the current (most evident in Figure 2a). This spatial current oscillation could have several origins. First, it could result from physical oscillations in the photoanode surface created as the TiO_2 colloid was spread in fabricating the photoanode.⁴ Or it could be the result of an interference pattern in the irradiation resulting from slightly non-parallel orientations of thin layers of material (solution, TiO_2 , FTO, etc.) with different refractive index. Interestingly, comparing Figures 2a and b, the pattern appears to change frequency and rotate slightly as the first increase in pressure is applied. Were the pattern due to structure in the photoanode surface this type of change would not be expected. Consequently, we conclude that the apparent structure (at least at this resolution) is an optical interference phenomenon.

Figures 2e-h are the same data as in Figures 2a-d, respectively, plotted on a more sensitive current scale. Visual inspection of the currents in the plateau reveal the qualitative changes discussed above but does not reveal any obvious quantitative

differences. Shorts which developed with increasing applied pressure should result in localized decreases in current (*vide supra*). Moreover, if the region over which the current was affected by such a short was only slightly smaller than the spatial resolution of the technique, the individual decreases might not be evident upon visual examinations of the current data but would be reflected in an increased standard deviation of the average current. To examine this possibility more closely, a representative rectangular patch was selected on the top of the current plateau which excluded the obvious hot spots and avoided regions near the edges of the plateau. The total area of this patch was slightly less than half of the total illuminated area of the cell.

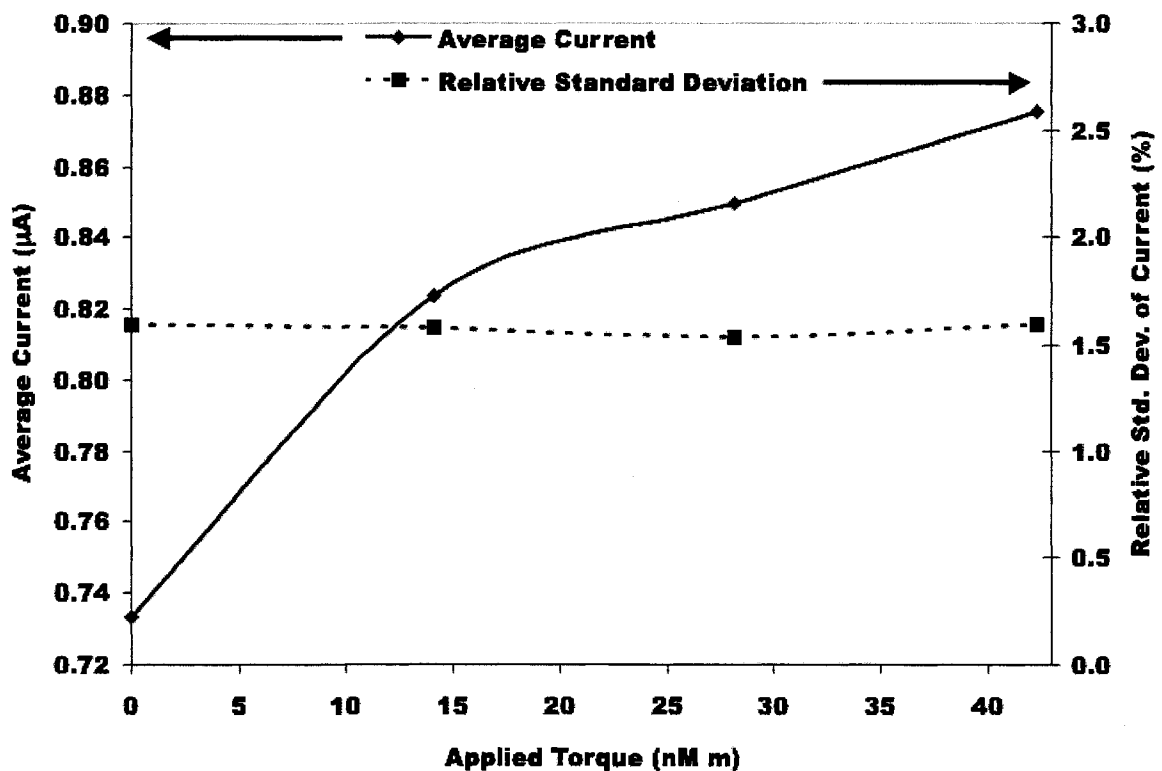


Figure 4. Effect of increasing inter-electrode pressure on average current (left axis, solid line) and relative standard deviation of current (right axis, dashed line). While the average current increases monotonically, the RSD remains constant.

As shown in Figure 4, when the pressure was progressively increased from finger-tight up to 42.3 mN m, the average current in the area monotonically increased by almost 20%

while the relative standard deviation of the current remained essentially constant at 1.5%. Consequently, if there are pressure-related phenomena at play (i.e., shorts, etc.) their effects are well below the spatial resolution of the technique as presently configured. It is interesting to note as well that the relative increase in average current in the representative area of the plateau is greater than the increase in the short-circuit photocurrent shown in Figure 3 (overall, ca. 10%). Since this latter measurement sums the current over the entire surface (including hot spots and edges), this may suggest that the current increase for the hot spots is relatively less than that for the electrode as a whole. This speculation comes with the caveat, however, that the light conditions are different for the two experiments. The i-V curve is obtained under CW white light irradiation while in the scan experiment the irradiation is monochromatic and spatially localized. In order to make a truly valid comparison, the scan experiment must be modified to allow the electrode to experience CW irradiation during the laser scan. Experiments of this type are planned.

The data represented in Figure 2 is just one example of data obtained from examinations of several cells. Typically, we have observed that some cells have relatively uniform current densities across the illuminated area while otherwise similar cells exhibit both “hot” and “cold” regions. Moreover, it is not at all obvious from visual inspection what these differences are due to. More in-depth studies incorporating spatially resolved measurements are called for (and in progress).

Finally, as part of their spatially resolved long-term stability studies of I/I_3^- mediated DSSCs, Macht et al. also observed unexplained local photocurrent spikes.⁴ These were smaller in relative (to the background photocurrent) amplitude and more

numerous (i.e., more spikes per unit area). Their apparatus incorporated a microscope objective through which the laser was focused, affording better spatial resolution. With the coarser resolution of our apparatus, spikes of the magnitude observed by Macht et al. would not be resolvable. Following the same reasoning, the current spikes shown in Figure 2 must therefore be much more pronounced—either in terms of a significantly larger relative amplitude and/or covering substantially larger area. We speculate that these “hot-spots” are fundamentally different in origin from those observed in the earlier study;⁴ moreover, we believe they are related to the special nature of the cobalt-based mediator system.

5.4 Conclusions

Spatially resolved photocurrent measurements can be valuable in studying the lateral variations in DSSC performance. Although not employed in the course of this study, spatially resolved V_{OC} measurements are possible as well.⁷ Through this approach we were able to identify regions of cobalt-mediated DSSCs which deviate substantially (i.e., both in terms of higher and lower currents) from the average performance obtained through more conventional current-voltage characterizations. The origins of those variations are under investigation.

5.5 Acknowledgements

Support for this work through grants from the US Department of Energy, Office of Science DE-FG02-04ER15591(C.M.E.) and DE-FG03-96ER14625(B.A.P.) is gratefully acknowledged.

5.6 References

1. Oregan, B.; Grätzel, M., A Low-Cost, High-Efficiency Solar-Cell Based on Dye-Sensitized Colloidal TiO₂ Films. *Nature* **1991**, 353, (6346), 737-740.
2. Nazeeruddin, M. K.; Kay, A.; Rodicio, I.; Humphry-Baker, R.; Mueller, E.; Liska, P.; Vlachopoulos, N.; Grätzel, M., Conversion of light to electricity by cis-X₂-bis(2,2'-bipyridyl-4,4'-dicarboxylate)ruthenium(II) charge-transfer sensitizers (X = Cl⁻, Br⁻, I⁻, CN⁻, and SCN⁻) on nanocrystalline titanium dioxide electrodes. *Journal of the American Chemical Society* **1993**, 115, (14), 6382-90.
3. Asano, T.; Kubo, T.; Nishikitani, Y., Short-circuit current density behavior of dye-sensitized solar cells. *Japanese Journal of Applied Physics Part 1-Regular Papers Brief Communications & Review Papers* **2005**, 44, (9A), 6776-6780.
4. Macht, B.; Turrion, M.; Barkschat, A.; Salvador, P.; Ellmer, K.; H., T., Patterns of efficiency and degradation in dye sensitization solar cells measured with imaging techniques. *Solar Energy Materials & Solar Cells* **2002**, 73, 163-173.
5. Cheek, G.; Inoue, N.; Goodnick, S.; Genis, A.; Wilmsen, C.; Dubow, J. B., Fabrication and Characterization of Indium Tin Oxide (ITO) Polycrystalline Silicon Solar-Cells. *Applied Physics Letters* **1978**, 33, (7), 643-645.
6. Furtak, T. E.; Canfield, D. C.; Parkinson, B. A., Scanning Light Spot Analysis of the Carrier Collection in Liquid-Junction Solar-Energy Converters. *Journal of Applied Physics* **1980**, 51, (11), 6018-6021.
7. Lana-Villarreal, T.; Monllor-Satoca, D.; Gomez, R.; Salvador, P., Determination of electron diffusion lengths in nanostructured oxide electrodes from photopotential maps obtained with the scanning microscope for semiconductor characterization. *Electrochemistry Communications* **2006**, 8, 1784-1790.

CHAPTER 6

Catalytic Phenothiazine Mediator Additives: Transient Laser Spectroscopy, DSSC Performance, and Catalytic Activity

This dissertation chapter describes the investigation of phenothiazine additives to cobalt mediator solutions employed in DSSCs. The ability of these compounds to reduce the photo-oxidized sensitizing dye was examined with transient absorption laser spectroscopy. The performance of the mixed mediator solutions was evaluated in operational DSSCs using current-voltage techniques. The electrochemistry of the mixed mediator solutions was studied using cyclic voltammetry. With the exception of the $E_{1/2}$ values quoted in Table 1, which were in part obtained from Jeremy Nelson, all data collection, manipulation, and manuscript preparation were completed by Michael Scott.

6.1 Introduction

To gain an increased understanding of the electron transfer processes in dye-sensitized solar cells it is desirable to separate the cell into its individual components and investigate each part individually. To accomplish an investigation of the recombination reactions that occur at the photoanode, transient absorption spectroscopy was employed.¹ Pseudo-photoanodes, where mesoporous TiO₂ is deposited on non-conducting glass and dyed, emulate an operational DSSC at open circuit. In this situation, when the sensitizing dye is excited by visible light, there are two reactions that can occur to reduce the photo-oxidized dye: (1) reduction of the photo-oxidized dye by the mediator, and (2) recombination of the photo-oxidized dye with the electron that was injected into the semi-conductor conduction band. This recombination reaction occurs in the microsecond to millisecond timeframe.²⁻⁴ In the open circuit situation of the transient absorption experiment, the reduced form of the mediator (i.e. Co(L)₃²⁺) reduces the photo-oxidized dye. The oxidized form of the mediator (i.e. Co(L)₃³⁺), is reduced by the electron that was injected into the semi-conductor conduction band. By measuring the lifetime of the photo-oxidized dye, which is accomplished by monitoring the change in the dye's absorbance as a function of time, the rate of photo-oxidized dye reduction by different mediator complexes can be compared. When the sensitizing dye is photo-oxidized, its absorbance at 480 nm is decreased resulting from a bleach of the dye. As the photo-oxidized dye is reduced, either by recombination or by the reduced form of the mediator, the original absorbance of the dye is restored. The ideal mediator will reduce the photo-oxidized dye at a rate much greater than that of the recombination reaction, so that the

largest amount of photo-injected electrons possible can be collected at the transparent conducting substrate and passed to the external circuit to do useful work.

In typical solution phase transient absorbance experiments a laser pulse excites the sample while a probe beam is used to measure the absorbance change at a particular wavelength.^{5,6} The wavelength of the pump beam corresponds to an absorbance feature of the analyte species. Typically, the pump and probe beams are aligned such that the pump beam enters the sample cuvette from one side while the probe beam enters the cuvette perpendicular to the pump beam. The sample cuvette is placed so the focal point of the probe beam is in the middle of the cuvette and the pump beam intersects the probe beam at the focal point. The probe beam emanates from a high power light source (e.g. a xenon lamp), is collimated, focused in the middle of the sample cuvette, recollimated, and focused on the entrance slit of a monochromator. The monochromator selects the wavelength of interest and the monochromatic light is then focused on a fast photomultiplier tube (PMT) that is connected to an oscilloscope. A chopper wheel that is synchronized with the laser pulse is placed in front of the monochromator to provide an optical experimental window, and to prevent continuous illumination of the PMT resulting in overloading of the PMT circuits.

It must be mentioned that there are special requirements when performing transient absorption spectroscopy experiments on thin films.^{1,3,4} First, consider a solution based spectroscopy experiment, using a 1 cm path-length cuvette to contain the sample. If the concentration of the analyte solution is 0.1 M, and the excitation laser beam has a diameter of 1 mm, there are ca. 10^{17} analyte molecules available for excitation in the volume of solution illuminated. With the same excitation beam, a 4 μm

thick film of mesoporous semiconductor (500x increase in surface area), and a molecular footprint of 1.65 nm^2 for the N3 dye,⁷ only ca. 10^{13} molecules will be available for excitation. By defocusing the laser beam to ca. 1 cm, the number of dye molecules available for excitation will increase by three orders of magnitude. Defocusing the laser not only increases the number of dye molecules on the thin film that are excited, it also decreases the laser fluence, more closely approximating incident sunlight. To take advantage of this greater area of excitation on the thin film, the sample is moved past the focal point of the probe beam so that the area of the sample probed is commensurate with the area excited. Because the sample consists of a thin film deposited on a glass substrate, it is impossible to utilize the perpendicular pump and probe beams configuration. The nature of the sample requires that the pump and probe beam are coincident, or the sample is placed at a 45 degree angle in a perpendicular pump-probe setup.⁴ A completely coincident pump-probe configuration would result in the excitation laser light propagating directly into the PMT, which would introduce a large background to the signal that represents the recovery of the photo-excited dye and overload the electronics of the PMT. To prevent this, the pump beam is brought in at a slight angle (ca. 5 degrees) to the probe beam. This results in the pump beam rapidly diverging from the probe beam when the probe beam is recollimated. Finally, a notch filter is placed in front of the entrance slit of the monochromator to absorb scatter from the pump beam and transmit a narrow band containing the wavelength of interest.

Current voltage (I-V) experiments have shown that bipyridyl-cobalt complexes function nearly as well as the iodide/tri-iodide redox couple that is typically used as a redox mediator in dye-sensitized solar cells.⁸ This is due to the low redox activity of

cobalt complexes on metal oxide electrodes (i.e., the mesoporous TiO₂ and underlying fluorine doped tin oxide, cf. Chapter 3). One of the benefits of using bipyridyl-cobalt complexes as the redox mediator in DSSCs is the ability to tune the E_{1/2} of the cobalt complex by substitution of electron donating or withdrawing functional groups on the bipyridyl ligands. Substitution of electron withdrawing functional groups will shift the E_{1/2} of the cobalt complex in the positive direction, increasing the maximum voltage of the cell (cf. Chapter 3). A potential drawback to this strategy is that, as the E_{1/2} of the cobalt complex is shifted more positive, the thermodynamic driving force for photo-oxidized dye reduction by the reduced form of the cobalt complex (Co(L)₃²⁺) will be decreased.

To investigate their ability to reduce the photo-oxidized dye, thin-film transient laser spectroscopy experiments were performed on three different cobalt complexes. The three complexes, tris(2,2'-bipyridyl-4,4'-di-*tert*-butyl)cobalt(II) perchlorate ([Co(DTB)₃](ClO₄)₂), tris(2,2'-bipyridyl-4,4'-di-*tert*-butylester)cobalt(II) perchlorate ([Co(DTBEST)₃](ClO₄)₂), and tris(2,2'-bipyridyl-4,4'-di-(bis-N,N-butylamide))cobalt(II) perchlorate ([Co(DBA)₃](ClO₄)₂), are shown in Figure 1.

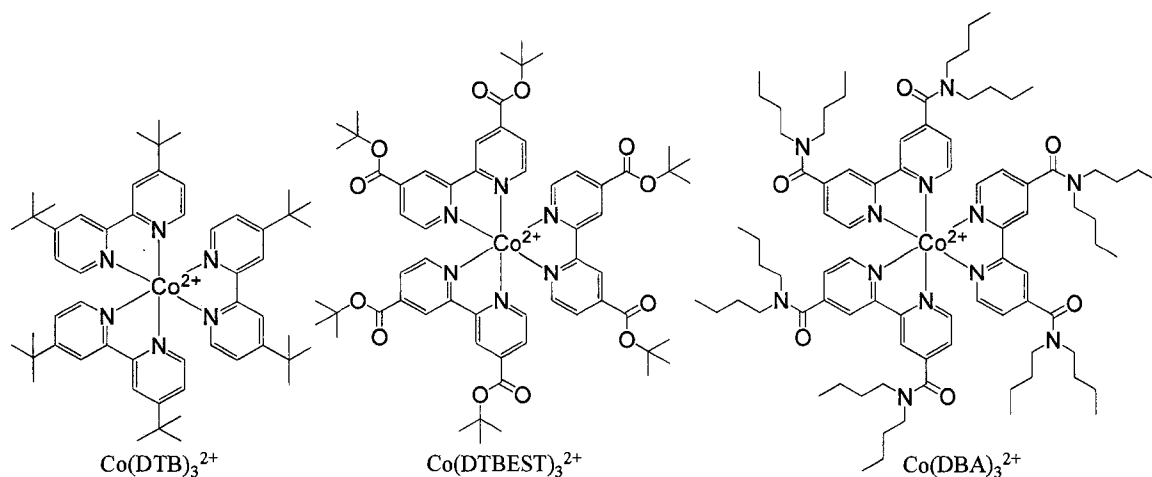
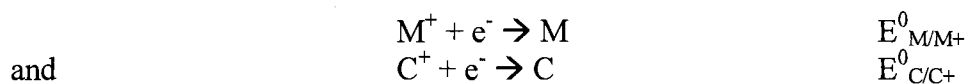


Figure 1. Structure of the 3 cobalt complexes considered in this chapter.

Our collaborators at the University of Ferrara, Italy, have shown that the addition of phenothiazine (PTZ) as co-mediator to $\text{Co}(\text{DTB})_3^{2+/3+}$ solutions can increase the photocurrent output of DSSCs.⁹ These solutions are in effect redox quadruples and can be illustrated with a system of two hypothetical redox couples:



where $E_{\text{C/C}^+}^0$ is more positive than $E_{\text{M/M}^+}^0$. Alone, neither the M/M^+ couple nor the C/C^+ couple is an optimum mediator: the reduction of the photo-oxidized dye by M is too slow, and the rate of recombination between photo-injected electrons and C^+ is too fast. In a solution where M^+ , M and C are present, added C^+ would immediately be reduced by M . In the corresponding mediator solution containing M^+ , M and C , if C could rapidly reduce the photo-oxidized dye, the generated C^+ would immediately be reduced by M . If this second step is kinetically fast, consuming the generated C^+ before recombination with the photo-injected electron, the issues associated with the M/M^+ and C/C^+ couples alone would be resolved. In this redox quadruple system M represents the $\text{Co}(\text{L})_3^{2+/3+}$ mediator and C represents the PTZ co-mediator.

To investigate the phenomenon involved with these redox quadruples, a study was launched involving PTZ moieties where the PTZ was an anion as a lithium salt, lithium 4-(10H-phenothiazine-10-yl)butane-1-sulfonate (LiPTZ4S), where the PTZ was neutral, N-methylphenothiazine (N-MePTZ), and where the PTZ was a cation as a hexafluorophosphate salt, *N,N,N*-trimethyl-3-(10H-phenothiazin-10-yl)propan-1-aminium hexafluorophosphate (PTZ3QPF_6). The structures of the three PTZ moieties are shown in Figure 2 and $E_{1/2}$ values for the cobalt complexes and PTZ moieties are tabulated in

Table 1. It is clear from the data presented in Table 1 that there is sufficient driving force for all three PTZ moieties to oxidize any of the three cobalt complexes.

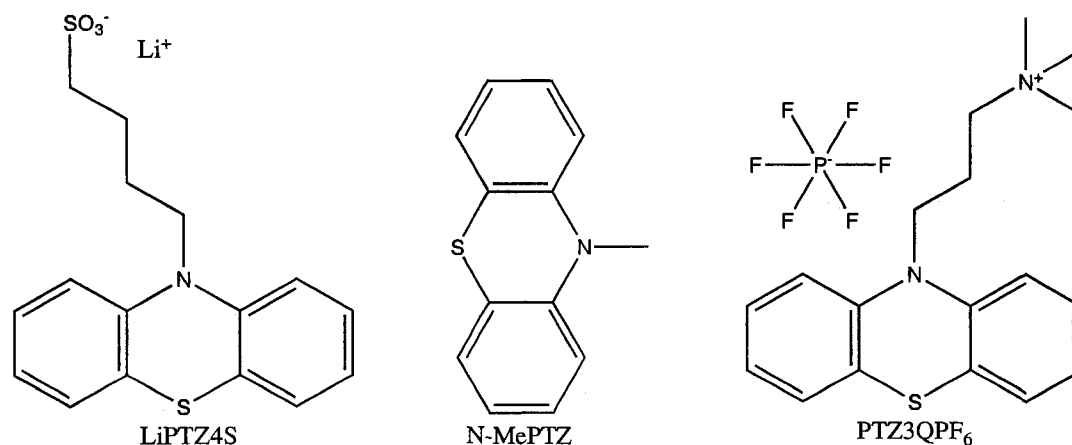


Figure 2. Structure of phenothiazine moieties investigated in this chapter.

Cobalt Complex	$E_{1/2}$	PTZ	$E_{1/2}$
[Co(DTB) ₃](ClO ₄) ₂	-250 mV	PTZ3QPF ₆	385 mV
[Co(DTBEST) ₃](ClO ₄) ₂	20 mV	N-MePTZ	335 mV
[Co(DBA) ₃](ClO ₄) ₂	75 mV	LiPTZ4S	275 mV

Table 1. $E_{1/2}$ values, determined by cyclic voltammetry and referenced to ferrocene, for the three cobalt complexes and three phenothiazine moieties investigated in this work. 0.1 M tetramethylammonium perchlorate supporting electrolyte, GC working electrode, Pt counter electrode, and SSCE reference electrode. Concentration of cobalt complexes and PTZ moieties was ca. 0.001 M.

Transient absorption laser experiments were performed on cobalt mediator solutions that contained the usual additives (lithium triflate and 4-*tert*-butylpyridine) and on cobalt mediator solutions that contained, in addition to the usual additives, one of the three PTZ moieties. These experiments were instructive in determining that LiPTZ4S is best suited as a co-mediator for use in cobalt mediated DSSCs.

Current-voltage experiments were performed on assembled DSSC employing the three cobalt complex mediator solutions alone and with added LiPTZ4S. To further investigate the catalytic oxidation of Co(L)₃²⁺ by LiPTZ4S⁺, cyclic voltammetry experiments were conducted to determine if the process was kinetically or diffusionally limited.

6.2 Results and Discussion

Transient Absorption of Cobalt Complexes

Immediately upon excitation by the 532 nm laser beam, the adsorbed N3 dye injects an electron into the conduction band of the mesoporous TiO₂ in the picosecond or femtosecond time range.¹⁰ This injection occurs with near unit efficiency, resulting in a bleach of the dye centered around 480 nm.² The transient decrease in absorption reflects the concentration of photo-oxidized dye present following electron injection into the conduction band of the TiO₂. When there is no solution species present to donate an electron to the photo-oxidized dye, the recovery of the ground state is very slow, with complete recombination requiring tens of microseconds to one millisecond.²⁻⁴ When an electron donor such as the reduced form of the redox mediator is present, the photo-oxidized dye is quickly reduced. In an operational DSSC, electrons in the mesoporous TiO₂ percolate through the semi-conductor to the current collecting substrate.¹¹ In the transient absorption experiment, electrons in the mesoporous TiO₂ reduce the oxidized mediator.

Data collected in transient absorption experiments in this work were normalized to unit initial intensity and fit to a double exponential decay using Origin[®] software. The use of a double exponential decay was necessary to account for a fast component that was evident in the transient absorbance spectra.¹ This fast component is due to over-excitation of the sample, in other words, the irradiance on the sample was greater than the desired 100 mW/cm² that would mimic sunlight conditions. This increased irradiance was necessary, however, to obtain an acceptable signal to noise ratio in the transient absorption spectra. Even with this experimental concession, including several spectra in

a single plot for comparison makes the figure difficult to interpret. For this reason, only the fits of the data are plotted for comparison. Individual spectra plotted along with the double exponential fits are provided in Appendix A.

Figure 3 shows thin-film transient laser spectra for a background solution, containing only 0.2 M lithium triflate and 0.2 M 4-*tert*-butylpyridine in γ BL, and for solutions containing, respectively, 0.15 M $[\text{Co}(\text{DTB})_3](\text{ClO}_4)_2$, 0.15 M $[\text{Co}(\text{DTBEST})_3](\text{ClO}_4)_2$, and 0.15 M $\text{Co}[(\text{DBA})_3](\text{ClO}_4)_2$, in the background solution.

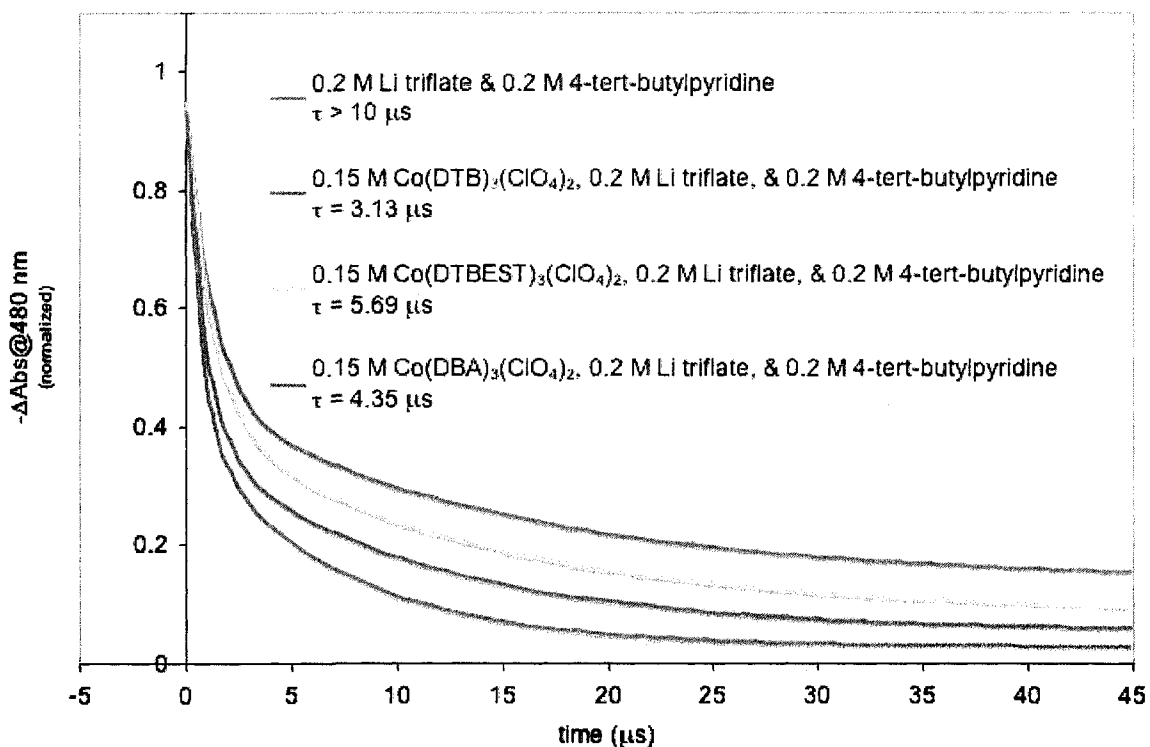


Figure 3. Transient absorption spectra for the background solution (blue trace), $[\text{Co}(\text{DTB})_3](\text{ClO}_4)_2$ (red trace), $[\text{Co}(\text{DTBEST})_3](\text{ClO}_4)_2$ (orange trace), $[\text{Co}(\text{DBA})_3](\text{ClO}_4)_2$ (green trace). Lifetimes calculated from double exponential fits are shown in legend.

Of note in Figure 3 is that all three of the cobalt complexes reduce the photo-oxidized dye faster than the recombination reaction, when no mediator is present, shown by the blue trace. This is essential for the cobalt complex to be effective at all as a mediator in an assembled DSSC. In fact, the order of effectiveness shown in Figure 3,

from least effective $[\text{Co}(\text{DTBEST})_3](\text{ClO}_4)_2$ to most effective $[\text{Co}(\text{DTB})_3](\text{ClO}_4)_2$, is the same order of performance observed using these mediators in operational DSSCs (cf. Chapter 3 Figure 8). The order of effectiveness in Figure 3 also confirms that shifting the $E_{1/2}$ of the cobalt complex in the positive direction reduces the thermodynamic driving force for dye reduction (*vide supra*).

The results presented in Figure 3 indicate that the cobalt mediators investigated are capable of reducing the photo-oxidized dye faster than recombination of photo-oxidized dye with conduction band electrons. It is important to note that since the cobalt mediators do not reduce the photo-oxidized dye as quickly as iodide, there will be a lower J_{sc} achieved with cobalt mediated cells. This has been shown in cell performance evaluation experiments.⁸ Employing a suitable co-mediator system may overcome the decreased performance observed in cobalt mediated DSSCs while avoiding the detrimental properties of I^-/I_3^- mediator systems.

Figure 4 shows thin-film transient laser spectra for the $[\text{Co}(\text{DTB})_3](\text{ClO}_4)_2$ mediator solution and $[\text{Co}(\text{DTB})_3](\text{ClO}_4)_2$ mediator solutions containing the three PTZ moieties, LiPTZ4S, N-Me-PTZ, and PTZ3QPF₆. All four solutions contained 0.15 M $[\text{Co}(\text{DTB})_3](\text{ClO}_4)_2$, 0.2 M lithium triflate and 0.2 M 4-*tert*-butylpyridine. The concentration of the PTZ moieties was 0.05 M.

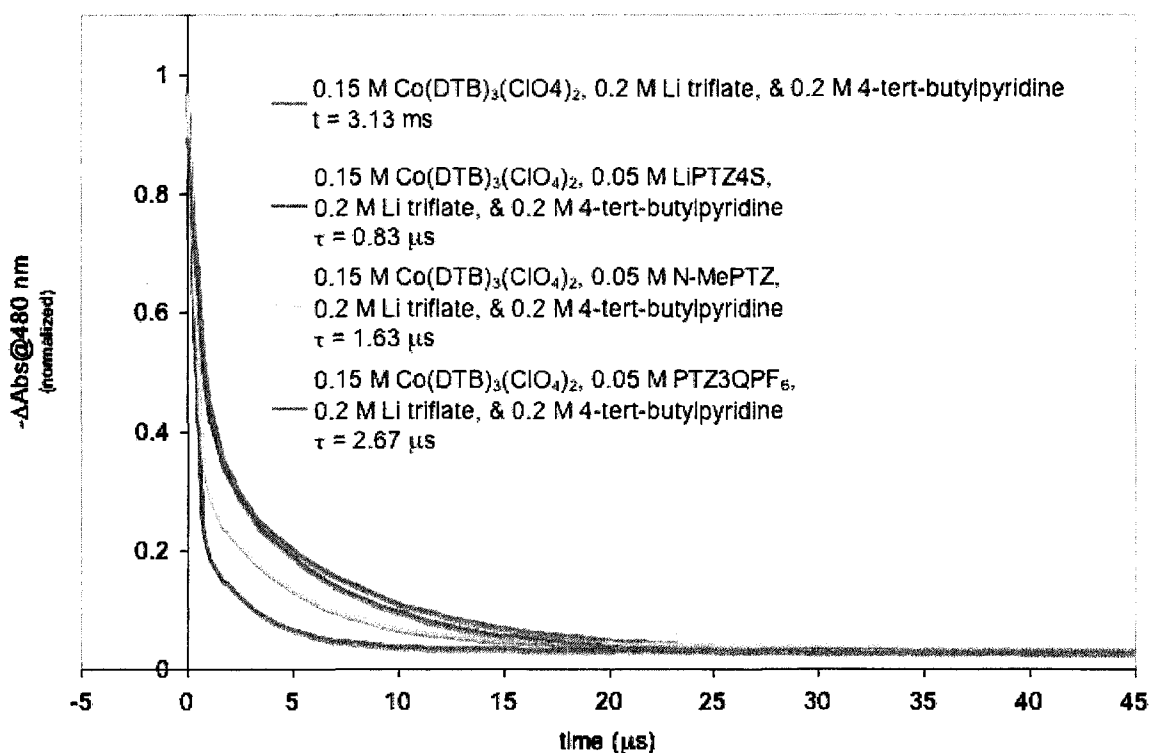


Figure 4. Transient absorption spectra for $[\text{Co}(\text{DTB})_3](\text{ClO}_4)_2$ mediator solution (blue trace), and $[\text{Co}(\text{DTB})_3](\text{ClO}_4)_2$ mediator solutions containing LiPTZ4S (red trace), N-MePTZ (orange trace), and PTZ3QPF₆ (green trace).

In Figure 4 the decay of the photo-oxidized dye signal is strongly accelerated when the anionic LiPTZ4S is present, shown by a ca. factor of 4 decrease in the photo-oxidized dye lifetime compared with $[\text{Co}(\text{DTB})_3](\text{ClO}_4)_2$ alone. The uncharged N-MePTZ does accelerate the decay of the photo-oxidized dye signal, but only by a factor of ca. two compared with $[\text{Co}(\text{DTB})_3](\text{ClO}_4)_2$ alone. The cationic PTZ3QPF₆ has no significant effect on the decay of the photo-oxidized dye signal compared to the decay when only $[\text{Co}(\text{DTB})_3](\text{ClO}_4)_2$ is present.

Figure 5 shows thin-film transient laser spectra for the $[\text{Co}(\text{DTBEST})_3](\text{ClO}_4)_2$ mediator solution and $[\text{Co}(\text{DTBEST})_3](\text{ClO}_4)_2$ mediator solutions containing the three PTZ moieties. All four mediator solutions contained 0.15 M $[\text{Co}(\text{DTBEST})_3](\text{ClO}_4)_2$, 0.2 M lithium triflate and 0.2 M 4-*tert*-butylpyridine. The concentration of the PTZ moieties was 0.05 M.

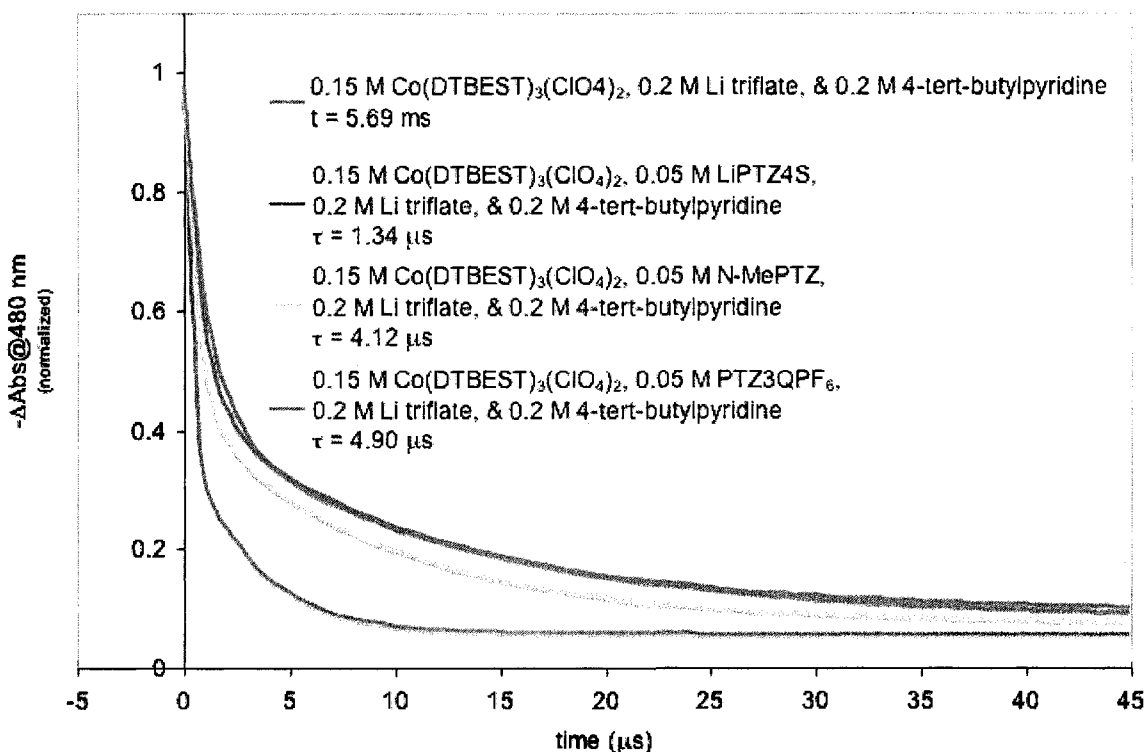


Figure 5. Transient absorption spectra for $[\text{Co}(\text{DTBEST})_3](\text{ClO}_4)_2$ mediator solution (blue trace), and $[\text{Co}(\text{DTBEST})_3](\text{ClO}_4)_2$ mediator solutions containing LiPTZ4S (red trace), N-MePTZ (orange trace), and PTZ3QPF₆ (green trace).

In Figure 5 the decay of the photo-oxidized dye signal is again accelerated when the anionic LiPTZ4S is present with $[\text{Co}(\text{DTBEST})_3](\text{ClO}_4)_2$, shown by a factor of ca. four decrease in the photo-oxidized dye lifetime compared with $[\text{Co}(\text{DTBEST})_3](\text{ClO}_4)_2$ alone. The uncharged N-MePTZ accelerates the decay of the photo-oxidized dye signal by a factor of ca. less than two compared with $[\text{Co}(\text{DTBEST})_3](\text{ClO}_4)_2$ alone. Again, the cationic PTZ3QPF₆ has no significant effect on the decay of the photo-oxidized dye signal compared to the decay when only $[\text{Co}(\text{DTBEST})_3](\text{ClO}_4)_2$ is present.

Figure 6 shows thin-film transient laser spectra for the $[\text{Co}(\text{DBA})_3](\text{ClO}_4)_2$ mediator solution and $[\text{Co}(\text{DBA})_3](\text{ClO}_4)_2$ mediator solutions containing the three PTZ moieties. All four mediator solutions contained 0.15 M $[\text{Co}(\text{DBA})_3](\text{ClO}_4)_2$, 0.2 M lithium triflate and 0.2 M 4-*tert*-butylpyridine. The concentration of the PTZ moieties was 0.05 M.

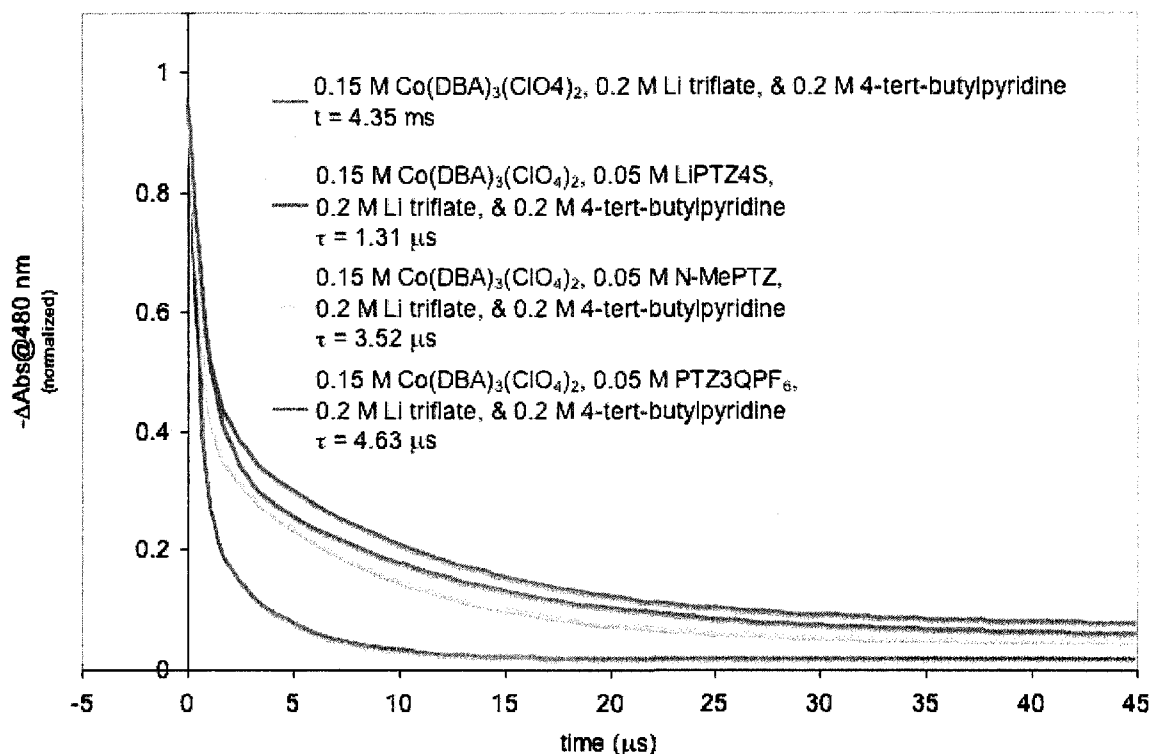


Figure 6. Transient absorption spectra for $[\text{Co}(\text{DBA})_3](\text{ClO}_4)_2$ mediator solution (blue trace), and $[\text{Co}(\text{DBA})_3](\text{ClO}_4)_2$ mediator solutions containing LiPTZ4S (red trace), N-MePTZ (orange trace), and PTZ3QPF₆ (green trace).

In Figure 6 the decay of the photo-oxidized dye signal is accelerated when the anionic LiPTZ4S is present with $[\text{Co}(\text{DBA})_3](\text{ClO}_4)_2$, shown by a factor of ca. three decrease in the photo-oxidized dye lifetime compared with $[\text{Co}(\text{DBA})_3](\text{ClO}_4)_2$ alone. The neutral N-MePTZ accelerates the decay of the photo-oxidized dye signal by a factor of ca. less than two compared with $[\text{Co}(\text{DBA})_3](\text{ClO}_4)_2$ alone. The cationic PTZ3QPF₆ does not significantly affect the decay of the photo-oxidized dye signal when present with $[\text{Co}(\text{DBA})_3](\text{ClO}_4)_2$ compared to the decay when $[\text{Co}(\text{DBA})_3](\text{ClO}_4)_2$ is present alone.

The charge on the phenothiazine affects how the molecule associates with the photo-oxidized dye. The N3 dye acquires an overall positive charge upon photo-oxidation, providing an electrostatic attraction between the photo-oxidized dye and the anionic LiPTZ4S reductant. This is shown by the factor of ca. four decrease in the lifetime of the photo-oxidized dye when LiPTZ4S is present in solution with all three

cobalt complexes (red traces in Figures 4, 5, and 6). The co-mediator effect is most pronounced when $[\text{Co}(\text{DTB})_3](\text{ClO}_4)_2$ is co-mediated by LiPTZ4S, reducing the lifetime of the photo-oxidized dye to the nanosecond regime. The neutral and cationic PTZ moieties have, respectively, no electrostatic interaction, and an electrostatic repulsion with the photo-oxidized dye, resulting in increasingly slower dye reduction moving from N-MePTZ to PTZ3QPF₆. This trend is shown in Figures 4, 5, and 6 by a ca. factor of two decrease in the lifetime of the photo-oxidized dye when N-MePTZ is present (orange traces), and no significant effect on the lifetime of the photo-oxidized dye when PTZ3QPF₆ is present (green traces).

The results from these thin-film transient absorption experiments suggest that the anionic LiPTZ4S is the best choice for use as a co-mediator in cobalt mediator systems used in DSSCs. The electron transfer process measured in the open circuit situation of the thin-film transient absorption experiment is the reduction of the photo-oxidized dye, either by the mediator or recombination with conduction band electrons. It is important that the reduction by the mediator occurs rapidly to limit the recombination of injected conduction band electrons with the photo-oxidized dye. The rate of reduction of the photo-oxidized dye by $\text{Co}(\text{L})_3^{2+}$ is slower than of I^- ,^{3, 8} particularly with the $[\text{Co}(\text{DTBEST})_3](\text{ClO}_4)_2$ and $[\text{Co}(\text{DBA})_3](\text{ClO}_4)_2$ (cf. Figures 5 and 6). When present, the LiPTZ4S co-mediator reduces the photo-oxidized dye at a rate that is a factor of ca. four faster than $\text{Co}(\text{L})_3^{2+}$ alone. The generated LiPTZ4S^{•+} is rapidly reduced by $\text{Co}(\text{L})_3^{2+}$ while $\text{Co}(\text{L})_3^{3+}$, which is not readily reduced at the photoanode, diffuses to the cathode for reduction.

Cell Performance

Transient absorption experiments on the cobalt mediator solutions with PTZ additives suggest that the anionic LiPTZ4S will enhance cell performance by quickly reducing the photo-oxidized dye, decreasing the rate of recombination between the photo-oxidized dye and electrons in the semiconductor conduction band (*vide supra*). To evaluate DSSCs employing LiPTZ4S as a co-mediator, current-voltage experiments were performed on cells that employed the cobalt mediator solutions, and on cells that employed cobalt mediator solutions with LiPTZ4S as a co-mediator. Mediator solutions were prepared as 0.15 M $[\text{Co}(\text{L})_3](\text{ClO}_4)_2$, 0.015 M NOBF₄, 0.2 M lithium triflate, and 0.2 M 4-*tert*-butylpyridine in γ BL (cf. Chapter 2). Co-mediated solutions contained 0.05 M LiPTZ4S.

Current-voltage curves for DSSCs employing the $[\text{Co}(\text{DTB})_3](\text{ClO}_4)_2$ mediator with and without 0.05 M LiPTZ4S are presented in Figure 7 with cell parameters summarized in Table 2.

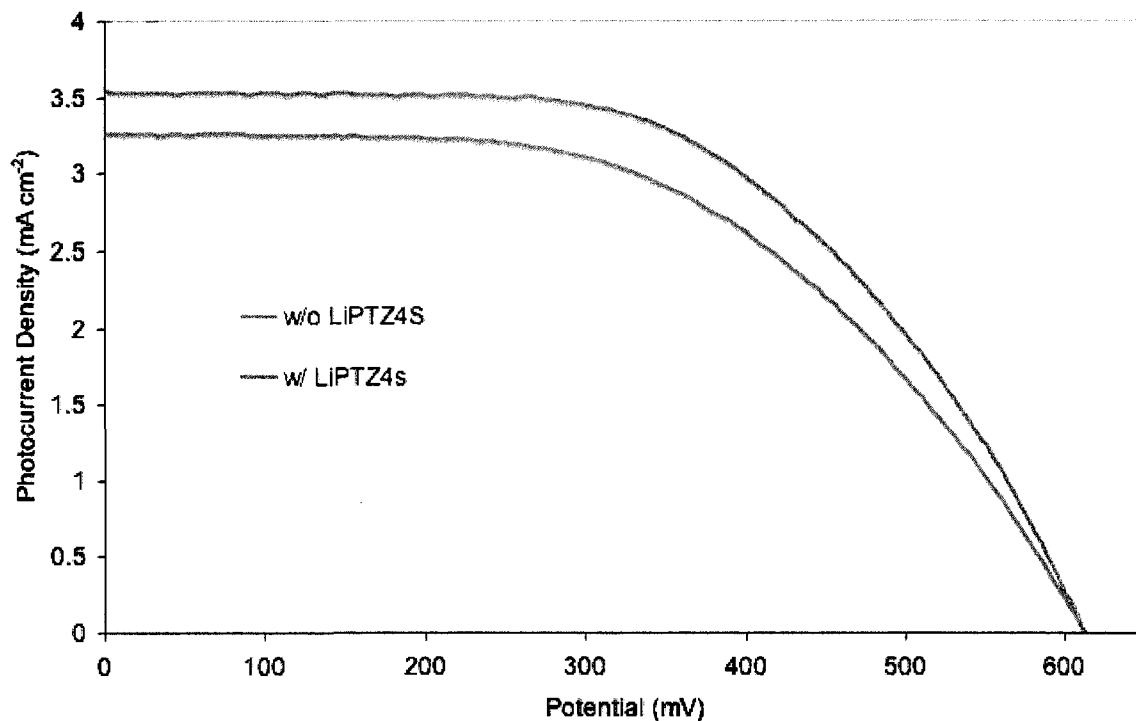


Figure 7. Current-voltage curves for DSSCs employing $[\text{Co}(\text{DTB})_3](\text{ClO}_4)_2$ mediator (blue trace) and $[\text{Co}(\text{DTB})_3](\text{ClO}_4)_2$ co-mediated with 0.05 M LIPTZ4S (red trace).

Mediator	V_{oc}	J_{sc}	Fill Factor	Efficiency
$\text{Co}(\text{DTB})_3(\text{ClO}_4)_2$	615 mV	3.26 mA/cm ²	52.4%	1.05%
$\text{Co}(\text{DTB})_3(\text{ClO}_4)_2$ w/ LIPTZ4S	615 mV	3.54 mA/cm ²	54.9%	1.19%

Table 2. Cell parameters for current-voltage curves shown in Figure 7.

The current-voltage curves presented in Figure 7 show an increased J_{sc} when LIPTZ4S is present as a co-mediator with $[\text{Co}(\text{DTB})_3](\text{ClO}_4)_2$ compared to $[\text{Co}(\text{DTB})_3](\text{ClO}_4)_2$ alone. The LIPTZ4S effectively reduces the photo-oxidized dye faster than $[\text{Co}(\text{DTB})_3](\text{ClO}_4)_2$ alone while the generated LIPTZ4S^{++} is quickly reduced by $[\text{Co}(\text{DTB})_3](\text{ClO}_4)_2$. This results in a decreased rate of recombination between conduction band electrons and photo-oxidized dye, shown by an increased J_{sc} .

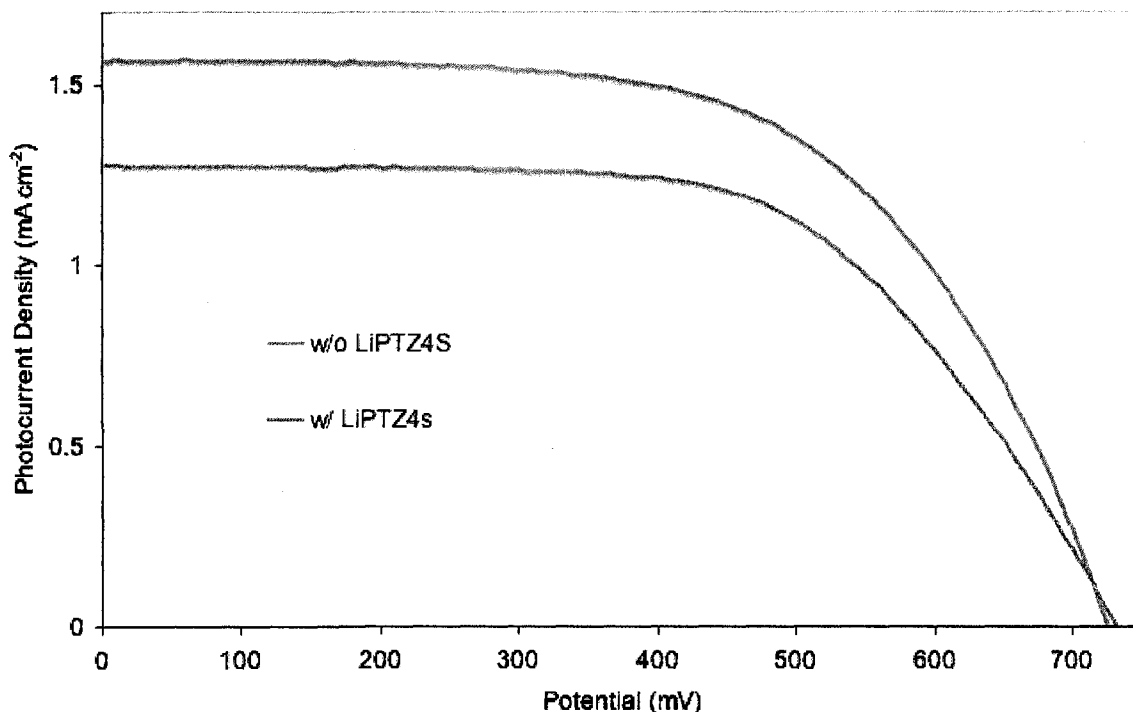


Figure 8. Current-voltage curves for DSSCs employing $[\text{Co}(\text{DTBEST})_3](\text{ClO}_4)_2$ mediator (blue trace) and $[\text{Co}(\text{DTBEST})_3](\text{ClO}_4)_2$ co-mediated with 0.05 M LiPTZ4S (red trace).

Mediator	V_{oc}	J_{sc}	Fill Factor	Efficiency
$\text{Co}(\text{DTBEST})_3(\text{ClO}_4)_2$	725 mV	1.56 mA/cm^2	59.8%	0.68%
$\text{Co}(\text{DTBEST})_3(\text{ClO}_4)_2$ w/ LiPTZ4S	730 mV	1.28 mA/cm^2	60.3%	0.56%

Table 3. Cell parameters for current-voltage shown in Figure 8.

Current-voltage curves for DSSCs employing the $[\text{Co}(\text{DTBEST})_3](\text{ClO}_4)_2$ mediator with and without 0.05 M LiPTZ4S are presented in Figure 8 with cell parameters summarized in Table 3. The current-voltage curves presented in Figure 8 show that LiPTZ4S as a co-mediator with $[\text{Co}(\text{DTBEST})_3](\text{ClO}_4)_2$ results in a lower J_{sc} compared to $[\text{Co}(\text{DTBEST})_3](\text{ClO}_4)_2$ alone. While transient absorption experiments shown in Figure 5 demonstrate that LiPTZ4S effectively reduces the photo-oxidized dye faster than $[\text{Co}(\text{DTBEST})_3](\text{ClO}_4)_2$ alone, Figure 5 suggests that reduction of LiPTZ4S^{+} by $\text{Co}(\text{DTBEST})_3^{2+}$ is slow, making LiPTZ4S^{+} available for reduction by conduction band electrons, resulting in decreased J_{sc} .

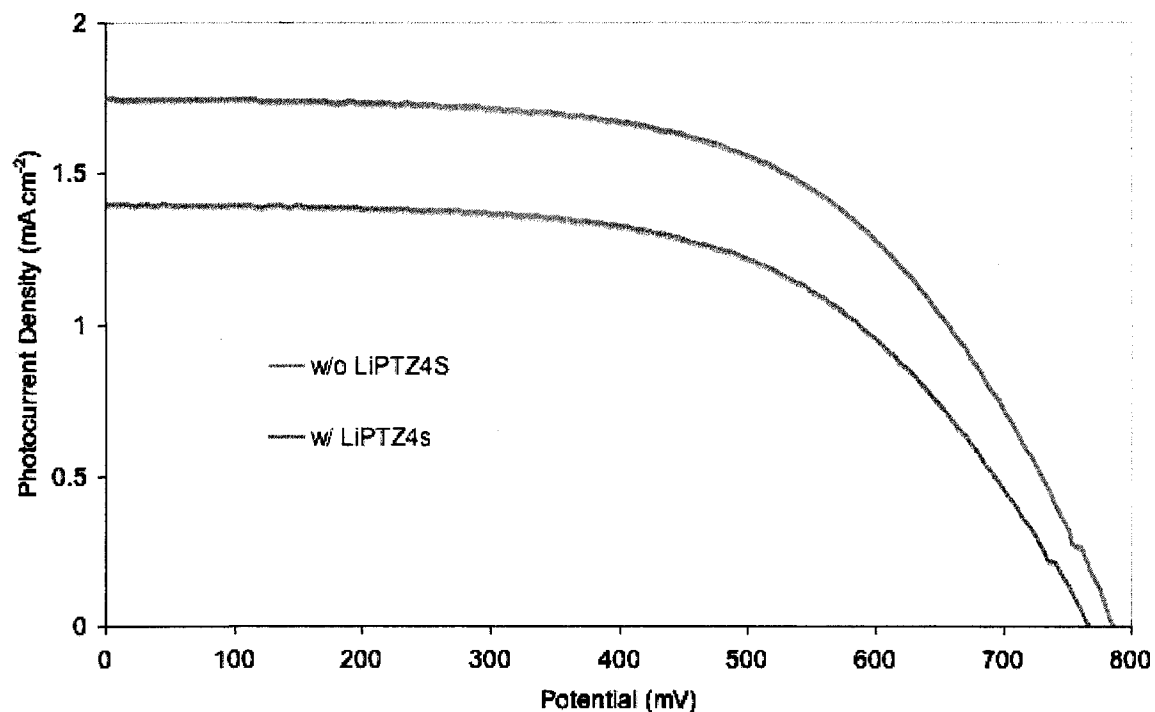


Figure 9. Current-voltage curves for DSSCs employing $[\text{Co}(\text{DBA})_3](\text{ClO}_4)_2$ mediator (blue trace) and $[\text{Co}(\text{DBA})_3](\text{ClO}_4)_2$ co-mediated with 0.05 M LiPTZ4S (red trace).

Mediator	V_{oc}	J_{sc}	Fill Factor	Efficiency
$\text{Co}(\text{DBA})_3(\text{ClO}_4)_2$	785 mV	1.75 mA/cm ²	58.2%	0.80%
$\text{Co}(\text{DBA})_3(\text{ClO}_4)_2$ w/ LiPTZ4S	765 mV	1.40 mA/cm ²	57.6%	0.62%

Table 4. Cell parameters for DSSCs shown in Figure 4.

Current-voltage curves for DSSCs employing the $[\text{Co}(\text{DBA})_3](\text{ClO}_4)_2$ mediator with and without 0.05 M LiPTZ4S are presented in Figure 9. Cell parameters are summarized in Table 4. The current-voltage curves presented in Figure 9 show that, similar to the case with $[\text{Co}(\text{DTBEST})_3](\text{ClO}_4)_2$, $[\text{Co}(\text{DBA})_3](\text{ClO}_4)_2$ co-mediated with LiPTZ4S does not enhance cell performance. Transient absorption data presented in Figure 6 demonstrates that the rate of reduction of the photo-oxidized dye is increased when LiPTZ4S is present. However, Figure 9 suggests that the reduction of LiPTZ4S^{+} by $\text{Co}(\text{DBA})_3^{2+}$ is slow, making LiPTZ4S^{+} available for reduction by conduction band electrons, resulting in decreased J_{sc} .

Catalyzed Oxidation of Cobalt(II)

Transient absorption experiments yielded promising results for LiPTZ4S as an additive to cobalt mediator solutions. Particularly when considering the $[\text{Co}(\text{DTBEST})_3](\text{ClO}_4)_2$ and $[\text{Co}(\text{DBA})_3](\text{ClO}_4)_2$ mediators, where initial current-voltage experiments showed increased V_{oc} but poor J_{sc} compared to $[\text{Co}(\text{DTB})_3](\text{ClO}_4)_2$ (cf. Chapter 3 Figure 8). Unfortunately, Figures 8 and 9 above indicate that while the rate of reduction of the photo-oxidized dye is increased over the cobalt complexes alone (cf. Figures 5 and 6), operational DSSCs employing LiPTZ4S as a co-mediator with $[\text{Co}(\text{DTBEST})_3](\text{ClO}_4)_2$ and $[\text{Co}(\text{DBA})_3](\text{ClO}_4)_2$ exhibit decreased J_{sc} .

To investigate the catalysis of $\text{Co}(\text{L})_3^{2+}$ oxidation by LiPTZ4S^{+} , cyclic voltammetry experiments were performed using an unmodified FTO working electrode on solutions that contained LiPTZ4S at low concentration (ca. 5×10^{-5} M) and the cobalt complexes at concentrations ranging from 0.0 to 5.0×10^{-3} M. All of the cobalt complexes investigated in this work are essentially redox inactive on unmodified FTO electrodes.^{8,12} As such, any current observed upon addition of cobalt complex to the solution must result from catalysis by the LiPTZ4S present in solution. The supporting electrolyte in the CV experiments was 0.1 M tetramethylammonium perchlorate in γBL . Voltammograms were recorded using a large area Pt mesh counter electrode, SSCE reference, and scan rate of 50 mV/s. All voltammograms are shown referenced to ferrocene.

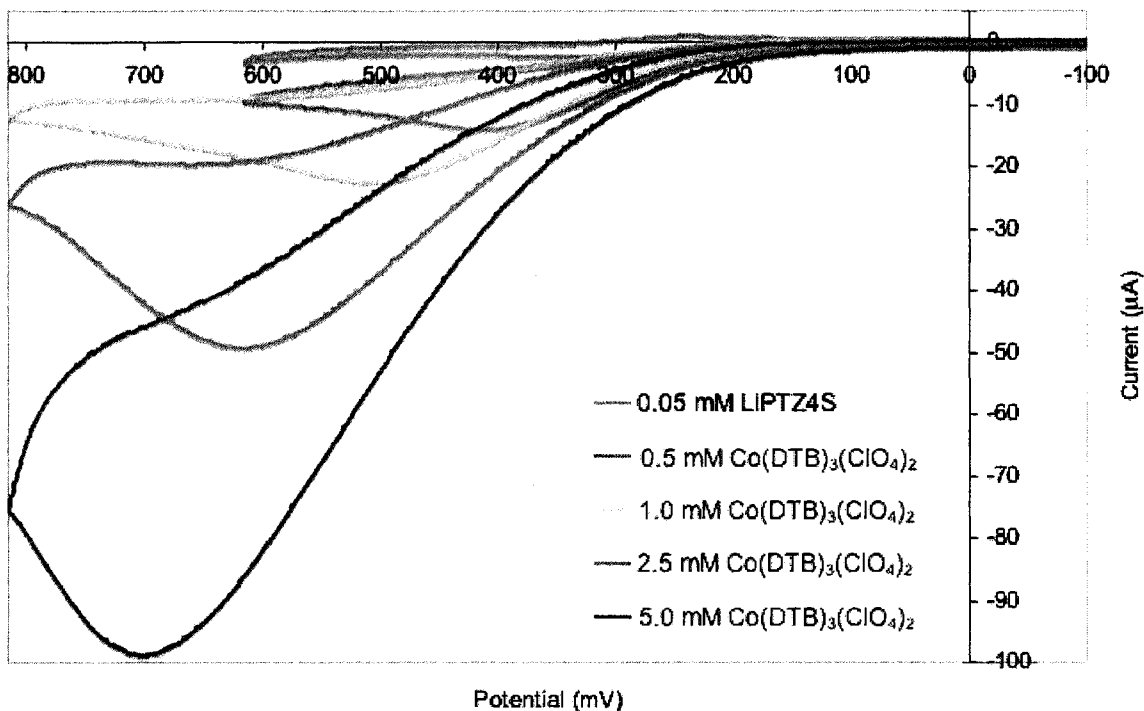


Figure 10. CV of catalytic oxidation of $[\text{Co}(\text{DTB})_3](\text{ClO}_4)_2$ by LiPTZ4S. CVs are shown referenced to ferrocene.

	$E_{p,a}$	$I_{p,a}$
LiPTZ4S	340 mV	-2.27 μA
0.5 mM $[\text{Co}(\text{DTB})_3](\text{ClO}_4)_2$	415 mV	-13.90 μA
1.0 mM $[\text{Co}(\text{DTB})_3](\text{ClO}_4)_2$	510 mV	-22.36 μA
2.5 mM $[\text{Co}(\text{DTB})_3](\text{ClO}_4)_2$	615 mV	-49.15 μA
5.0 mM $[\text{Co}(\text{DTB})_3](\text{ClO}_4)_2$	700 mV	-98.73 μA

Table 5. Electrochemical data from catalytic oxidation CVs shown in figure 10.

Figure 10 shows CVs obtained from catalysis experiments conducted on $[\text{Co}(\text{DTB})_3](\text{ClO}_4)_2$ with electrochemical data tabulated in Table 5. The peak oxidation current for the highest concentration of $\text{Co}(\text{DTB})_3^{2+}$ observed in Figure 10 is over 30 times larger than that of the LiPTZ4S alone. The peak potential for the catalytic oxidation of $\text{Co}(\text{DTB})_3^{2+}$ lies ca. 700 mV positive of the $E_{1/2}$ of $\text{Co}(\text{DTB})_3^{2+}$ at a glassy carbon electrode, and is slightly positive of the $E_{1/2}$ of LiPTZ4S at low concentrations of $[\text{Co}(\text{DTB})_3](\text{ClO}_4)_2$.

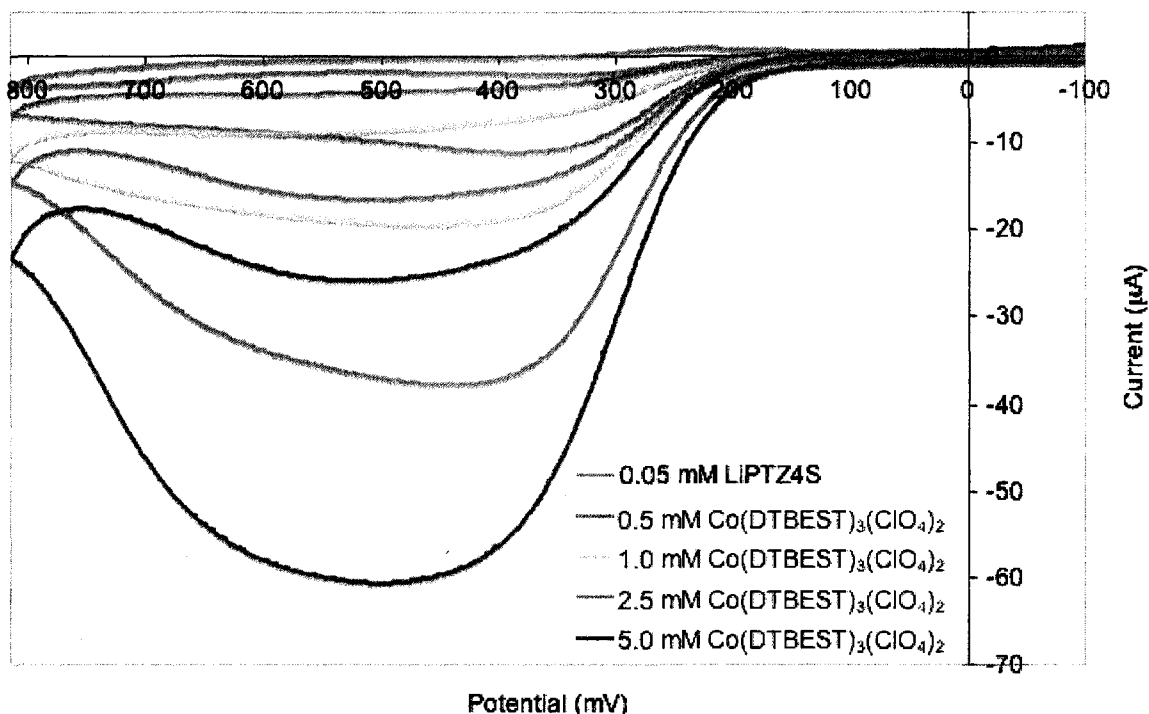


Figure 11. CV of catalytic oxidation of $[\text{Co}(\text{DTBEST})_3](\text{ClO}_4)_2$ by LiPTZ4S. CVs are shown referenced to ferrocene.

	$E_{p,a}$	$I_{p,a}$
LiPTZ4S	355 mV	-2.05 μA
0.5 mM $[\text{Co}(\text{DTBEST})_3](\text{ClO}_4)_2$	385 mV	-11.13 μA
1.0 mM $[\text{Co}(\text{DTBEST})_3](\text{ClO}_4)_2$	460 mV	-19.27 μA
2.5 mM $[\text{Co}(\text{DTBEST})_3](\text{ClO}_4)_2$	440 mV	-37.61 μA
5.0 mM $[\text{Co}(\text{DTBEST})_3](\text{ClO}_4)_2$	500 mV	-60.58 μA

Table 6. Electrochemical data from catalytic oxidation CVs shown in figure 11.

Figure 11 shows CVs obtained from catalysis experiments conducted on $[\text{Co}(\text{DTBEST})_3](\text{ClO}_4)_2$ with electrochemical data tabulated in Table 6. The peak oxidation current for the highest concentration of $\text{Co}(\text{DTBEST})_3^{2+}$ observed in Figure 11 is less than 20 times larger than that of the LiPTZ4S alone. The peak potential for the catalytic oxidation of $\text{Co}(\text{DTBEST})_3^{2+}$ lies ca. 300 mV positive of the $E_{1/2}$ of $\text{Co}(\text{DTBEST})_3^{2+}$ at a glassy carbon electrode, and is slightly positive of the $E_{1/2}$ of LiPTZ4S at all concentrations of $[\text{Co}(\text{DTBEST})_3](\text{ClO}_4)_2$. The broadness of the peaks indicates slow electron transfer from $\text{Co}(\text{DTBEST})_3^{2+}$ to LiPTZ4S^{+} .

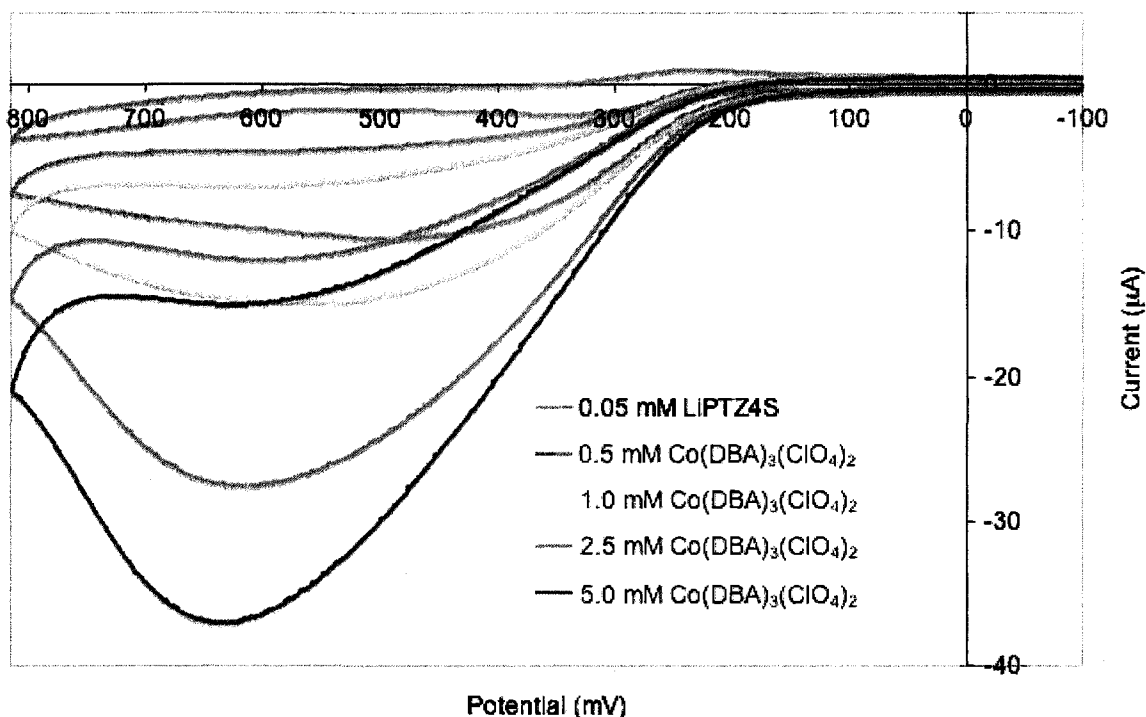


Figure 12. CV of catalytic oxidation of $[\text{Co}(\text{DBA})_3](\text{ClO}_4)_2$ by LiPTZ4S. CVs are shown referenced to ferrocene.

	$E_{p,a}$	$I_{p,a}$
LiPTZ4S	345 mV	-2.09 μA
0.5 mM $[\text{Co}(\text{DBA})_3](\text{ClO}_4)_2$	490 mV	-10.45 μA
1.0 mM $[\text{Co}(\text{DBA})_3](\text{ClO}_4)_2$	555 mV	-14.88 μA
2.5 mM $[\text{Co}(\text{DBA})_3](\text{ClO}_4)_2$	615 mV	-27.58 μA
5.0 mM $[\text{Co}(\text{DBA})_3](\text{ClO}_4)_2$	635 mV	-37.02 μA

Table 7. Electrochemical data from catalytic oxidation CVs shown in figure 12.

Figure 12 shows CVs obtained from catalysis experiments conducted on $[\text{Co}(\text{DBA})_3](\text{ClO}_4)_2$ with electrochemical data tabulated in Table 7. The peak oxidation current for the highest concentration of $\text{Co}(\text{DBA})_3^{2+}$ observed in Figure 12 is less than 10 times larger than that of the LiPTZ4S alone. The peak potential for the catalytic oxidation of $\text{Co}(\text{DBA})_3^{2+}$ lies ca. 600 mV positive of the $E_{1/2}$ of $\text{Co}(\text{DBA})_3^{2+}$ at a glassy carbon electrode, and is slightly positive of the $E_{1/2}$ of LiPTZ4S at low concentrations of $\text{Co}(\text{DBA})_3(\text{ClO}_4)_2$. Similar to the case with $[\text{Co}(\text{DTBEST})_3](\text{ClO}_4)_2$, the broadness of the oxidation peaks indicates slow electron transfer between $\text{Co}(\text{DBA})_3^{2+}$ and LiPTZ4S^{+} .

Figures 10 through 12 show that LiPTZ4S⁺⁺ is moderately efficient at catalyzing the oxidation of all three cobalt complexes by means of an EC' mechanism.¹³ The catalytic oxidation of [Co(DTB)₃](ClO₄)₂ is the most efficient, which explains the enhanced performance of DSSCs employing [Co(DTB)₃(ClO₄)₂] co-mediated with LiPTZ4S (cf. Figure 7). The lower efficiency of catalytic oxidation of [Co(DTBEST)₃](ClO₄)₂ and [Co(DBA)₃](ClO₄)₂ helps explain the decreased J_{sc} of operational DSSCs employing these two cobalt complexes with LiPTZ4S as a co-mediator. When LiPTZ4S reduces the photo-oxidized sensitizing dye, the resulting LiPTZ4S⁺⁺ is in close proximity to the TiO₂ and underlying FTO of the photoanode. While the cobalt complexes are redox inactive on these surfaces, LiPTZ4S is not. If the generated LiPTZ4S⁺⁺ is not eliminated by catalyzing the oxidation of Co(L)₃²⁺ it will be reduced by conduction band electrons at the photoanode. This results in decreased photo-injected electrons available to contribute to J_{sc}.

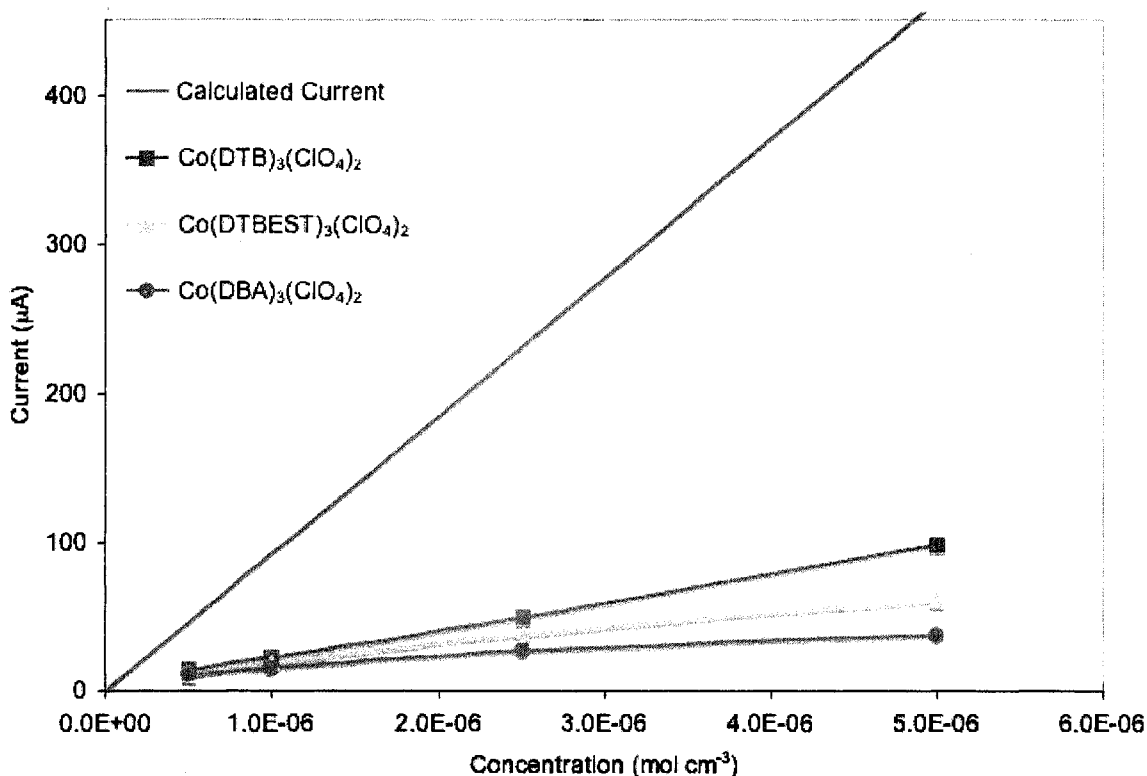


Figure 13. Catalytic peak current versus concentration. Theoretical diffusion controlled peak current (blue trace) plotted with experimental peak currents for $[\text{Co}(\text{DTB})_3](\text{ClO}_4)_2$ (red trace), $[\text{Co}(\text{DTBEST})_3](\text{ClO}_4)_2$ (orange trace), and $[\text{Co}(\text{DBA})_3](\text{ClO}_4)_2$ (green trace). Scan rate was 50 mV/s.

Figure 13, where peak current is plotted as a function of concentration, illustrates that the catalyzed oxidation of $[\text{Co}(\text{DTB})_3](\text{ClO}_4)_2$, $[\text{Co}(\text{DTBEST})_3](\text{ClO}_4)_2$, and $[\text{Co}(\text{DBA})_3](\text{ClO}_4)_2$ are not diffusionally controlled processes. The blue line in Figure 13 is the theoretical diffusion controlled current,¹³ calculated using the diffusion coefficient of $\text{Co}(\text{DTB})_3^{2+}$ reported elsewhere ($9.86 \times 10^{-6} \text{ cm}^2/\text{s}$).¹⁴ $[\text{Co}(\text{DTBEST})_3](\text{ClO}_4)_2$, and $[\text{Co}(\text{DBA})_3](\text{ClO}_4)_2$ are also compared to the calculated curve for $\text{Co}(\text{DTB})_3^{2+}$ in Figure 13 as there is likely no large difference in diffusion coefficients for the three complexes. At all concentrations considered the experimental peak current was significantly less than the theoretically predicted value. At the highest concentration the predicted current value was about 5 times greater than the experimental current for $[\text{Co}(\text{DTB})_3](\text{ClO}_4)_2$, about 8

times greater than the experimental current for $[\text{Co}(\text{DTBEST})_3](\text{ClO}_4)_2$, and about 12 times greater than the experimental current for $[\text{Co}(\text{DBA})_3](\text{ClO}_4)_2$.

Marcus theory predicts that the rate of catalyzed oxidation depends on electronic coupling (H_{AB}) and driving force ($\Delta E_{1/2}$) between the electron acceptor (LiPTZ4S^{++}) and the electron donor ($\text{Co}(\text{L})_3^{2+}$). $\Delta E_{1/2}$ values for the three cobalt complexes and LiPTZ4S are tabulated in Table 8. While the driving force for catalyzed oxidation of $[\text{Co}(\text{DTB})_3](\text{ClO}_4)_2$ is greater than the other two complexes, if driving force alone were responsible for the poorer catalytic oxidation of $[\text{Co}(\text{DTBEST})_3](\text{ClO}_4)_2$ and $[\text{Co}(\text{DBA})_3](\text{ClO}_4)_2$ by LiPTZ4S^{++} , one would expect their catalytic efficiency to be roughly equal, which they are not as shown by overlaid plots in Figure 13.

Cobalt Complex	$\Delta E_{1/2}$
$[\text{Co}(\text{DTB})_3](\text{ClO}_4)_2$	525 mV
$[\text{Co}(\text{DTBEST})_3](\text{ClO}_4)_2$	255 mV
$[\text{Co}(\text{DBA})_3](\text{ClO}_4)_2$	200 mV

Table 8. Driving force, represented by $\Delta E_{1/2}$, for catalytic oxidation of $[\text{Co}(\text{L})_3](\text{ClO}_4)_2$ by LiPTZ4S^{++} . $E_{1/2}$ values were determined for each species in 0.1 M tetramethylammonium perchlorate in γBL electrolyte with GC working electrode, Pt mesh counter electrode, SSCE reference, and scan rate of 50 mV/s.

Together, Figure 13 and Table 8 suggest that the catalyzed oxidation of $\text{Co}(\text{L})_3^{2+}$ is a kinetically controlled process where poor electronic coupling between the cobalt complexes and LiPTZ4S^{++} limits the catalysis, and decreased driving force for the catalytic oxidation of $[\text{Co}(\text{DTBEST})_3](\text{ClO}_4)_2$ and $[\text{Co}(\text{DBA})_3](\text{ClO}_4)_2$ further reduces their catalytic efficiency.

6.3 Conclusions

Transient absorption experiments presented in this chapter have shown that the cobalt complexes discussed display a reduction of the photo-oxidized sensitizing dye in DSSCs that occurs faster than recombination with conduction band electrons. These experiments also showed that the electron withdrawing ester and amide functionalities present on the $[\text{Co}(\text{DTBEST})_3](\text{ClO}_4)_2$ and $[\text{Co}(\text{DBA})_3](\text{ClO}_4)_2$ complexes reduce the rate of reduction of the photo-oxidized dye due to a decreased thermodynamic driving force.

An investigation of phenothiazine additives to the cobalt mediator solutions demonstrated that the solutions containing the anionic phenothiazine moiety LiPTZ4S are capable of reducing the photo-oxidized sensitizing dye much faster than solutions containing the cobalt complexes alone. These results indicated that employing these mixed PTZ/cobalt mediator solutions would result in enhanced performance of operational DSSCs.

Cell performance evaluations using current-voltage experiments showed that this enhancement was realized to some extent with $[\text{Co}(\text{DTB})_3](\text{ClO}_4)_2$ mediated DSSCs, where an increase in J_{sc} due to a slower rate of recombination between conduction band electrons and photo-oxidized dye was observed. Unfortunately, DSSCs employing the $[\text{Co}(\text{DTBEST})_3](\text{ClO}_4)_2$ and $[\text{Co}(\text{DBA})_3](\text{ClO}_4)_2$ complexes as mediators did not display enhanced performance.

Electrochemical investigation of the LiPTZ4S catalyzed oxidation of the cobalt complexes revealed that while the oxidation of $\text{Co}(\text{DTB})_3^{2+}$ was catalyzed with moderate efficiency, the oxidation of $\text{Co}(\text{DTBEST})_3^{2+}$ and $\text{Co}(\text{DBA})_3^{2+}$ was not. This low catalytic

efficiency is most likely due to a combination of decreased driving force for catalytic oxidation and poor electronic coupling between LiPTZ4S and the cobalt complexes that contain electron withdrawing functionalities.

6.4 References

1. Kelly, C. A.; Farzad, F.; Thompson, D. W.; Meyer, G. J., Excited-State Deactivation of Ruthenium(II) Polypyridyl Chromophores Bound to Nanocrystalline TiO₂ Mesoporous Thin Films. *Langmuir* **1999**, *15*, 731-737.
2. Boschloo, G.; Hagfeldt, A., Photoinduced absorption spectroscopy of dye-sensitized nanostructured TiO₂. *Chemical Physics Letters* **2003**, *370*, 381-386.
3. Nusbaumer, H.; Moser, J.-E.; Zakeeruddin, S. M.; Nazeeruddin, M. K.; Grätzel, M., Co^{II}(dbbip)₂²⁺ Complex Rivals Tri-iodide/Iodide Redox Mediator in Dye-Sensitized Photovoltaic Cells. *Journal of Physical Chemistry B* **2001**, *105*, 10461-10464.
4. Oskam, G.; Bergeron, B. V.; Meyer, G. J.; Searson, P. C., Pseudohalogens for Dye-Sensitized TiO₂ Photoelectrochemical Cells. *Journal of Physical Chemistry B* **2001**, *105*, 6867-6873.
5. Larson, S. L.; Cooley, L. F.; Elliott, C. M.; Kelley, D. F., Charge separation in donor-chromophore-acceptor complexes: inverted region behavior in reverse electron transfer reactions. *J. Am. Chem. Soc.* **1992**, *114*, (24), 9504-9.
6. Larson, S. L.; Elliott, C. M.; Kelley, D. F., Charge Separation in Donor-Chromophore-Acceptor Assemblies: Linkage and Driving Force Dependence of Photoinduced Electron Transfers. *J. Phys. Chem.* **1995**, *99*, (17), 6530-9.
7. Nazeeruddin, M. K.; Kay, A.; Rodicio, I.; Humphry-Baker, R.; Mueller, E.; Liska, P.; Vlachopoulos, N.; Grätzel, M., Conversion of light to electricity by cis-X₂-bis(2,2'-bipyridyl-4,4'-dicarboxylate)ruthenium(II) charge-transfer sensitizers (X = Cl⁻, Br⁻, I⁻, CN⁻, and SCN⁻) on nanocrystalline titanium dioxide electrodes. *Journal of the American Chemical Society* **1993**, *115*, (14), 6382-90.
8. Sapp, S. A.; Elliott, C. M.; Contado, C.; Caramori, S.; Bignozzi, C. A., Substituted Polypyridine Complexes of Cobalt(II/III) as Efficient Electron-Transfer Mediators in Dye-Sensitized Solar Cells. *Journal of the American Chemical Society* **2002**, *124*, (37), 11215-11222.
9. Cazzanti, S.; Caramori, S.; Argazzi, R.; Elliott, C. M.; Bignozzi, C. A., Efficient Non-corrosive Electron-Transfer Mediator Mixtures for Dye-Sensitized Solar Cells. *Journal of the American Chemical Society* **2006**, *128*, (31), 9996-9997.
10. Hagfeldt, A.; Grätzel, M., Light-Induced Redox Reactions in Nanocrystalline Systems. *Chemical Reviews* **1995**, *95*, (1), 49-68.

11. Nelson, J.; Chandler, R. E., Random walk models of charge transfer and transport in dye sensitized systems. *Coordination Chemistry Reviews* **2004**, 248, (13-14), 1181-1194.
12. Scott, M. J.; Nelson, J. J.; Caramori, S.; Bignozzi, C. A.; Elliott, C. M., cis-Dichloro-bis(4,4'-dicarboxy-2,2'-bipyridine)osmium(II)-Modified Optically Transparent Electrodes: Application as Cathodes in Stacked Dye Sensitized Solar Cells. *Inorganic Chemistry* **2007**, 46, (24), 10071-10078.
13. Bard, A. J.; Faulkner, L. R., *Electrochemical Methods: Fundamentals and Applications*. 2nd ed. ed.; John Wiley & Sons, Inc.: New York, 2001.
14. Elliott, C. M.; Caramori, S.; Bignozzi, C. A., Indium Tin Oxide Electrodes Modified with Tris(2,2'-bipyridine-4,4'-dicarboxylic acid) Iron(II) and the Catalytic Oxidation of Tris(4,4'-di-tert-butyl-2,2'-bipyridine) Cobalt(II) *Langmuir* **2005**, 21, (7), 3022-3027.

Appendix A

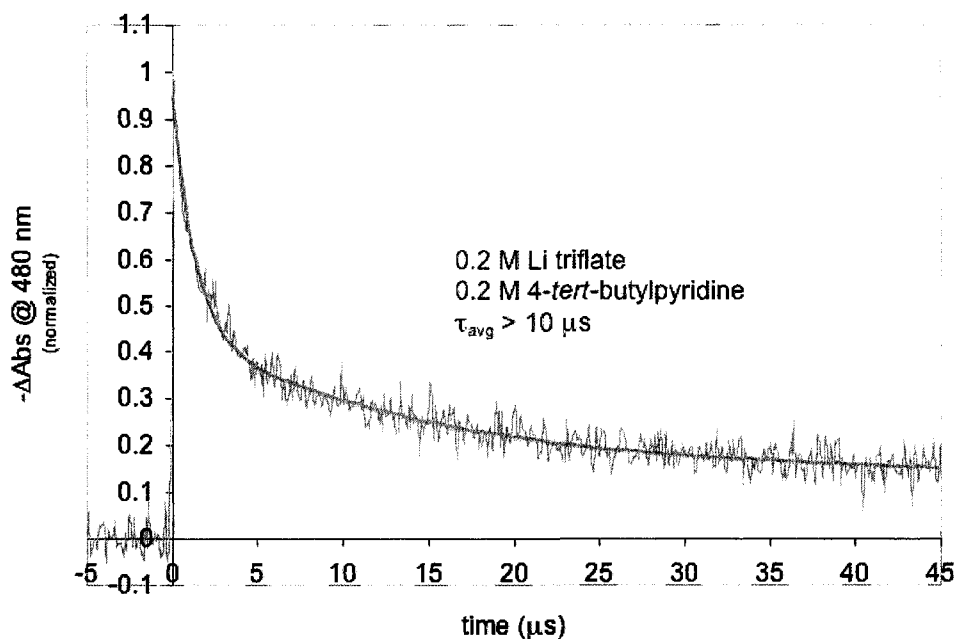
Transient Absorption Spectroscopy Data

Appendix A contains individual plots and fits for all transient absorption data presented in Chapter 6. Raw data was normalized to unit initial intensity and fit to a double exponential with constant using Origin® Software.

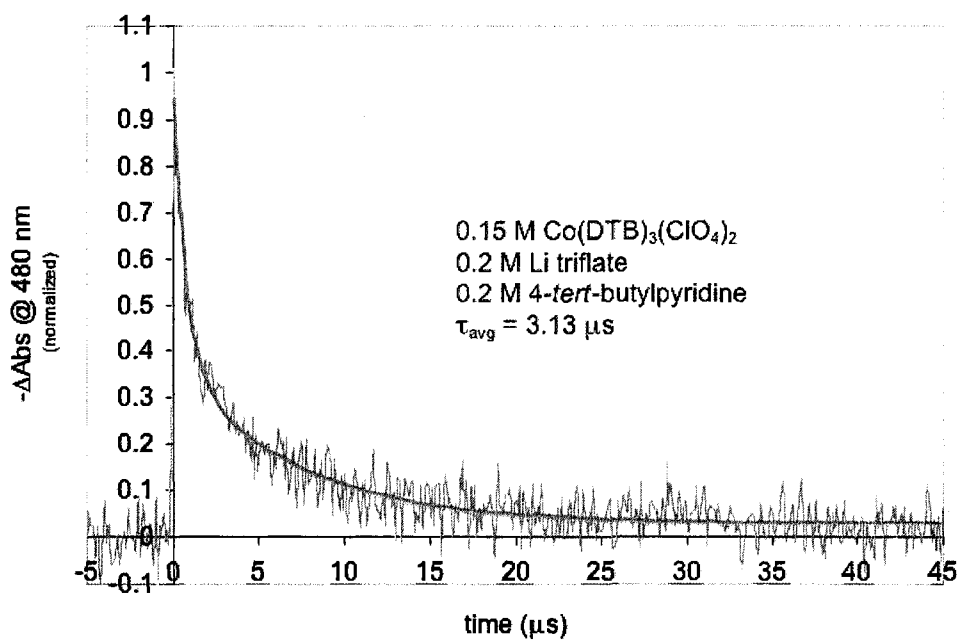
$$y = A_1 e^{\frac{-x}{t_1}} + A_2 e^{\frac{-x}{t_2}} + C$$

Average lifetimes (τ_{avg}) were calculated as:

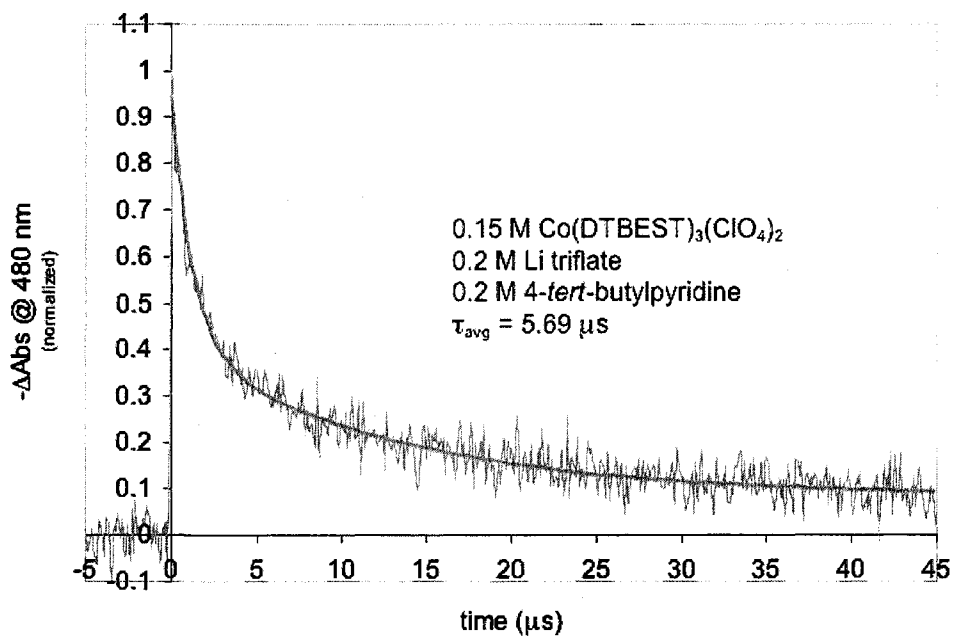
$$\tau_{avg} = \frac{A_1}{A_1 + A_2} t_1 + \frac{A_2}{A_1 + A_2} t_2$$



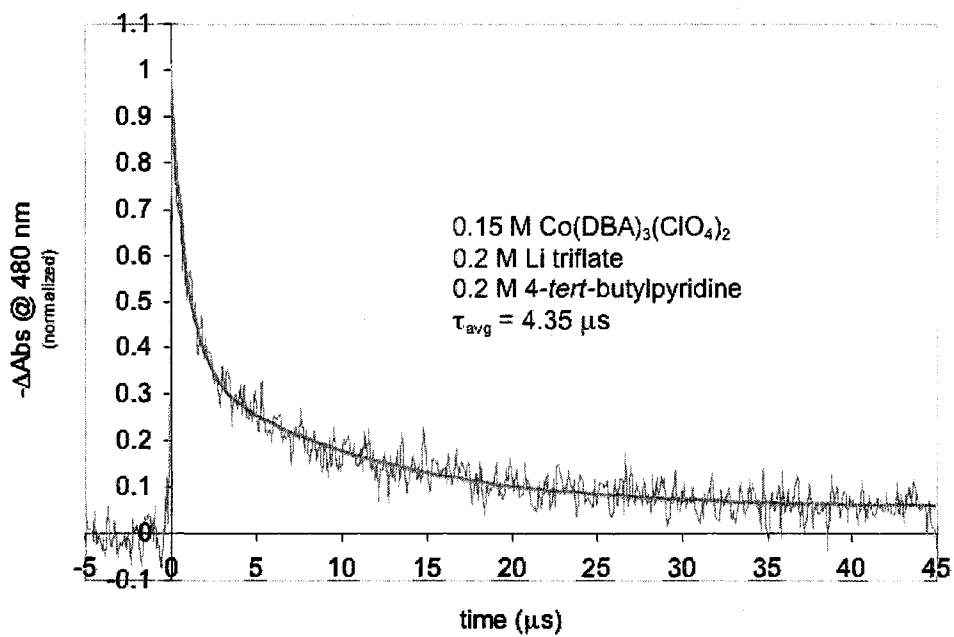
C	A ₁	t ₁	A ₂	t ₂	τ_{avg}
0.14036	0.31287	14.42955	0.49986	1.22577	> 10 μs



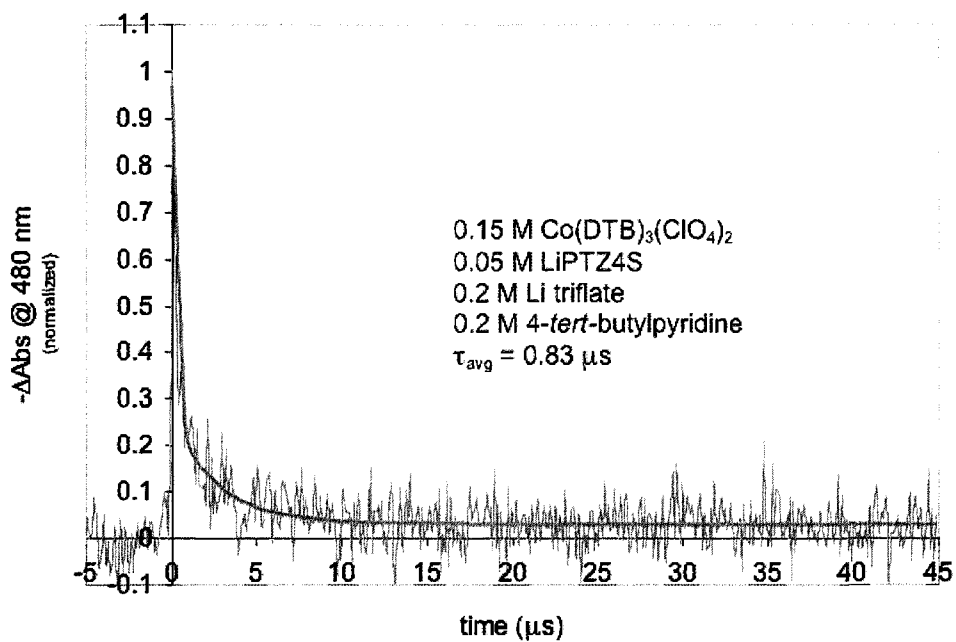
C	A ₁	t ₁	A ₂	t ₂	τ_{avg}
0.02946	0.35859	6.90859	0.56005	0.7035	3.13 μs



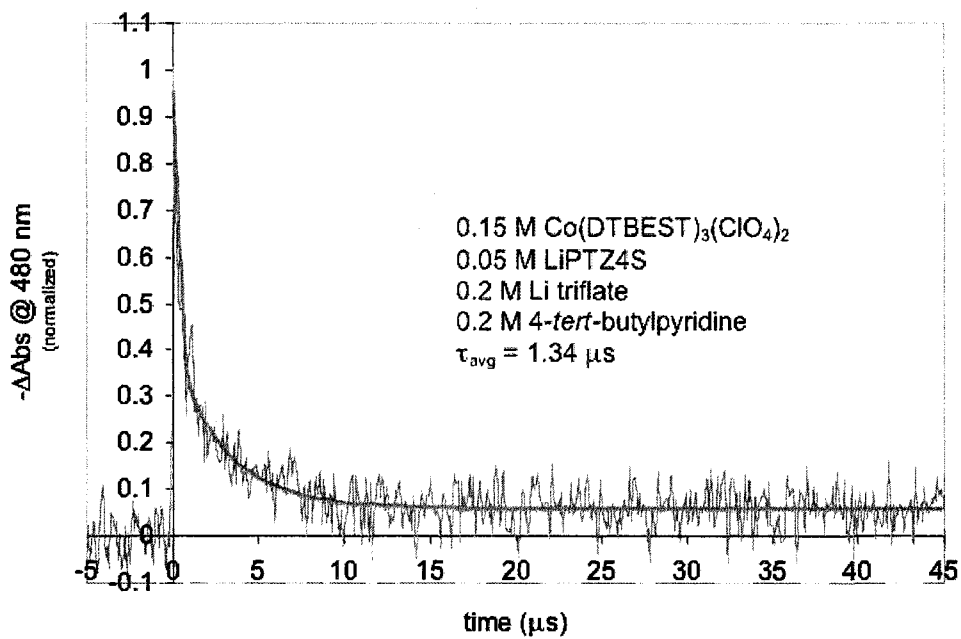
C	A ₁	t ₁	A ₂	t ₂	τ_{avg}
0.08603	0.52963	1.19657	0.3315	12.87312	5.69 μs



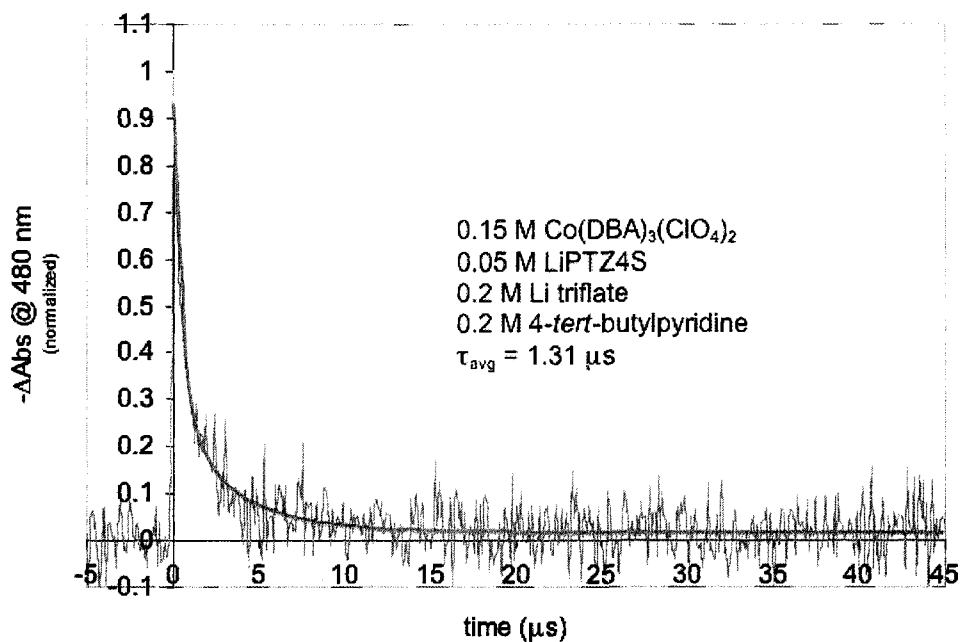
C	A ₁	t ₁	A ₂	t ₂	τ_{avg}
0.05705	0.55808	0.89698	0.32275	10.31817	4.35 μs



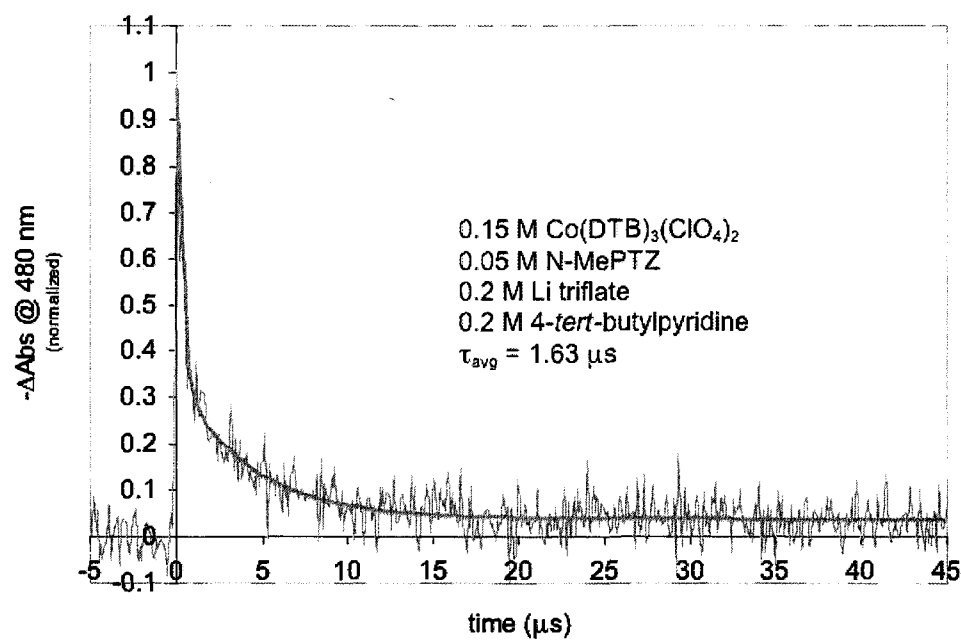
C	A_1	t_1	A_2	t_2	τ_{avg}
0.03283	0.23074	2.66203	0.70844	0.23426	0.830 μs



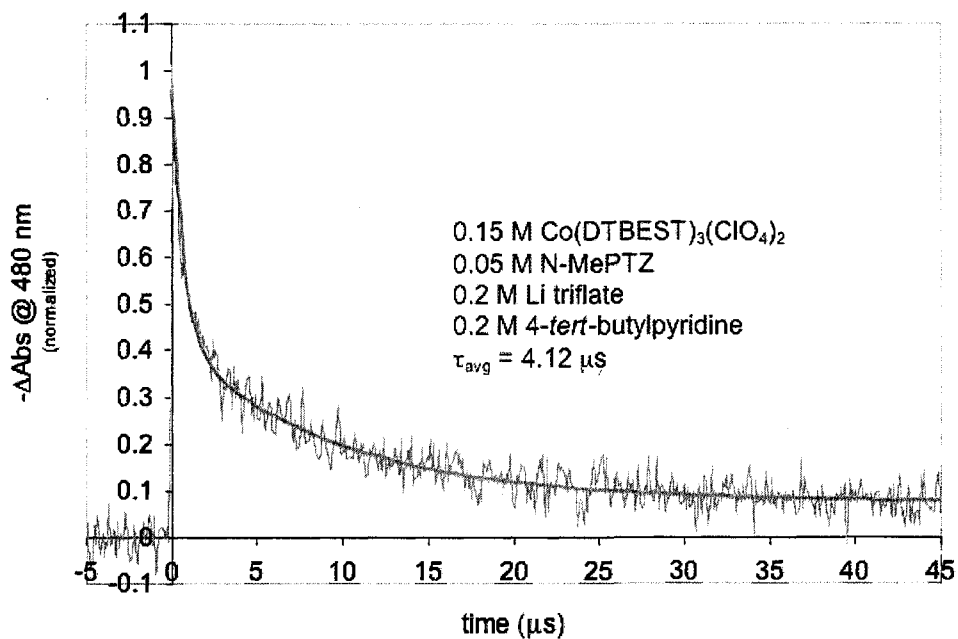
C	A_1	t_1	A_2	t_2	τ_{avg}
0.05969	0.56078	0.28155	0.33769	3.08787	1.34 μs



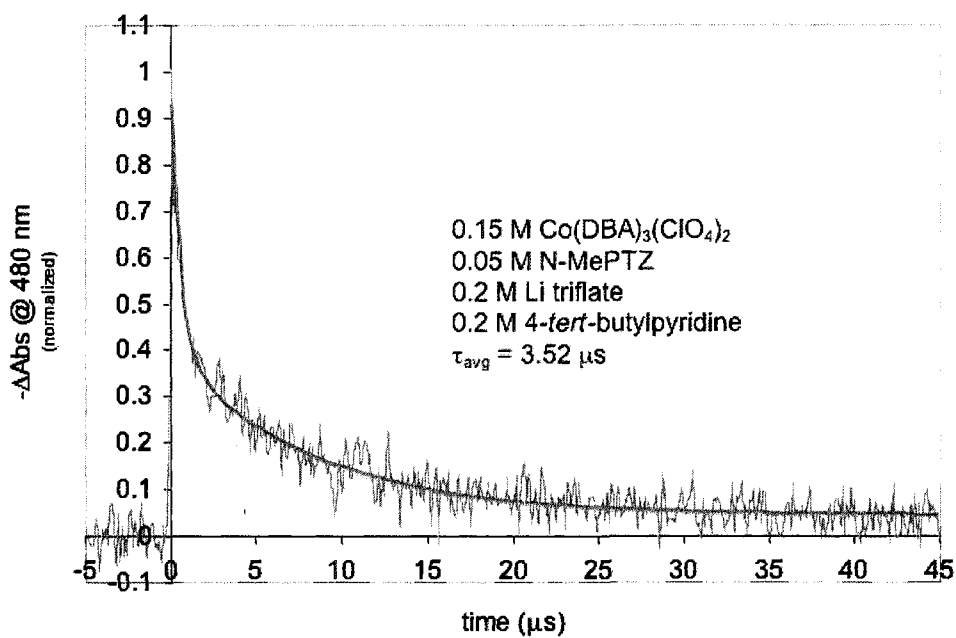
C	A ₁	t ₁	A ₂	t ₂	τ _{avg}
0.01975	0.25492	3.39331	0.65818	0.49948	1.31 μs



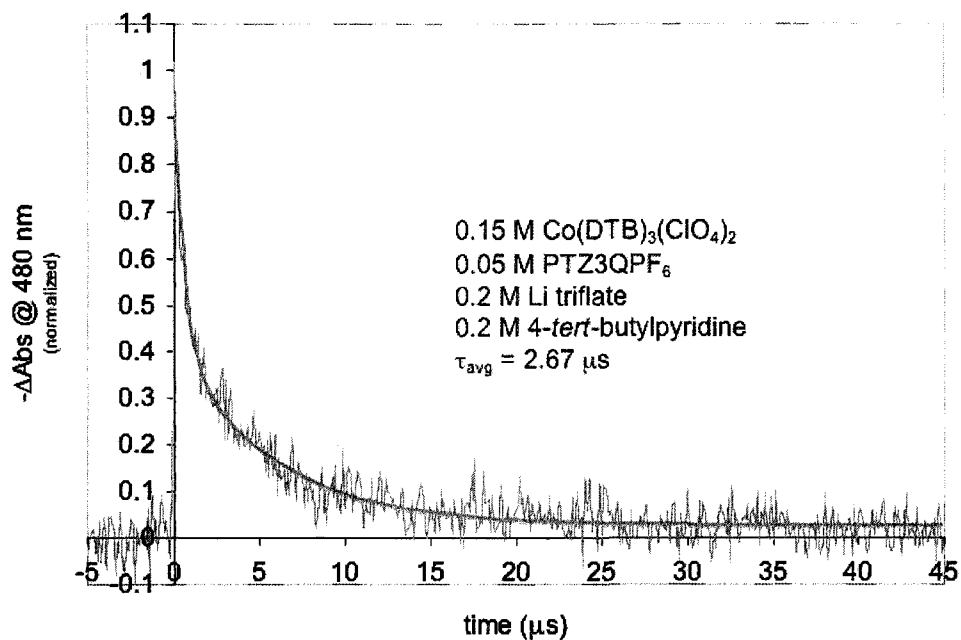
C	A ₁	t ₁	A ₂	t ₂	τ _{avg}
0.03925	0.30403	4.33189	0.62592	0.32419	1.63 μs



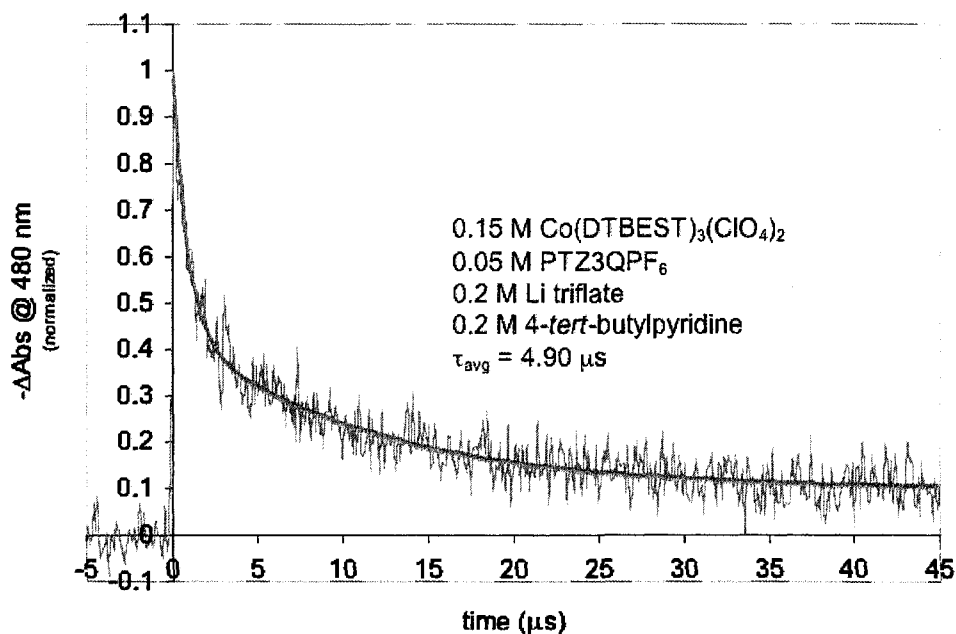
C	A ₁	t ₁	A ₂	t ₂	τ _{avg}
0.07871	0.5321	0.65481	0.35014	9.37379	4.12 μs



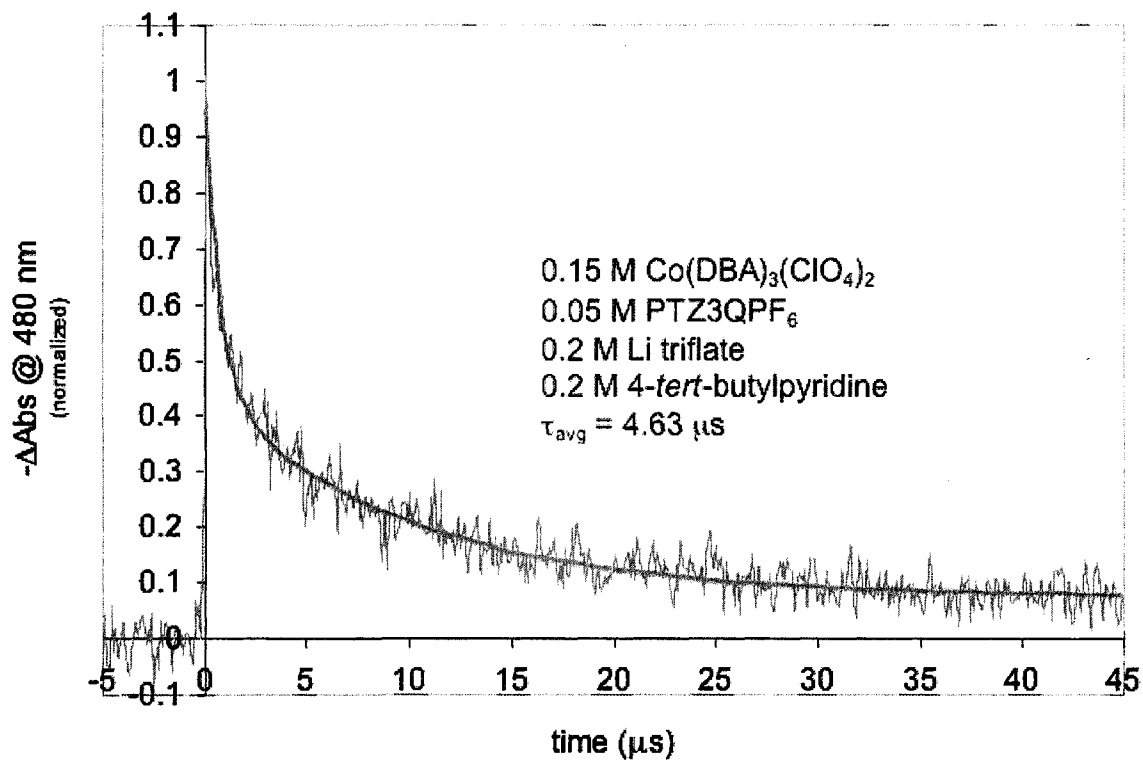
C	A ₁	t ₁	A ₂	t ₂	τ _{avg}
0.04712	0.53046	0.52321	0.35773	7.97297	3.52 μs



C	A ₁	t ₁	A ₂	t ₂	τ _{avg}
0.02885	0.407	5.49704	0.52598	0.48921	2.67 μs



C	A ₁	t ₁	A ₂	t ₂	τ _{avg}
0.09975	0.53374	0.83489	0.34771	11.13491	4.90 μs



C	A ₁	t ₁	A ₂	t ₂	τ_{avg}
0.07514	0.49692	0.73793	0.37736	9.76463	4.63 μs